Experimental Characterization and Theoretical Calculations of Responsive Polymeric Systems

by

Salim Khouri

A thesis
presented to the University of Waterloo
in fulfillment of the
thesis requirement for the degree of
Master of Applied Science
in
Chemical Engineering

Waterloo, Ontario, Canada, 2010

AUTHOR’s DECLARATION

I hereby declare that I am the sole author of this thesis. This is a true copy of the thesis, including any required final revisions, as accepted by my examiners.

I understand that my thesis may be made electronically available to the public.

ABSTRACT

Due to their controllable size, low cytotoxicity, and unique architecture, cyclodextrin based pseudopolyrotaxanes have been developed to encompass a broad range of diverse medical and chemical engineering applications. The study of complexation between α-cyclodextrin (α-CD) grafted PEG segments on the surface of PAMAM dendrimers was carried out to investigate the physical properties and driving force of this so called host guest interaction. At pH of 10, complexation between α-CD and PEGylated-PAMAM occurred once α-CD was titrated to the PAMAM solution. However, at pH of 2 no binding took place until a critical α-CD concentration (C*) of ~ 8.0 mM was exceeded. The size of the nanostructures increased with α-CD concentration ranging from 0.5 to 25 mM at pH value of 2. From zeta potential measurements it was found that the PEGylated-PAMAM possessed positive charges, attributed to the protonation of primary amine groups on PAMAM chains that impart electrostatic repulsive forces to the system. As observed from DLS and SLS study at increasing α-CD concentration and pH values, the morphology of the complex changed from a start shaped to a Gaussian like structure.

The dynamics and dimensions (length, diameter, translation and diffusion coefficients) of rod-like cellulose micro crystallites (whisker) were also investigated using simulated parameter estimation technique. For rod with L/d ratio equal to 17 (ROD 17), experimental D and Θ values produced length and diameter values showing close resemblance to experimental results with a significant reduction in the percentage error approaching 0.22 and 0.27% after 1000 iterations, respectively. The proposed approach provides a suitable and simple method to determine the length and diameter of rod-like nanoparticles, such as nanocrystalline cellulose.

ACKNOWLEDGMENTS

I would like take this opportunity to express my heartfelt thanks to Professor Kam Chiu Tam for his support and encouragement throughout my two year period of study. I am very grateful to Professors Ali ElKamel and Zhongwei Chen for agreeing to be my readers of this thesis and for their inspirations and motivations throughout all my research work.

I would like to acknowledge all my lab coworkers and friends who have provided me with support, assistance, and enthusiasm during my research studies, and during the course of writing this thesis. I also very much appreciate the assistance and time spent by David Suh (May God Bless His Soul), Dr. Ashraf Al-Daoud, Parinaz Akhlaki, Imad Azzam and Prodip Kundu during proof reading this thesis.

I also offer my gratitude to University of Waterloo for providing financial support to pursue this research project. Last but not least, I thank my family particularly my father, mother and brother for their guidance and mental support throughout all my academic years at school and universities.

Contents

LIST OF FIGURES

LIST OF TABLES

LIST OF SYMBOLS

(D_t)	:	Translational Diffusion Coefficient
(Θ)	:	Rotational Diffusion Coefficient
(L)	:	Length
(L^*)	:	Experimental Length,
($\bar{L}$)	:	Average calculated length
(d)	:	Diameter
(d^*)	:	Experimental diameter,
($\overline{d}$)	:	Average calculated diameter
(q or Q)	:	Neutron Scattering Intensity
S (q)	:	Structural Factor
M (q)	:	Mobility
(Γ)	:	Decay rate
(T)	:	Torque
(ω)	:	Angular Velocity
(b)	:	Half width
(η)	:	viscosity
(D_r)	:	Rotational frictional drag coefficient
(f_r)	:	Drag Force
(k_B)	:	Boltzmann constant
(T)	:	Absolute temperature
i	:	Sub-script index
α, β	:	Fitting parameters
b (k)	:	Decay exponent
ε %	:	Error percent

LIST OF ABBREVIATIONS

PAMAM	:	Poly (amido amine)
PEG	:	Poly (ethylene glycol)
α-CD	:	α-cyclodextrin
β-CD	:	β –cyclodextrin
γ-CD	:	γ-cyclodextrin
LPEI	:	Linear polyethylenimines
PAA	:	Poly (acrylic acid)
PMOz	:	Poly (methyl oxazoline)
PNIPAM	:	Poly (N-isopropylacrylamide)
NCC	:	Nanocrystaline cellulose
^{1}H NMR	:	High resonance neutron spectroscopy
SANS	:	Small angle neutron scattering
MRI	:	Magnetic resonance imaging
ITC	:	Isothermal titration calorimetry
UV/VIS	:	Ultraviolet visible spectroscopy
DLS	:	Dynamic light scattering
SLS	:	Static light scattering
IACF	:	Intensity Autocorrelation Fucntion

Chapter 1.0 Introduction

1.1 Introduction

Since the discovery of nanoscale structures, they have attracted significant attention by researchers because of their promising and exciting industrial applications. Due to the development of science and engineering, the past 100 years have shown a dramatic increase in the design, production, and manufacture of artificially created nano-devices. These have shown numerous potential applications in different fields such as, gene delivery, catalysis, electronics, pharmaceuticals, cosmetic and food processing, nano / microreactors; and polymers (Philp et al. 1996). With respect to nanoparticles, understanding of the definitions, such as self organization / assembly, host-guest interactions and molecular recognition, is vital for explaining the types of interactions and behavior. Ultimately, all these phenomena belong to an emerging and important field of science called supramolecular chemistry, which means chemistry "beyond the molecule" (Alexei A. 1997). Various types of interaction forces, such as hydrophobic, Van Der Waals, and other non-covalent interactions are driving forces that induce the molecules to undergo spontaneous self-assembly (Szejtli, 1984). In the present study, the properties and behavior of four different supramolecular systems were studied, involving cyclodextrins (cyclic oligosaccharides), dendrimers (synthetically designed molecules that are often referred to as ("building blocks for a nanoscopic chemistry"),and block copolymer. Dendrimer, such as poly (amido amine) (PAMAM) possesses positive charges at low pH attributed to the protonation of primary amine groups on the PAMAM chains, which imparts electrostatic repulsive forces to the system. Other systems were studied theoretically, including nanocrystalline cellulose whiskers which are naturally found as microfibrils.

1.2 Motivation and objectives

The first objective of this research is to study the interaction between α-CD and PEGylated PAMAM dendrimers using different physical techniques. PAMAM dendrimers are potentially important in drug delivery, gene delivery, catalysis etc. Therefore, studies on the physical properties of these modified dendrimers and their aggregation mechanism in the presence of additives, such as cyclodextrins are of great interest to researchers. This thesis describes the particle surface charge, binding mechanism and morphological structure of PEGylated-PAMAM/α-CD complex, using zeta potential, isothermal titration calorimetry (ITC) and light scattering. PEGylated PAMAM dendrimers are attractive nanostructures because of colloidal stability imparted by the extended PEG chains via steric hindrance. At low pH (e.g. pH < 2), PAMAM would swell and entrap more molecules within the cavity of the core since all of the amine groups are fully protonated. At neutral pHs (pH=7-8), studies showed that only the amines at the surface of PAMAM are protonated, whereas those in the core are deprotonated due to the fact that their pKa values (3-6) are lower than the pH condition. This unique property is expected to play a vital role in the binding between cyclodextrin and grafted PEG on the dendrimer's surface.

On the other hand, cyclodextrin inclusion complexation (IC) with polymeric chains has been extensively studied, because of their wide applications in fields of drug delivery, pharmaceutical and cosmetic formulations, food processing and environmental protection. Through these studies, it was found that strong ionic strength on the polymer backbone will prevent the commencement of the threading process, which inhibits the formation of ICs. This is because the electrostatic repulsive forces present on the polymer are much stronger than the non-covalent interactions, such as hydrogen bonding that is essential for the formation of the CD-polymer complexes (Liu, et al. 2007,Lee, et al. 2004).

The second aim of our work is to evaluate the physical properties of rod like nanoparticles, such as nanocrystalline cellulose (NCC) using theoretical modeling and simulation techniques. The proposed approach provides a suitable and simple method to determine the length and diameter of the NCCs. The method utilizes an optimization routine with built-in MatLab functions to solve a model developed by previous researchers (Broersma et al. 1960, 1980) yielding averaged values of both dimensional and dynamic properties of cellulose.

1.3 Organization of thesis

This thesis is divided into 5 main chapters. The first chapter provides an oveview of the current work and applications of both cyclodextrin induced supramolecular and dendritic systems. The topics discussed are responsive α-CD based polymers, physical properties of dendrimers, overview of NCC, and recent applications of these systems.

The third chapter describes the detailed methodologies and experimental techniques on the synthesis, characterizations and theoretical calculations of the systems. It also presents the ^{1}H Nuclear Magnetic Resonance (NMR) spectrum of the synthesized products.

The fourth chapter is divided into four sections. The first one briefly discusses the results obtained on the binding between α-CD and homopolymeric polyethyleneimine (PEI) system. The second part describes the physical characterization of the binding between α-CD and PEGylated-PAMAM dendrimers at low and high pH values. The third one describes the same binding process but at various pH values and at constant α-CD concentration. Finally the fourth section, discusses the determination and prediction of the physical properties of cellulose whiskers.

Lastly, chapter five summarizes the key conclusions and chapter six provides several recommendations on possible future studies of this research study.

Chapter 2.0 Literature Review

2.1 Background on CD Supramolecular Structures

In this section general background on cyclodextrin and its supramolecular structures will be presented.

2.1.1 Cyclodextrin and CD-polyrotoxanes

Cyclodextrin

Discovered in 1891 by Villiers (Wenz, et al. 2006), cyclodextrin has attracted the attention of scientists and engineers for more than a century, mainly due to its extraordinary abilities to host guest molecules within its ring cavity as shown in Figure 2.1. In general, cyclodextrins are water soluble, biocompatible, easily modified and well-defined molecules that are commercially available in different cavity diameters.

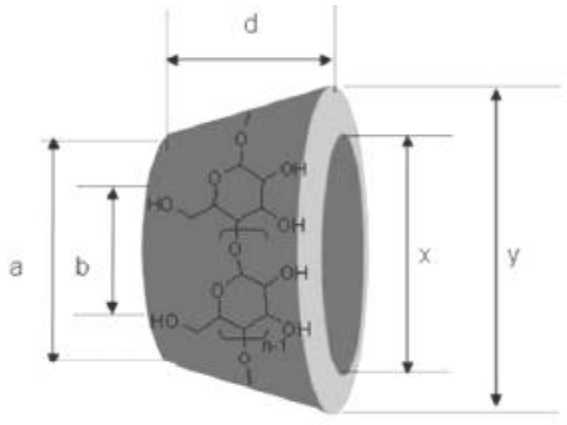

Figure 2.1 Dimensions of α, β, γ cyclodextrins (A^o) (Wenz, et al. 2006)

CD Type	n (# of repeating units)	a	b	d	x	y
α-CD	**6**	**13.2**	**4.5**	**7.8**	**5.0**	**13.7**
β-CD	**7**	**14.9**	**6.1**	**7.8**	**6.5**	**15.3**
γ-CD	**8**	**16.1**	**7.7**	**7.8**	**8.5**	**16.9**

Table 2.1 Dimensions of cyclodextrin compounds

The three most important types of cyclodextrins are α, β and γ-CD, which contain 6, 7 and 8 glucose units, respectively (Figure 2.1). The average diameters of the cavities of α , β and γ CD are 4.5, 7.0, and 8.5 Å, respectively, while the height of each CD's torus is 7.8 Å (Del Valle 2004). Generally, the interior of cyclodextrin is not hydrophobic, yet considerably less hydrophilic than the aqueous environment and thus able to incorporate other hydrophobic molecules. In contrast, the exterior is sufficiently hydrophilic due to the presence of hydroxyl groups that enhance the solubility of cyclodextrins (Bender, 1978). As discussed previously, the widespread use of CDs is due to their valuable property in complexing with guest molecules within their ring structure, a process called inclusion complexation. Because of the different sizes of CD molecules, many different types of compounds can be encapsulated within their ring structure, ranging in size from small inorganic ions to large organic molecules. The main binding forces in these host-guest complexes are generally non-covalent interactions, particularly hydrogen bonding and Van Der Waals forces.

Cyclodextrin Rotoxanes

The word rotoxane is derived from the Latin word for wheel and axle (Harada, et al. 1992). These materials consist of three key components: the wheel (i.e., a macrocycle such as cyclodextrins), the axle (i.e., the molecule threaded through the macrocycle, usually a linear polymer), and bulky blocking groups appended to the axle, which prevent the dethreading of the wheel(s). The threading efficiency and polyrotaxane dynamics are governed by non-covalent

interactions, mainly hydrogen bonding and Van der Waals, between the wheel(s), axle and between the adjacent wheels. If the bulky blocking groups (also called endcaps or stoppers) on the ends of the axle are smaller than the cavity of the macrocycle, then the complex is termed a pseudorotaxane (i.e., a false wheel and axle) (Scott Loethen, 2008). Since polyrotaxanes are a novel class of polymer molecular topology, it is anticipated that their properties are distinct from other polymeric architectures. The distinguishing feature of polyrotaxanes is the potential for lateral and translational motion of the cyclic molecules relative to the linear chain that penetrates it. Figure 2.2-a shows a typical illustration of a polyrotoxane with its three necessary "ingredients".

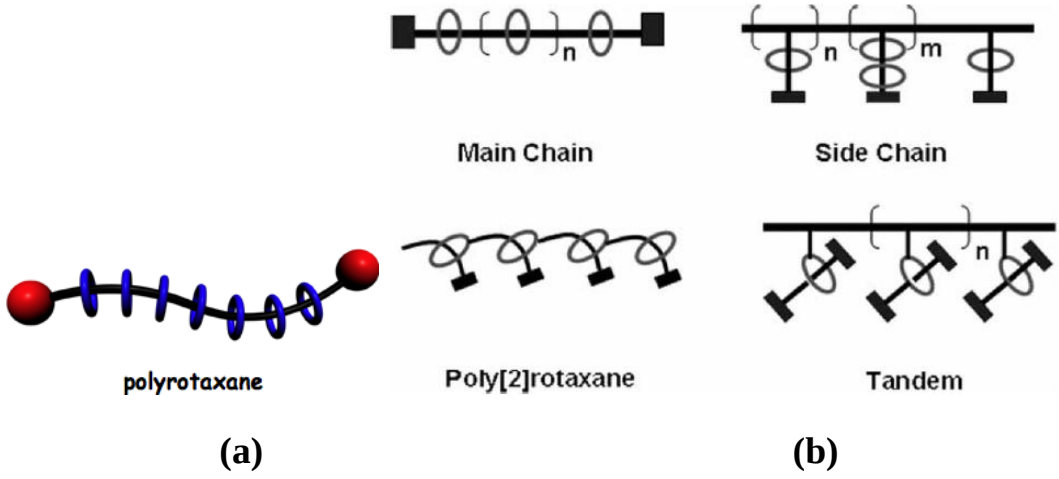

Figure 2.2 (a) Polyrotoxane with cyclic materials (blue), polymer chain (black), and capping materials (red) (b) Schematic diagrams of CD based rotoxanes(Scott Loethen, 2008)

There are in principle many subclasses of CD polyrotaxanes that differ in the nature and location of the covalent and physical linkages (Gupta, et al. 2006)**.** Basically, the major requirement for the formation of these supramolecular structures is an axle with a cross-section that is smaller than the CD cavity and a length greater than that of CD. Since the CD-polymer complex is rigid

and stable, it prevents the hemolytic activity of free unmodified CD molecules and therefore it can be used in biological systems for delivery purposes.

Some ways of assembling them include (Harada, et al.1992 and 1996; Scott Loethen, 2008) :

1) Threading, followed by endcapping
2) slippage
3) clipping

When pseudorotoxanes are formed, threading is the only process required for the complexation between CD and the polymer. In some cases, a relatively small capping material is used to cap the end groups of the complexed CD/polymer system as shown in Figure 2.3.

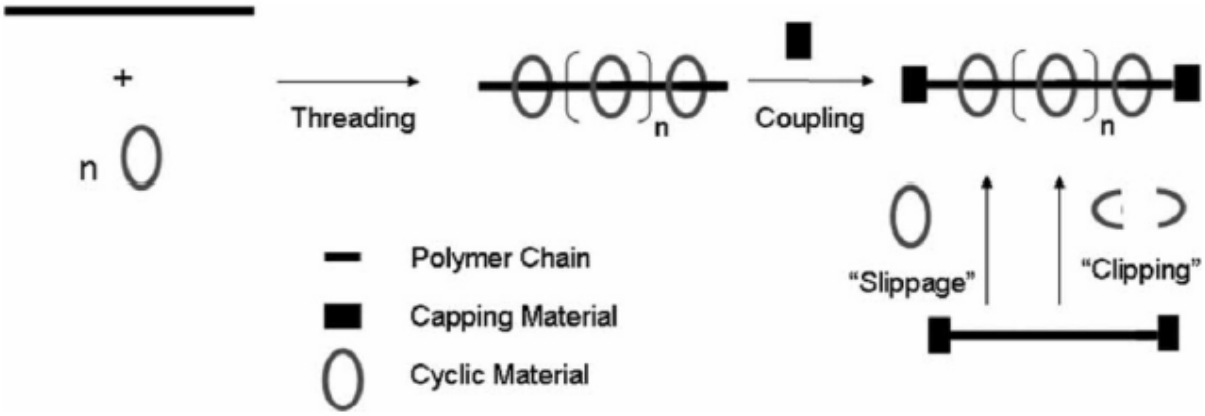

Figure 2.3 Method of production of a Polyrotoxane (Scott Loethen, 2008)

Appropriate selection of the polymer-macrocycle pair is crucial for the successful and efficient preparation of polyrotaxanes. The polymer must have the correct cross-sectional area and a relatively hydrophobic surface to form a well-fitting and stable inclusion complex with the CD units. Also, the polymer chain should be sufficiently long (i.e., M.W. >250 Daltons) and should be soluble in the solvent used for threading (Loftsson et al. 2007).

Hydrogen bonding between CD and the polymer chain also plays a vital role in the formation of CD polyrotoxanes. As shown in Figure 2.4, there are three well-known configurations between CD and the polymer (PEG) including: head-to-head (H-H), tail-to-tail (T-T) or head-to-tail (H-T) orientations (Van, et al. 2009; Wenz, et al. 2006). It was shown by molecular dynamics simulation that alternating H-H and T-T results in the lowest molecular basis with the most favourable thermodynamics consideration, and therefore produces the most favorable CD-polymer complex configuration.

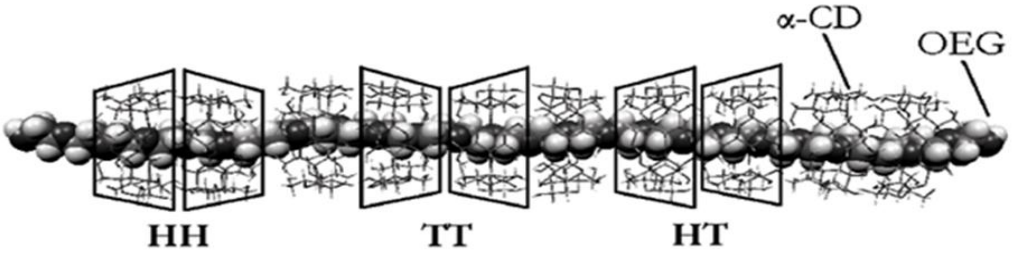

Figure 2.4 Orientation between α-CD and PEG induced by hydrogen bonding (Wenz, et al. 2006).

2.2 Studies on responsive CD based polymers

Due to their controllable size, low cytotoxicity, and unique architecture, CD-polymer supramolecular structures have been extensively studied. In this section we will provide a brief overview of several case studies in the design, synthesis and characterization of cyclodextrin based polymer complexes.

2.2.1 Properties of α-CD-Polymer complexes

Recently, numerous studies have been reported on the synthesis, characterization and applications of cyclodextrin (α, β, and γ)-polymeric nanostructures. As shown in Table 2.1,

various types of polymers having hydrophobic, hydrophilic or even polyelectrolytic properties have been studied.

Polymer	Formula	CD Threaded
Poly (ethylene glycol)	$-CH_2CH_2O-$	α, β, γ
Poly (propylene glycol)	$-CH_2CH(CH_3)O-$	α, β, γ
Poly (methyl vinyl ether)	$-CH_2CH(OCH_3)-$	γ
Oligoethylene	$-CH_2CH_2-$	α
poly (isobutylene)	$-CH_2C(CH_3)_2-$	β, γ
poly (tetrahydrofuran)	$-(CH_2)_4O-$	α, β
poly(oxytrimethylene)	$-(CH_2)3O-$	α
poly (dimethylsiloxane)	$-Si(CH_3)_2O-$	β, γ
poly (dimethylsilane)	$-Si(CH_3)_2-$	β, γ
Poly (ε-lysine)	$NH-(CH_2)_4-CH-CO-NH$	α
poly (ethyleneimine)	$-CH_2CH_2-NH$	α, β, γ

Table 2.2 List of common polymer-CD complexes (Scott Loethen May 2008) **.**

New methods and protocols in CD-polymer synthesis have provided us with more control and higher yield in the preparation of polyrotoxane, and the choice of solvent is vital. For example, the solvent must not form a better complex with the macrocycle than the threaded polymers; otherwise, the solvent will dethread from the macrocycle. In the case of CD-based polyrotaxane, many common organic solvents such as benzene, toluene, and tert-butyl alcohol should not be used. Polar solvents, such as water, DMSO, DMF, and DMAC, which interact poorly with the hydrophobic core of the CD, are most commonly used (Loethen, et al. 2007).

Complex formation between the family of cyclodextrins and hydrophilic polymers were extensively studied by Harada and co workers (Harada, etl al. 1992 and 1996). They found out that α-CD will complex with poly (ethylene glycol) (PEG) in high yield, producing highly

crystalline gels (Harada, 1996). “When aqueous solutions of PEG were added to a saturated solution of α -CD at room temperature, the solution became turbid and the complexes were formed when the average molecular weight of PEG was more than 200 Da ” (Harada, et al. 1992) . They also showed that the highest kinetics of the threading process were obtained when using PEG of molecular weight 1000g/mol in comparison to other molecular weight PEGs. It was also proven that one α-CD molecules threads on two PEG repeating units, resulting in a 2:1 ratio (ethylene glycol unit: CD) as shown in Figure 2.5. The formation of the complex was reversible and highly dependent on temperature. In solution, complexes are in equilibrium with its component. It was noted that the addition of salts, such as NaCl and KC1 did not cause any change in the solubility of the complexes since the binding of CD on non-ionizable polymers such as PEG has no ionic interactions.

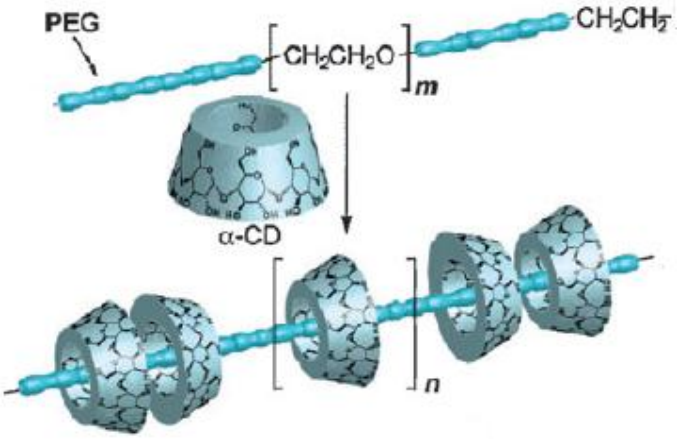

Figure 2.5 Threading of α-CD on PEG polymeric chain (Harada 1997)

Complex formation between β and γ-CD and PEG did not take place since the cavity of both cyclic molecules is too large to act as hosts for the PEG repeating units.

Several studies have been carried out on the complexation between CD and various polymers with different hydrophilic and hydrophobic properties. In the case of hydrophilic polymers, it

was shown that α- CD does not form stable complexes with poly (propylene glycol) (PPG) of any molecular weight. PPG is structurally similar to PEG but has extra methyl groups. The reason that α-CD does not form complexes with PPG is due to the small cavity diameter of α-CD and hence the steric hindrance between α-CD and the methyl groups on the main chain of PPG. On the other hand, β-CD was able to form stable complexes with PPG (Harada, et al. 1992). Similar to the case of PEG, low molecular weight PPGs did not form any supramolecular structures, with β-CD, because their number of repeating units was insufficient to form stable complexes.

Complexation between cyclodextrins and other polymers with hydrophobic chains has also been thoroughly studied. Binding between α-CD and oilgoethylene (OE) and γ-CD with polyisobutylene are two examples of these studies. The former case showed a 3:1 stoichiometric ratio (ethylene unit: α-CD). X-Ray diffraction studies, ^{13}C CP/MAS and PST/MAS NMR spectra suggested that the OE chain is included in the channel formed by α -CDs and the OE backbone in the complexes. Similar results were observed when poly (dimethylsiloxane) was allowed to complex with cyclodextrins (Okumura, et al. 2000). An interesting phenomenon was observed for the latter where β-CD formed complexes with the low molecular weight analogs, monomer and dimer; whereas γ-CD did not form complexes with these low molecular weight compounds. This indicates that the chain length selectivity is totally reversed between β-CD and γ-CD.

α-CD complexation with Poly (ε-lysine) (PL)

Initially, the majority of research work in the field of CD pseudorotoxanes was focused on the interaction between CD and linear polymers having nonionic nature such as PEG, PPG, etc. However, more studies involving the threading of CDs onto polyelectrolytes were performed later. Because of their pH responsiveness, it is believed that these polymers will potentially be

sued in a wide range of applications, such as in chemical, biochemical and biomedical engineering domains. Poly (ε-lysine) (PL) is one of these polymers. Embedded within its chain, is an amino acid repeating unit (ε-lysine NH-$(CH_2)_4$-CH-CO-NH), with a pKa value close to 8.5-9 making its amino groups ionizable in acid and neutral conditions (Huh, et al. 2002). The precipitation of PL in aqueous solutions saturated with α-CD revealed the initiation of complexation. However, β and γ-CD could not form ICs with PL because their cavity sizes were too large to accommodate the ε-lysine repeating unit. The stoichiometric ratio was found to follow a 1:1 ratio; half to that obtained for PEG (α-CD: lysine unit). The inclusion complexation, however, was absent in acidic and highly alkaline conditions. As explained by Huh and coworkers (Huh, et al. 2002), it can be considered that this pH-dependent complexation is closely related to the protonation of amino side groups (pKa = 9) in the PL at low pH values, and the dissociation of hydroxyl groups (pKa = 11.3) at basic pH. At low and high pH values the strong electrostatic repulsion forces will dominate over the non-covalent forces (mainly hydrogen bonds) forcing a dethreading process of the α-CD molecules from the PL polymeric chain (Huh, et al. 2002).

Threading process between α-CD and PEI

In the past few decades, the effect of pH, salt and temperature on inclusion complexation of CDs with various ionic guests has been studied. However, CDs did not show an appreciable change in their properties within a moderate range of pH and salt concentration. For example, Wenz et al. reported on the preparation of polypseudorotaxanes based on α-CD and polycation guests such as poly-(iminooligomethylene) in acidic pH conditions (Wenz et al. 1994 and 2006). They demonstrated that the inclusion process largely depends on the degree of protonation of the

amino groups along the polymer chain. Later, they reported on the kinetics and temperature-dependent threading of the CDs onto the polymer chain.

Soon after, homopolymeric polyethylenimine (PEI) was investigated for its complexation with CD molecules. PEI is structurally very similar to PEG, having nitrogen replacing the oxygenatom in the repeating CH_2CH_2O unit. PEI is also commonly used in gene delivery agents, transfection agents, cell attachment promoters and many other biomedical applications (Boussif, et al. 1995). Choi et al. investigated the pH-dependent PEI polypseudorotaxane formation with α or γ-cyclodextrins (Choi, et al. 2004). The advantage of using PEI polymers is that they are easy to synthesize unlike natural ones, such as poly (ε-lysine). It was shown that the polypseudorotaxane formation is significantly dependent on the pH of the aqueous media similar to the observations seen for the homopolymeric PLs. Having secondary amine groups with a pKa of 8.9, PEI is ionizable below pH ≈ 8.5, and thus is expected to form a pH responsive inclusion complexation with CDs. The yield percentage of IC formation showed a significant increase at pH≈8.5, which coincides with the pKa values of PEI (Figure 2.6), which is in accordance with previous reports. Previously, it was shown that the dissociation of CDs resulted in a decrease in the yield at low pH conditions due to the fact that the hydrophobic cavities of CDs were energetically unfavorable to the protonated amino groups (Choi et al. 2004).

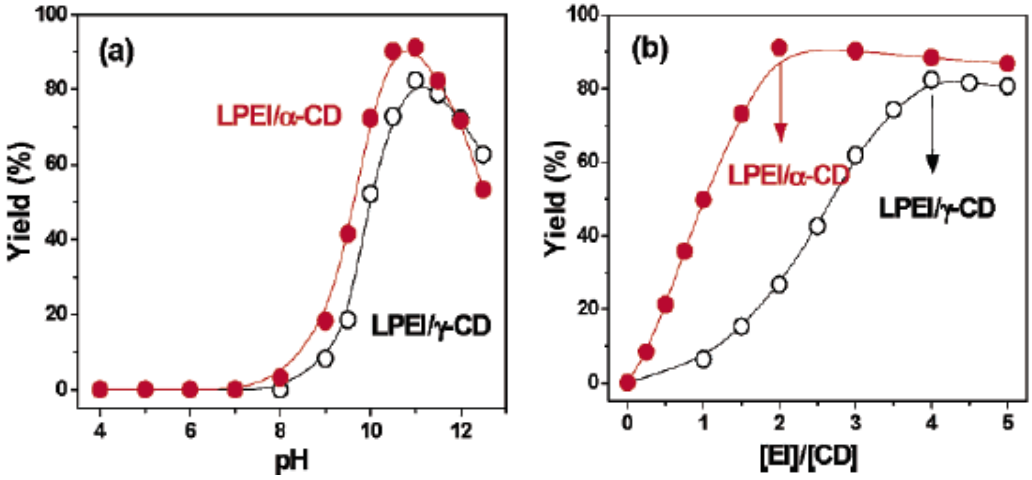

Figure 2.6. a) Yield percentage with pH, b) yield percentage changes with [EI]/ [CD] ratio for α /γ-[CD] (Choi, et al. 2004).

The observed stoichiometric ratio of 2:1 ([EI]/α-[CD]) was similar to that previously reported for the α-CD/PEG-based complexes. This is because the length of the PEI repeating unit is identical to that of PEG (3.3 Å).

Linear polyethylenimine (PEI) could also be conjugated with different polymers as di or tri block copolymers to produce pH responsive systems with two segments, one or two of which, is able to complex with α-CD. Lee et al. synthesized a PEI-PEG-PEI triblock copolymer and studied its complexation with α-CD molecules. Although they observed no complexation for the mixture of α-CDs and PEI homopolymers at low pH values, ^{1}H NMR analysis showed that the stoichiometry for the polypseudorotaxane was about 2:1 ([EG +EI]: [α-CD]) at pH 11.0 but was 4:1 at pH< 8 (Lee, et al. 2004). This indicated that at high pH values, both PEI and PEG segments were able to bind to cyclodextrin resulting in a stoichiometric value similar to that between PEG and α-CD. On the other hand, at low pH values, PEI was not able to bind to α-CD due to the strong electrostatic forces caused by the positive charges on the PEI segment. Alternating stoichiometric ratios between [EG +EI] and [α-CD] was seen when changing the pH

values from 2.0 to 11.0. This change accounted for the fact that α-CDs will be threaded on PEI as well as the PEG segments at pH 11.0, but will be subsequently dethreaded when the pH is decreased to less than 8.0 as seen in Figure 2.7. These observations are of significant importance since they show a reversible complexation between α-CDs and the PEI blocks (Lee, et al. 2004) (Figure 2.7)

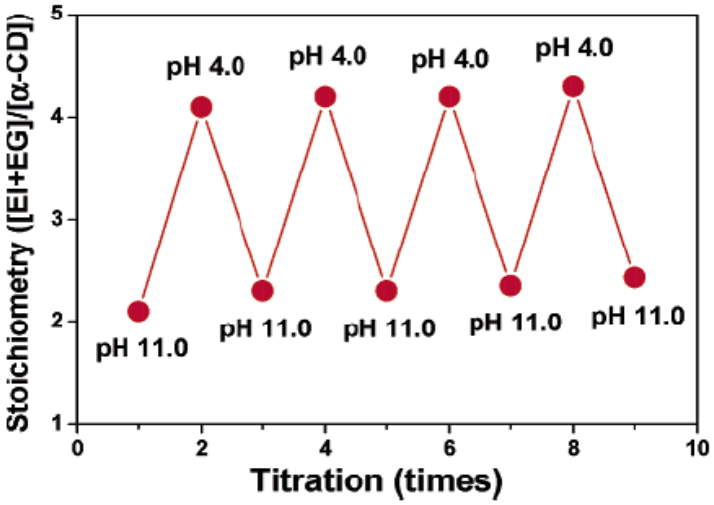

Figure 2.7 pH dependent stoichiometric changes between [EG +EI] and [α-CD]
(Lee, et al. 2004)

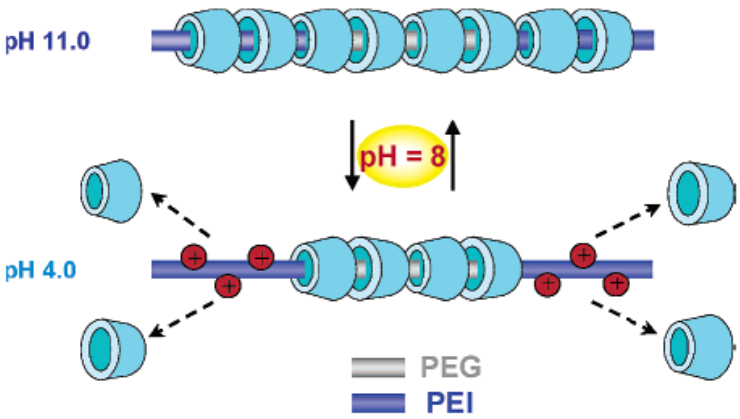

Figure 2.8 Threading and Dethreading process between CD and PEG-PEI-PEG triblock copolymer

(Lee, et al. 2004)

2.2.2 pH, thermo and photo responsive Inclusion Complexes

pH Responsive Behavior

In this section we will provide an overview of other responsive α-CD/polymer complexes. In one study conducted by Tam and coworkers, a PEG-PAA block copolymer synthesized via ATRP methods, was studied for the complexation with α-CD (Liu, et al. 2007). In their study, the focus was on examining the solution properties, such as the self-assembly behavior, dissociation, particle size, and morphology. These properties and parameters play a vital role when applying nano-supramolecular structures in areas of biomedical and chemical engineering applications. They noted the formation of a turbid solution at low pH which became clear at high pH values in the presence of α-CD. At low pH (pH=3), it was expected that the protonation of the carboxylic acid groups on the PAA segment will cause the CD-polymer complex to precipitate. This is because of two hydrophobic blocks in proximity to each other resulting in their precipitation. At high pH (pH=11), deprotonation of carboxylic groups induced significant hydrophilic character to the PAA segments, resulting in the complete dissolution of the PEO-b-PAA/α-CD complex. They used the titration calorimetry technique to study the threading process of α-CD on the polymeric system at low pH values. The exothermic energy favorable curve was only ascribed to the complexation between α-CD and the polymer (PEO segments) in a 2:1 ratio (one α-CD was bound to 2 repeat units of EO segments). Furthermore, using light scattering techniques (DLS and SLS) the morphological structure of the solution at pH =3 was found to be a vesicle having an R_g/R_h ratio close to 1.0. This α-CD induced "micellization" process resulted in the formation of α-CD/PEO bilayers surrounded by a shell of ionized PAA chains extended to the external and internal regions of the vesicle as shown in Figure 2.9.

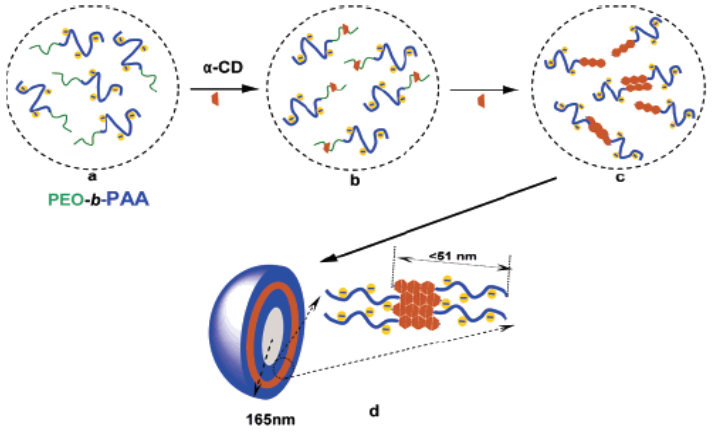

Figure 2.9 Self assembled α-CD/PEO-PAA vesicular structure (Liu, et al. 2007)

Thermo-responsive Behavior

CD-polymer complexes were also designed for thermo-responsive systems. Polymers such as poly (alkyloxazoline), poly (propylene glycol), poly (N,N-dimethylacrylamide), poly (N-isopropylacrylamide) (PNIPAM) and many others were used for this purpose (Mias, et al. 2008). PNIPAM is the most widely studied thermo-responsive polymer that possesses a LCST close to 32^{o}C; which is close to the internal temperature of biological systems. Tu et al. have studied the conformational structure of a thermo-responsive α-CD/PEO-b-PNIPAM complex. They showed that the inclusion complex consisted of coiled segments of free PEO/PNIPAM and rod segments of α-CD/PEO units. Because of the unique thermo-responsive characteristic of PNIPAM, they observed the self-assembled structure of α-CD/PEO-b-PNIPAM IC into long-range-ordered lamellar structure containing alternating layers of a-CD/PEO ICs (Tu, et al. 2009). Ooya and coworkers prepared a thermo-responsive Pluronic system consisting of PEG-b-PPG-b-PEG (Ooya, et al. 2005). Initially, they synthesized β-CD based polyrotaxanes in which many β-CDs were threaded onto PEG-b-PPG-b-PEG capped with fluorescein diisothiocyanate (FITC). Their polyrotaxane showed a temperature-responsive sliding motion of β-CDs between PEG and PPG

segments. Recently, they prepared new biodegradable polyrotaxanes in which β-CDs are threaded onto PEG-b-PPG-b-PEG capped with α-CDs which are expected to act as host molecules for the self-assembled formation of complexes with some guest molecules. It was shown that the cleavage of the terminal hydrazone bond, triggered under acidic conditions, would provide the polymeric system with a delivery carrier property applicable in biological or catalyzed acidic conditions (Ooya, et al. 2005).

Photo-responsive Behaviour

Generally, most photo-responsive systems include components of energy and electron transfers governed by non-covalent interactions, mainly hydrogen bonds, aromatic pi-stacking and metal ligand coordination. A series of polyrotaxanes as light-harvesting antenna models were constructed by Tamura et al (Tamura, et al. 2001). These polyrotaxanes consist of various ratios of α-CD and naphthalene-appended α-CD threaded onto a PEG chain bearing anthracene moieties at each end. Here, naphthalene and anthracene moieties act as energy donors and energy acceptors, respectively. It was observed that the antenna effect becomes more pronounced by increasing the number of naphthalene-appended α-CD units in the polyrotaxanes, however, the energy transfer efficiency decreases. Ongoing studies are focused on the exploration of new methods in order to increase this efficiency. Hu and co-workers also used the thermo-responsive property of some hydrophobically modified (HM) polymers to study their complexation with α-CD (Zheng, et al. 2005). They used an azobenzene functionalized hydroxypropyl methylcellulose (AZO-HPMC) which not only acts as a photo-responsive trigger, but also as a guest molecule that can form inclusion complexes with α-CD. A “one binding site” model was used to evaluate their ITC results of the inclusion complexation between α-CD and AZO-HPMC, showing an exothermic enthalpic driven reaction with a stoichiometric ratio close to 1.0. The

stoichiometric number n was independent of azobenzene content, but significantly reduced upon trans-cis isomerization of the azobenzene groups. This proved that the cis-azobenzene groups cannot form inclusion complexes with α-CD.

2.3 General applications of cyclodextrins

Since CDs have various applications in pharmaceutical, chemical, and food industries, research on these systems has become remarkably important. In pharmaceutical industry, the cyclic ring structure of CD has made it a suitable carrier for different drugs in sustained release formulations. It has been shown that drug availability in CD containing formulations will be hindered by the slow release of drug molecules from the CD cavities (Loftsson et al. 2007). However, the presence of water-soluble drug/cyclodextrin complexes at the hydrated epithelial surface will frequently increase the availability of dissolved drug molecules, especially of lipophilic drugs with poor aqueous solubility (Stella et al. 1997). Also, CD derivatives have been widely used in dispersed vehicle systems such as emulsions, microcapsules, microspheres, nanospheres, nanocapsules, liposomes (Challa, et al. 2005).

2.3.1 Gene Delivery

Over the last decade, cationic polymers have been receiving growing attention as gene delivery carriers. CDs were used to modify and functionalize cationic polymers, or serve as a template for the synthesis of new cationic polymers with star architectures. Generally, the CD containing cationic polymers showed lower cytotoxicity and efficient gene transfection in cell cultures. The most important feature of CD containing cationic polymers in gene delivery systems is that the polyplexes formed between the polymers and DNA can be further modified by inclusion complex formation. A recent study on the application of α-CD threaded polymer complex on gene delivery was thoroughly investigated by Li and co-workers (Li et al. 2008).

They synthesized a poly [(ethylene oxide)-ran-(propylene oxide)] with threaded α-CD molecules on the EO repeating units, and grafted oligoethylenimine (OEI) chains on the CD moieties. The complexation increased the mobility of the cationic α-CD rings and the flexibility of the polyrotaxanes. This led to enhanced interaction of the cationic α-CD rings with DNA and/or the cellular membranes (Li et al. 2008). All the cationic polyrotaxanes synthesized have been effectively condensed with plasmid DNA to form nanoparticles that were suitable for gene delivery. In addition, their cytotoxicity studies confirmed that the cationic polyrotaxanes with all linear OEI chains of molecular weight up to 423 Da exhibited much less cytotoxicity than high-molecular-weight branched polyethylenimine (PEI). Later, PEGylation of adamantane through the inclusion complex formation between the terminal adamantane and β-CD moieties on the DNA polyplexes was found to stabilize the polyplex nanoparticles and resulted in enhanced gene transfection (Pun et al. 2002). Another work was also presented by Ooya et al. in which dimethylaminoethyl-modified α-CDs were threaded onto a PEO chain and capped by cleavable end groups, where the α-CD possesses tertiary amines (Ooya et al. 2006). The major advantage of the synthesized complexes is the dethreading process of CD in the intracelleular region to release DNA in the cells. This is a vital process in the intracellular trafficking of the DNA after being delivered into the cells by the polyplexes (Ooya et al. 2006, Li et al. 2008) .

2.3.2 Drug Delivery

Polymeric hydrogels have attracted a lot of interest in biomedical applications because of their biocompatibility. Extensive research was performed that focuses on designing a delivery formulation that promotes gelation and drug loading simultaneously. Recently, investigations showed that the inclusion complexes formed between CDs and polymers led to the development of supramolecular hydrogels. These hydrogels could potentially be used as biomaterials for

controlled drug delivery. It is believed that those ICs will overcome problems such as inefficient time consumption of drug loading and intermolecular conjugation between drugs and hydrogels due to a cross linking reaction (Cavalli et al. 2006). In this section we will present three case studies showing the promising drug delivery properties of α-CD hydrogels.

I) The precipitation of the inclusion complexes of α-CD and PEO from aqueous solutions indicates that the resulting complexes self-assemble into larger supramolecular structures with altered hydrophilicity. As discussed earlier, Harada and coworkers were the first to show an example of a hydrogel formation between CDs and polymers (Figure. 2.10). Since both CD and PEO are biocompatible and bioabsorbable, it is expected that a new class of injectable drug delivery systems based on supramolecular hydrogels containing these polymers would become effective for implementation (Li el al. 2003, 2008).

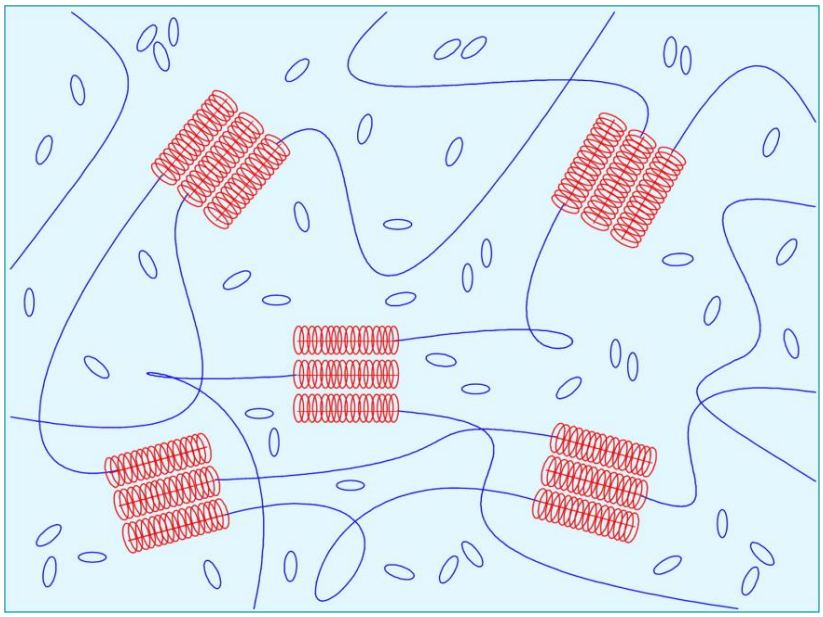

Figure 2.10 Partial inclusion complexation between high M.W. PEO and α-CD
(Li el al. 2003, 2008)

The supramolecular hydrogels formed from PEO/α-CD were found to be thixotropic and reversible. It was noted that the viscosity values changes with time. At first the viscosity of the

hydrogel greatly diminished as it was agitated, then it eventually restored towards its original value (Li et al. 2003) . From this property one can incorporate bioactive agents, such as drugs, proteins, vaccines, or plasmid DNAs into the gel in a syringe at room temperature without any contact with organic solvents. The drug-loaded hydrogel formulation can then be injected into the tissue under pressure because of the thixotropic property, and served as a depot for controlled release (Li, et al. 2003). After studying the gene delivery ability, Li and coworkers showed the releasing ability of α-CD/PEO hydrogels. They used a model drug made of Fluorescein isothiocyanate labeled with dextran (dextran-FITC), which was physically entrapped in the hydrogels. Their results are shown in Figure 2.11 revealing a steady release of the model drug from the hydrogels. However the release rate decreases sharply with an increase in the molecular weight of PEO up to 35,000 Da, presumably because of the chain entanglement effect and different complex stability (Li, et al. 2003) .

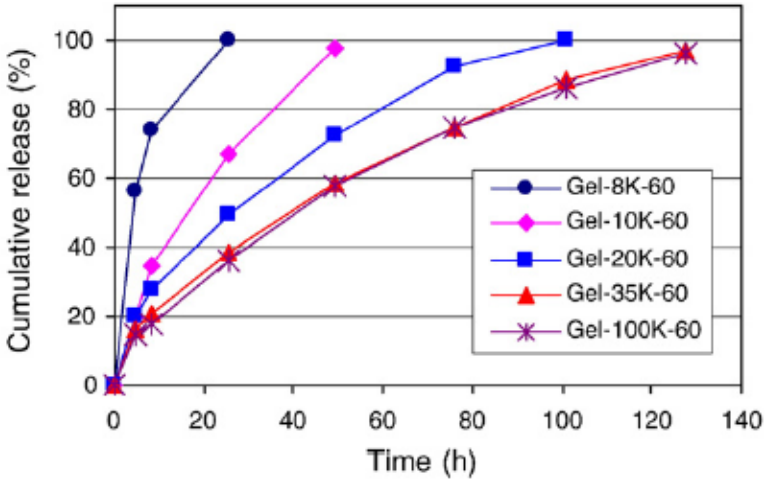

Figure 2.11 In vitro release profiles for dextran-FITC released from α-CD–PEO hydrogels formed from PEO of different molecular weights. (Li, et al. 2003)

There are two major challenges in applying α-CD/PEO hydrogels as drug delivery carriers. First, the fast release kinetics and the short-term drug release of hydrogels, because of the rapid

dissociation of them in aqueous environments due to the hydrophilic nature of PEO; and secondly the problems associated with the in vivo use of high molecular weight PEO of more than 10,000 Da. This problem is because PEO is not biodegradable and the high molecular weight PEO cannot be filtered through human kidney membranes due to the large hydrodynamic radius (Li et al. 2003, 2008).

II) Ni el al. hypothesized that using a triblock co-polymeric system will solve the problems listed above. They suggested that extra inter-molecular hydrophobic interaction of the middle blocks can further strengthen the hydrogel network, inducing the formation of more stable hydrogels for long-term controlled release of drugs (Ni et al. 2009). Initially, it was found that supramolecular hydrogel systems composed of α-CD and Pluronic (PEO–PPO–PEO) triblock copolymers could be formed (Li et al. 2003). Then it was observed that α-CD could aid the formation of hydrogels of PEO–PPO–PEO triblock copolymers at much lower copolymer concentrations. This is because α-CD could form inclusion complexes with parts of the flanking PEO blocks. This was proved using phase diagrams and comparing the polymer gelation concentrations in the absence and presence of α-CD. At very high concentrations of the triblock copolymer, a small part of it could form a hydrogel. With an increase in α-CD concentration, the gelation regions became larger and the hydrogels were formed at much lower concentrations (Ni et al. 2009 , Li et al. 2008). The in vitro controlled release properties were studied using BSA-FITC as a model protein drug released from the synthesized hydrogels. The hydrogels showed a wide range of release kinetics. The smaller copolymers showed a sustained release of BSA for more than one week with linear release kinetics. However, larger copolymer compositions were too unstable for long-term sustained delivery (Ni et al. 2009). Therefore, it was concluded that a good balance

between the PEO and PPO block lengths is important for controlled drug release from the hydrogels.

III) Finally, it is important to mention another type of CD drug delivery system based on conjugated drugs on the cyclodextrin-polyrotaxanes complex. These systems could be achieved via end-modification of the polyrotaxanes to incorporate recognizable moieties for targeted applications. In 1995, the first example of biodegradable polyrotaxanes was reported, in which α-CDs were threaded onto PEO chains and capped with L-phenylalanine (L-Phe) via biodegradable peptide linkages (Li et al. 2008). When the peptide linkages were enzymatically degraded by papain, the polyrotaxane degraded to PEO, α-CD, and L-phenylalanine (Li et al. 2008). Figure 2.12 shows the mechanism of this process:

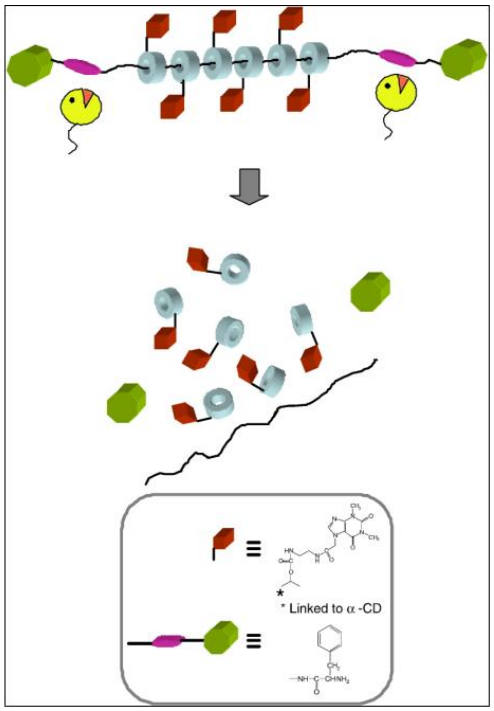

Figure 2.12 Schematic illustrations of drug-conjugated polyrotaxanes and concept of drug release (Li et al. 2008).

2.3.3 Other industrial applications of cyclodextrins

Food agents

CDs are used in food formulations for flavor protection or flavor delivery. They became accepted during the 1980s as a common ingredient for the food manufacturer; their production and consumption have been steady over the last decade (Szente et al. 2004).They form inclusion complexes with a variety of molecules including fats, flavors and colors. Most natural and artificial flavors are volatile oils or liquids and complexation with CDs provides a promising alternative to the conventional encapsulation technologies used for flavor protection (Del Valle 2004; Szente et al. 2004). Most importantly, emulsions like mayonnaise, margarine or butter creams can be stabilized with free α-CD or α-CD/polymer biodegradable complexes (Szente et al. 2004). Many food processing techniques found CD to be an effective agent to facilitate the processing methods involved, for example it was found that β-CD as a molecular encapsulant allows the flavor quality and quantity to be preserved to a greater extent and longer period compared to other encapsulants (Del Valle, 2004).

Cosmetics, personal care and toiletry

Cosmetic preparation is another area where CD can be effectively utilized. They are mainly used in the area of suppression of volatiles in perfumes, room fresheners and detergents (Del Valle 2004). Other applications include uses in skin creams, liquid and solid fabric softeners. The essential functions of fragrance materials are to provide a pleasant odour, to mask the base smell of the product, and to give the product an identity (Ulya et al., 2007). However, this is sometimes a tedious process since most fragrance agents are not water soluble. The solubilizing ability of CD can alter these poorly water-soluble fragrance materials and provide an effective solution for the presented problem (Ulya et al., 2007). Likewise, through CD

complexation it is possible to obtain controlled release of fragrances. In a patent produced by Prasad et al., it was noted that the stabilisation, odour control, and process improvement could all be achieved upon conversion of a liquid ingredient to a solid form of a fragrance using CD molecules (Prasad, et al. 1999).

CDs also showed applications in some household products such as toothpaste. Loftsson et al. implemented CD inclusion complexation in silica-based toothpastes to study the increase and availability of triclosan (an antimicrobial agent). They observed an almost threefold enhancement of triclosan availability, which could be used in combination with fluoride in toothpaste products (Loftsson, et al. 1999).

2.4 Dendrimers

Polymers can be categorized into four groups: linear polymers, cross linked polymers, hyperbranched polymers, and dendrimers as shown in Figure 2.13 (Lim, 2008**).** Dendrimers are branched-chain, three-dimensional macromolecules. Due to the similarity of their structures to branching trees, they were called dendrimers (dendron is a Greek word for a tree) (Esfand et al. 2001). Around half a century ago, Flory established a theoretical background for the existence of such macromolecules, but only about forty years later the production of the first set of synthetic dendritic systems was made possible. Despite their differences, all dendrimers have the same structural features: a central core (or reference point), repeating units, and terminal (functional) groups (Figure 2.14) (Tomalia and Dvornic, 1994).

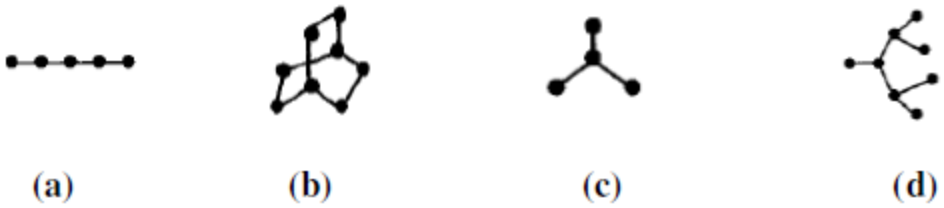

Figure 2.13 Categorization of a) linear polymers, b) cross linked polymers, c) hyperbranched polymers and d) dendrimers (Tomalia and Dvornic, 1994)

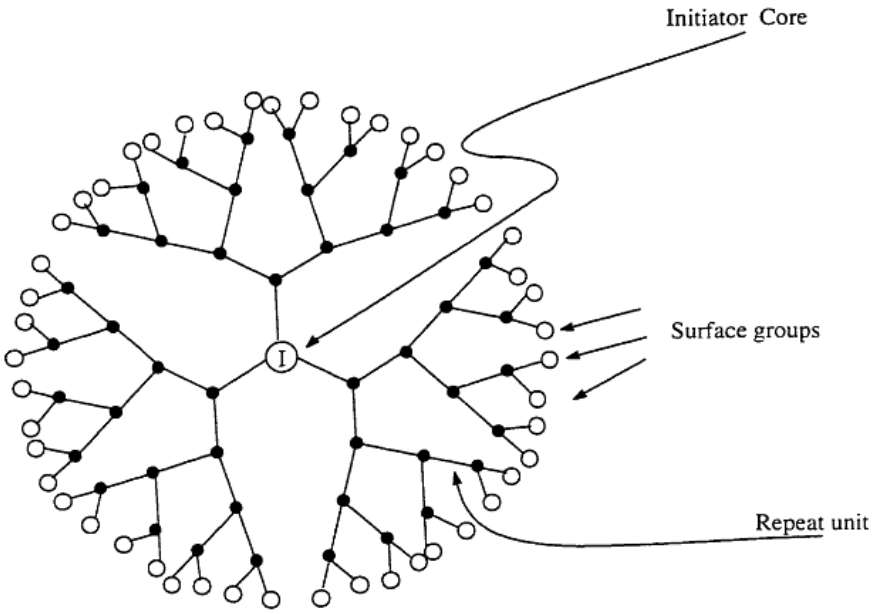

Figure 2.14 Structural Representation of a Dendrimer Molecule (Tomalia and Dvornic, 1994)

All dendrimers contain a core which possesses N_c reactive sites, where N_c is called the core multiplicity. For example, NH_3 (N_c=3), ethylenediamine $H_2NCH_2CH_2NH_2$ (N_c=4), SiH_4 (N_c=4), and benzene C_6H_6 (N_c=3), can be used as potential reactive sites (Alexei A.Fedortchenko, 1997). The radial branching out of layers of the repeating chemical groups, results in many generations until reaching the final exterior layer which is known as the surface group. The surface group can be chemically modified with a variety of terminal functionalities to give the desired properties. One of the most popular dendrimers are poly (amido amine) (PAMAM) dendrimers, which were

first synthesized by Tomalia et al (Tomalia et al.1994**).** These dendrimers consist of a diamine core with either carboxylic acid terminated dendrimers (half generation), or amine terminated dendrimers (full generation). Each generation of PAMAM dendrimers correspond to the covalently bonded repeating units of $(NCH_2CH_2CONHCH_2CH_2N)_2$. The potential applications of dendrimers, particularly, PAMAM dendrimers, are diverse mainly in the field of drug and gene delivery. This is due to their robust, well defined and highly branched globular structure (Klajnert et al., 2001).

From the beginning, similar properties between dendrimers and micelles were noted (Klajnert et al., 2001). For instance, both micelles and dendrimers have a similar size 10-300 A^o. Also, both structures are spherical and can bind to different molecules (Alexei A.Fedortchenko, 1997). However, one important difference between them is that micelles are dynamic molecular aggregates, whereas dendrimers are discrete molecules (Esfand et al., 2001; Lim 2008). For instance, conjugation of PEG has been widely used to improve the properties of a PAMAM parent molecule. PEGylation of PAMAM could resolve the problem of precipitation of dendrimers with surfactants by introducing PEGylation-induced-steric stabilization to the system (Wang, et al. 2007). Dendrimers have also been reported to host both hydrophilic and hydrophobic drugs, thus demonstrating their versatility. However, PAMAM dendrimers suffer some downsides specifically that they do not generate highly soluble polymers and show some toxicity to polymeric systems (Lim, 2008). Nevertheless, the nanoscopic particle size of dendrimers (ranging from 1 to100 nm) makes them less susceptible for uptake by the reticuloendothelial system. This fact drove the researchers' interest specifically on focusing on drug delivery applications and future nano-catalysis prospects (Klajnert et al. 2001; Gupta, et al.

2006). In this section we will explore the different synthetic procedures, physical properties and applications of dendrimers.

2.4.1 General methods for synthesis of dendrimers

The complexity of dendrimers required significant innovation and digression from classical organic synthesis methods. Nowadays, commercial quantities of controlled macromolecular structures with polydispersities of 1.0005−1.1000 are routinely being synthesized using traditional organic reagents and monomers, such as ethylenediamine and alkyl acrylates (Esfand et al. 2001). Although we will not cover the details of the synthesis, it is worth mentioning the two most popularly utilized methods including the divergent and convergent techniques.

Divergent synthesis method

This method employs branching from the amine core to produce each subsequent generation. Figure 2.14 shows the schematic synthesis of a dendrimer via the divergent. This method involves two sequential steps; in which assembling monomeric modules in a radial fashion is adopted by a branch-upon-branch configuration. Firstly, a half generation of dendrimer (PAMAM in this case) is produced by the Michael addition from a nucleophilic core (amine or ethylene diamine). After that, generation 1 of a PAMAM dendrimer will be generated on the amine chain by the subsequent amidation reaction of the resultant ester with large access of ethylenediamine (Figure 2.15-a)

Convergent synthesis method

Fréchet and colleagues introduced the convergent growth process (Esfand et al. 2001) It proceeds from what will become the dendron molecular surface (i.e. from the leaves of the molecular tree) inward to a reactive focal point at the root. This produces a single reactive dendron, which itself can be used as a starting point for obtaining a full dendritic structure as shown in Figure 2.15-b.

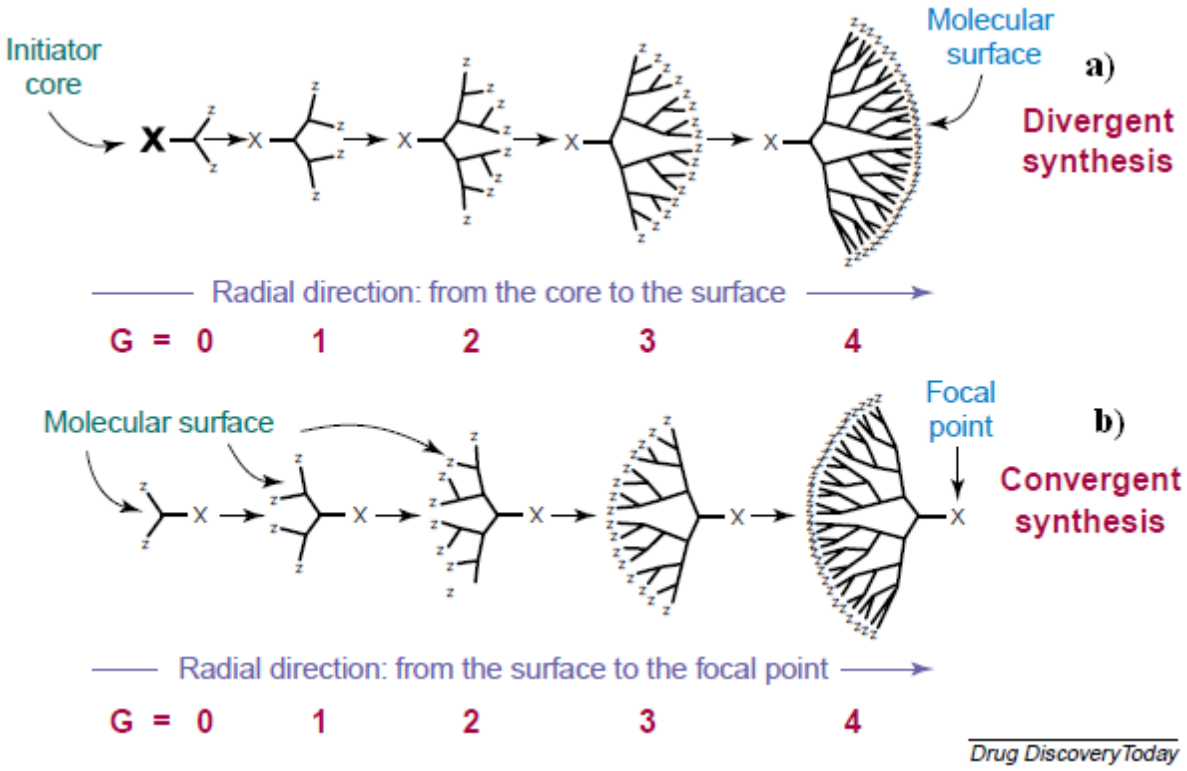

Figure 2.15 Methods for synthesizing dendrimers a) Divergent and b) Convergent method (Esfand et al. 2001)

2.4.2. Physicochemical Effects on PAMAM dendrimers

pH Effect

PAMAM dendrimers in host guest systems are greatly influenced by pH. This is because the conformation of PAMAM dendrimers is dependent on pH and the ionic strength of the solvent as shown in Figure 2.16 (Boas et al. 2004). Protonation of PAMAM dendrimers has

made them applicable as gene and drug carriers via interaction with negatively charged DNA or anionic drugs (Lim, 2008).

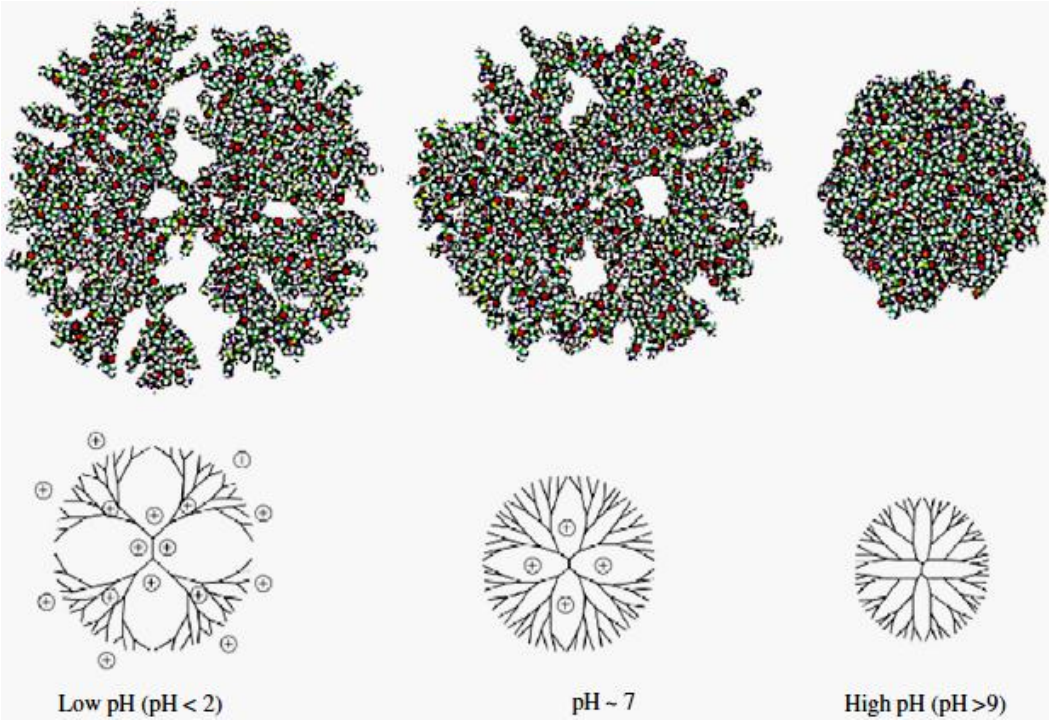

Figure 2.16 pH dependent PAMAM dendrimers

It is generally known that dendrimers are on average less compact than proteins, i.e. the interior is not packed as efficiently as in typical proteins. Also, dendrimers contain a substantially higher number of surface functional groups than proteins of comparable molecular weights. Using molecular dynamic simulations and NMR techniques, it was demonstrated that the electrostatic repulsion between protonated cationic inner tertiary amines at low pH, will force the dendritic branches to stay apart from each other (Boas et al. 2004). However, absence or reduction of those charges will cause back-folding of the dendrimers, resulting in a denser core.

C**oncentration Effect**

The encapsulation of molecules within the dendrimer core is dependent on the concentration and generation of the dendrimers. Cheng and coworkers demonstrated that by increasing the concentration of PAMAM dendrimers the solubility of non-steroid anti inflammatory drugs (NSAIDs) will also increase. This is because there would be more accessible amine sites and internal cavities for drugs encapsulation (Cheng, et al. 2008). They showed that with about 10 mg/mL of PAMAM G4 dendrimers, the solubility was increased from 0.88 to 16.92 mg/ml for ketoprofen, from 0.02 to 31.41 mg/ml for naproxen, from 0.10 to 7.45 mg/ml for ibuprofen, and from 0.19 to 4.94 mg/ml for diflunisal (Cheng, et al. 2008).

2.4.3 Dendrimers as drug agents, gene, and drug delivery vehicles

Drug agents

Antiviral Drugs: Dendrimers can act as antiviral agents. They inhibit viruses from binding to cells of host organisms by using their cluster effect. In general, antiviral dendrimers work as artificial mimics of anionic cell surfaces. Thus, the dendrimers are generally designed to have anionic surface groups such as sulfonate residues or sialic acid residues (Boas et al. 2004). Virus particles bind with cellular surfaces causing viral infection. However, using their anionic surfaces, dendrimers compete for the surface binding of virus, leading to a lower cell-virus infection probability (Figure 2.17).

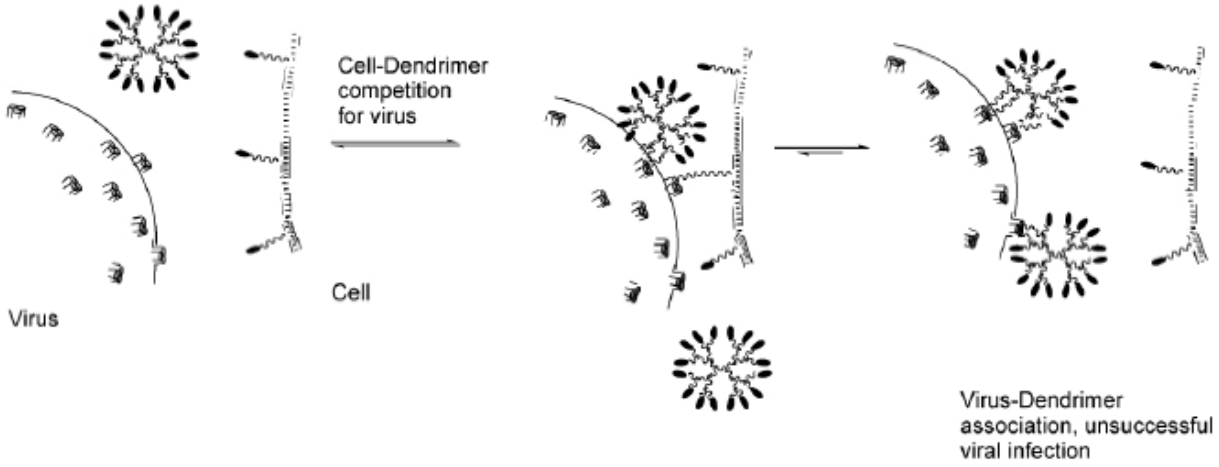

Figure 2.17 Anti-viral actions of dendrimers (Boas et al. 2004)

It was found that poly (lysine) dendrimers modified with naphtyl residues having sulfonate surface groups, were useful as viral inhibitors for Herpes Simplex virus in vitro (Boas et al. 2004). VivaGelTM, a commercially known PAMAM dendrimer grafted with naphthalene disulfonate surface groups, was a major breakthrough in pharmaceutics as an antiviral agent in preventing HIV infection.

Antibacterial Drugs: In contrast to the antiviral dendrimers, the antibacterial dendrimers generally contain cationic surface functionalities such as amines or tetraalkyl ammonium groups (Boas et al. 2004).The general mode of action of the antibacterial dendrimer is to adhere to and damage the anionic bacterial membrane, causing bacterial lysis. This is a similar mechanism to most of the commercially used antibacterial agents nowadays. Chen et al. revealed that with surface functionalization of poly (propylenimine) (PPI) dendrimers with tertiary alkyl ammonium groups, PPI dendrimers could be very potent antibacterial biocides against Gram positive and Gram negative bacteria (Chen et al. 2002).

Gene Delivery Carriers

In gene therapy, dendrimers can act as carriers called vectors (Klajnert et al. 2001). Dendrimers, such as PAMAM have high density of ionizable surface sites that serve as ideal DNA binding agents via electrostatic interactions between positively charged PAMAM with negatively charged phosphate backbones of DNA. This allows the vectors to transfer genes through the cell membrane directly into the nucleus. In addition, this ensures consistent formation of transfection complexes (Klajnert et al. 2001). A commercialized dendrimer gene delivery system called SuperFect® is currently being used as a transfection reagent. SuperFect®–DNA complexes are characterized by high stability and provide more efficient transport of DNA into the nucleus than liposomes (Klajnert et al. 2001). Some recent studies indicated that neutralization of dendrimers with DNA reduced the interaction with cell membranes, which enhanced gene transfection through the cell membranes and consequent uptake of DNA into the cells (Braun et al. 2005).

Drug Delivery Vehicles

PAMAM and PPI dendrimers have large molecular sizes and multivalent surfaces that make them suitable scaffolds for synthetic macromolecular hosts. Subsequent surface modification on these polymers can yield a host molecule with desired properties (Boas et al. 2004). As noted by Boas et al., the host–guest binding can either take place in the cavities within the core of the dendrimer (endoreceptor), or at the multivalent surface or outer shell of the dendrimer (exoreceptor). Recently, there appears to be a significant renaissance in the macromolecular drug delivery field; this revolutionary concept was first introduced by Ringsdorf in the mid-1970s. Sialated dendrimers, called sialodendrimers, have been shown to be potent inhibitors of the haemagglutination of human erythrocytes by influenza viruses. They could be useful as

therapeutic agents in the prevention of bacterial and viral infections. Attaching a α-sialinic acid moiety to the dendrimer surface enhances its therapeutic property (Esfand and Tomalia 2001).

Ibuprofen (a non-steroidal anti-inflammatory drug (NSAID)) was applied by Kolhe et al. to demonstrate its incorporation with PAMAM Generation 4 (64 amine groups) (Kolhe et al. 2003). Seventy eight iburofen drug molecules formed stable complexes with PAMAM dendrimers and showed steady release profiles in water and methanol as shown in Figure 2.18.

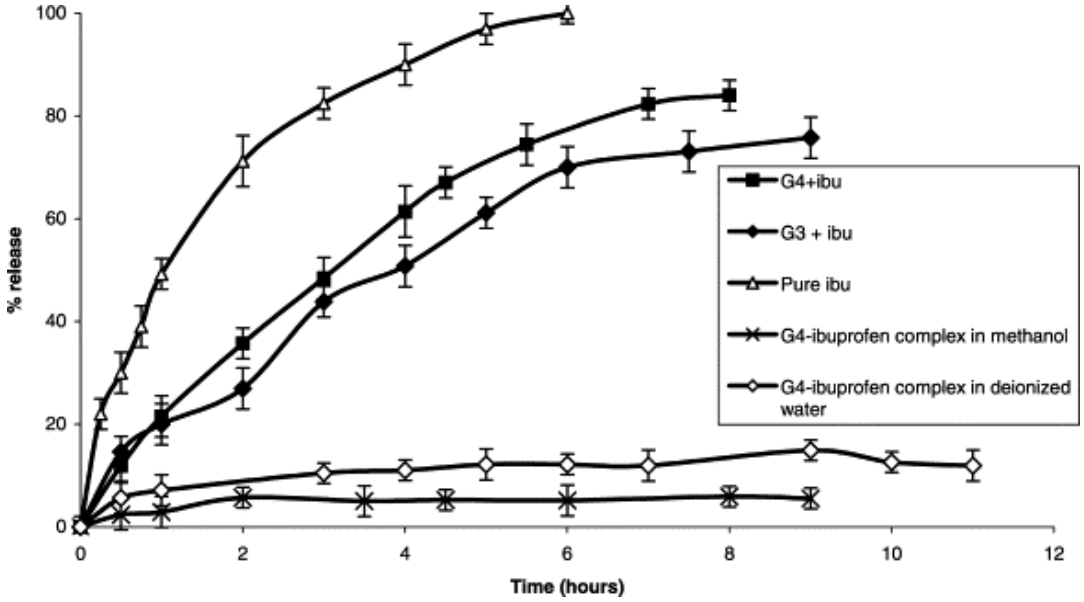

Figure 2.18 Sustained and controlled release of ibuprofen from stable complexes of ibuprofen/PAMAM (Kolhe et al. 2003)

Despite recent clinical progress in applications of dendrimers in gene and drug delivery, many challenges exist that cannot be overcome without further research innovation in designing dendritic nanostrucures.

2.4.4 Dendrimers as Nanocatalysts

Besides biomedical applications, dendrimers can be used to improve many industrial processes. The combination of high surface area and high solubility makes dendrimers useful as nanoscale catalysts. The aim is to make dendrimers function as homogeneous catalysts with faster kinetics through accessibility of the metal site dissolved in a solvent with the substrates. Their advantage is that they have large surface areas along with relatively rigid backbones which allow them to be removed from the solvent streams by ultrafitration methods (Tomalia et al. 1994). Figure 2.19 shows a comparison between the catalytic activities of three different polymeric structural configurations. Classical polymers have exerted tremendous influences on the field of chemical reaction catalysis. They are considered to be less corrosive, more stable, active, and selective than their mononuclear counter parts. Cross-linked polymers have an important advantage over linear polymers. Some linear polymers are notsoluble with the catalyst allowing for heterogeneous catalysis and thus, can be easily separated by filtration from the product reaction mixture. However, a major downside is that the reactions take place on the interior surface of the porous material which may result in counter resistance to the mass transport of the particles. It is believed that some dendritic properties, listed below, will provide a solution to the problems faced with polymer catalyzed reactions. Some of those properties and advantages include (Tomalia et al. 1994): 1) persistent and controllable nanoscale dimensions (1-100nm); 2) controlled shape design based on the choice of the core unit; 3) precise and monodisperse molecular weight (PDI≈1.0005); 4) chemically reactive surfaces; 5) specifically designed interiors that can contain hydrolytically or thermally demanding reactions; and finally, 6) designed dendrimers that can solubilise either hydrophobic or hydrophilic solvent types.

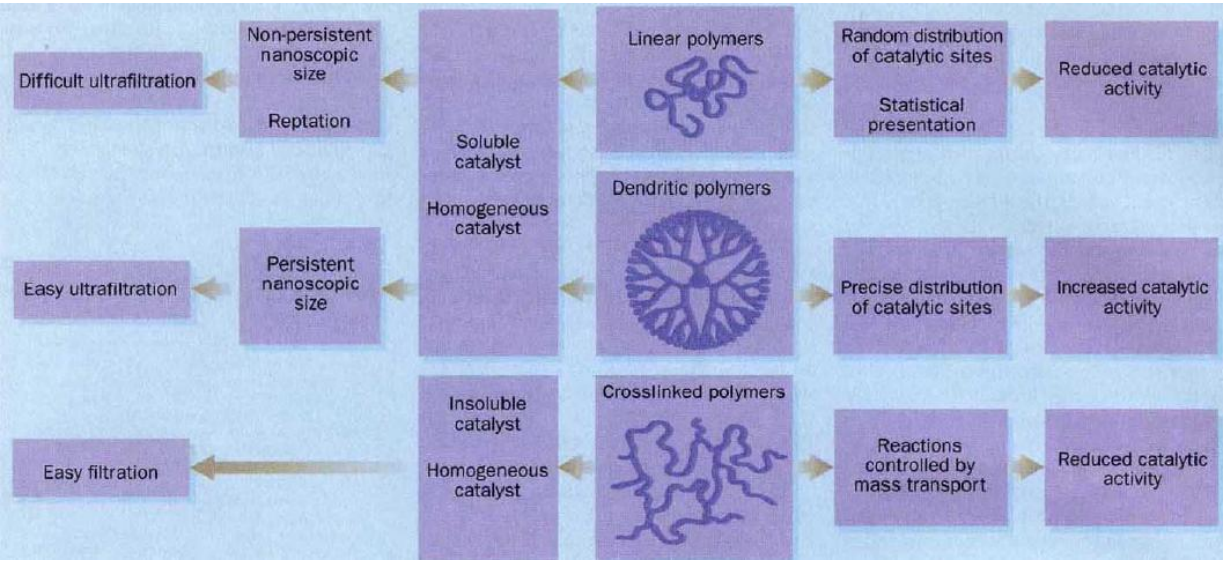

Figure 2.19 Comparison between catalytic properties of three different polymeric structures
(picture taken from Tomalia 1994)

In general, the properties of a homogeneous polymeric catalyst is determined by the physical and chemical properties of the catalytic sites, the distribution of these sites along the polymer backbone, and finally by the accessibility of these sites to the reaction substrates. Some of these factors are governed by the polymer chain and its configuration under given reaction conditions. Knapen et al. have prepared a soluble polycarbosilane dendrimer with amino arylnickel (II) complexes presented as precisely ordered groups on the surface of the nanoscale scaffold (Knapen et al. 1994). These polysilane dendrimers are highly branched macromolecules and could be functionalized at their periphery with metal-containing catalytically active sites. They showed that they can be employed as homogeneous catalysts with regio-specific catalytic activity for Kharasch addition reaction of polyhalogenoalkanes to carbon-carbon double bonds. They also argued that it is possible to remove the nanoscale catalysts from the solution of products using filtration techniques and thus providing us with a heterogeneous process advantage.

2.4.5 PEGylation of PAMAM dendrimers

PEGylation was first introduced by Davis et al. in 1970s with the objective of improving the properties of therapeutic drugs and proteins (Harris et al. 2003).Usually, PEGylation is a term describing the conjugation of poly (ethylene glycol) onto another chemical compounds to improve the properties of the conjugated molecules. It has been used for several years in order to design long circulating drug carriers. In addition, it is thought that problems such as drug leakage, stability and hemolytic toxicity could be overcome by PEGylation (Gupta et al., 2006).

Occurrence as unimolecular micelles:

PEGylated PAMAM dendrimers have similar characteristics as micelles. They have been proposed as unimolecular micelles as they exhibit both polar and non-polar properties. Studies on the encapsulation of drugs with PEGylated PAMAM dendrimers demonstrated an enhancement in the solubility and entrapment of drugs. In one study, Kojima et al. synthesized PAMAM dendrimers having PEG grafts and studied their ability to encapsulate two anticancer drugs: adriamycin (ADR) and methotrexate (MTX). Methylated PEG with average molecular weights of 550 and 2000 Da were attached to the end groups of 3G (Generation) and 4G PAMAM dendrimers (Kojima, et al. 2000). ADR was found to be encapsulated in the M-PEG attached to 3G and 4G PAMAM dendrimers. The study revealed the contribution of both dendrimer and PEG chains. Table 2.3 shows the results of the maximum number of ADR molecules per dendrimer.

Product	M-PEG (550)-3G	M-PEG (2000)-3G	M-PEG (550)-4G	M-PEG (2000)-4G
Number of ADR molecules / dendrimer	**1.2**	**1.3**	**1.6**	**6.5**

Table 2.3 Maximum number of ADR molecules per dendrimers for different synthesized products (Kojima, et al. 2000)

It was clearly demonstrated that by increasing both the generations of the dendrimers and the molecular weight of PEG attached, the encapsulation efficiency increased. The other drug that was studied was MTX, which differs from ADR due to its acidic nature. Similarly, the results showed an increase of encapsulation with increase of generation (Kojima, et al. 2000) .

2.5 Rodlike cellulose micro crystallites

Inspired by the growing environmental issues, there is a major interest in finding new materials that are biodegradable and environmental friendly (Azizi el al., 2005). Therefore, materials derived from natural resources have attracted a lot of interest in the industrial and scientific communities. Preparation of novel bio-nanocomposites, such as nanocrystalline cellulose, based on biopolymers has drawn specific attention. It is expected that these types of nanocomposites will open new areas for medical, packaging and electronic applications. Cellulose is the most common organic compound on earth. This renewable natural polymer is present in plants and algae. Cellulose of the tunicin type forms a shell of certain marine creatures and it is also synthesized by some microorganisms. Figure 2.20 shows a micrograph of a cellulose fiber, which is basically a linear; stereo-regular polysaccharide built from D- Glucose pyranose units liked by 1, 4-β glycoside bonds (Ioelovich, 2008). Generally, cellulose samples are extracted from wood which undergo mechanical treatments to yield wood flakes. Further

chemical processes, such as cooking and bleaching produces the so-called cellulose pulp which has elementary fibrils and two distinct regions: a distorted amorphous region, and a crystalline region as shown in Figure 2.21. Under steam explosion and acid hydrolysis, cellulose pulp is converted to rigid micro sized microcrystalline cellulose (MCC), which upon further acid hydrolysis produces cellulose whiskers (Ioelovich et al. 2008, Battista et al. 1956).

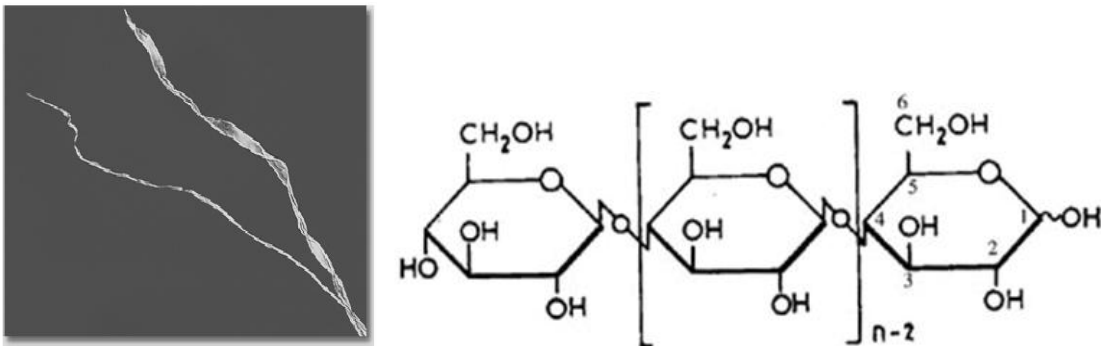

a) **b)**

Figure 2.20 a- Twisted cellulose microfibrils taken from cotton samples.
b- Molecular structure of cellulose (Ioelovich et al. 2008)

Along with its unique dimensions, cellulose possesses a special structure having three walls making up a 4-6 μm wall thickness. The primary and secondary wall are quite thin with a thickness of 2 μm and an average length of 100 nm, whereas the tertiary wall has multiple layers. Table 2.4 shows the sizes of a list of naturally occurring or synthesized cellulose products.

It is difficult to characterize the size of cellulose nanowhisker dispersions. This is because both the matrix and reinforcement are soft, light and non-conductive materials. However, due to their significant importance, many techniques and instruments have been developed for measuring the length and diameter of these polymers.

Source	L (nm)	d (nm)	technique
Bacterial	100- 1000	10-50	TEM
Cotton	100-150	5-10	TEM
	200-300	8	E-SEM
MCC	~500	10	AFM
ramie	50-150	5-10	TEM
sisal	100-500	3-5	TEM
tunicate	1160	16	DDL
	100- 1000	15-30	TEM
Valonia	>1000	10-20	TEM
Wood	100-300	3-5	AFM

Table 2.4 Experimentally measured dimensions of several naturally obtained Nanocomposites (Habibi et al., 2010)

The main advantages of cellulose in our daily applications are: 1) renewable nature, 2) wide variety of fillers available throughout the world, 3) non-food agricultural based economy, 4) low energy consumption, 5) low cost, 6) low density, 7) high specific strength and modulus (Favier et al., 1997), 8) high sound attenuation of lingo-cellulosic based composites (Azizi et al., 2005), 9) comparatively easy processability due to their nonabrasive nature (Siqueria et al., 2009) which allows high filling levels resulting in significant cost savings, and finally, 10) relatively reactive surfaces which can be used for grafting specific groups (Azizi et al., 2005). At the same time, because nanocellulose is harmless to human, biocompatible, and quite stable, it could have various uses in health care applications, such as personal hygiene products, cosmetics, and

biomedicine. One of the simplest applications of nanocellulose dispersions is its use to stabilize medical suspensions against phase separation and sedimentation of heavy ingredients. It was proven that chemically modified cellulose can be a promising carrier for the immobilization of enzymes and drugs (Ioelovich et al., 2008). The crystallinity and dimensions of these crystallites depend on the origin of the cellulose fibers. For the cotton whiskers, electron microscopy gives averaged dimensions of about 10-15 nm in diameter and 250-300 nm in length and about 15 nm in diameter, and 2000 nm in length for the tunicate (De Souza et al., 2002).

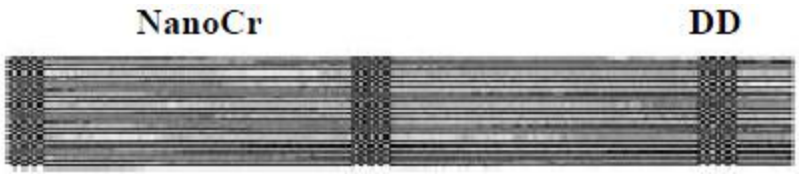

Figure 2.21 Cellulose Nanofibril: NanoCr-nanocrystallite. DD-disordered domain (Ioelovich 2008)

Cellulose rod-like whiskers are known to possess anisotropic character, that is, they are directionally dependent in both shape and optical properties. This property makes them suitable candidates for studying by dynamic depolarized light scattering (DDLS). This technique is quite powerful in determining the dynamic properties of the microcrystallites namely, the translational and rotational diffusion coefficients (D_t in m^2/s and Θ in s^{-1} respectively). Among different characterization techniques, microscopy is currently the most popular technique for estimating the aspect ratio (Length/diameter) (Kvien et al., 2005). However, it is pertinent that accurate dimensions of the whiskers could be determined as they are important parameters for mechanical modeling where cellulose is used as a reinforcing phase in polymeric matrix composites. Terech and co-workers (Terech et al., 1999) have conducted experimental measurements on cellulose monocrystalline rods with an average length of 1 μm using small-angle scattering technique (neutron and X-rays). The cross-sectional morphology was found to have a radius of 88 A^o. Their neutron scattering intensity, Q, was also measured and was found to have no influence on

the shape of the scattering curves, even at low Q and so there is no significant concentration-dependence on the aggregation process. Van Der Zande and co-workers (Van Der Zande et al., 2000) performed the characterization of gold nano-rods using dynamic light scattering and electrophoresis techniques. They found that the average length of the gold particles ranges between 390 and 730 nm, and the diameter was approximately 17 nm. The experimentally and theoretically calculated dynamics of the gold nano-rods (using modified version of Broersma models) showed better agreement when poly (vinyl pyrrolidone) (PVP) adsorption layers were included in the theoretical calculations. One significant aspect of their study is that comparisons were made between experimental and theoretical values that suggested that theoretical modeling can provide a good insight on the characteristics of the nanostructures. However, a detailed explanation of these theoretical models was not provided. Soon after, De Souza and co workers (De Souza et al., 2002, 2003) used similar techniques to determine the dynamic properties of fractionated microcrystal cellulose whiskers utilizing elastic and quasi-elastic light scattering techniques. It was noted that effective diffusion coefficient ($D_t = \Gamma (q)/q^2$) was inversely proportional to the structure factor S (q), which is directly related to the dimensions of the cellulose. In addition, the results showed that the mobility M (q) is independent of q (scattering angle) according to the general Ferrel-Kawasaki expression for the apparent diffusion coefficient. This result has often been seen in other whiskers where the mobility has minimal dependency to its scattering angle. At high q values the diffusion is dominated by D_t and D_{rot} (Θ), which are the only motions capable of modulating the intensity when the rods are oriented nearly perpendicular to q^6. The same group also conducted a study on the dynamics and dimensions of cellulose whiskers using similar techniques in addition to using electric birefringence (TEB). Using their experimentally calculated dynamics with $D_t = 5.5 \times 10^{-8}$ cm^2/s,

Θ_{DDLS} =552 s^{-1}, and Θ_{TEB} =536/s (De Souza et al.; 2003) and the full version of Broersma's relations (Broersma 1960, 1967, 1981), the rotational and translational diffusion coefficients produced dimensional values with length equal to 255 nm and cross-section diameters of 15 nm which are very close to the experimentally obtained values. These and other experimentally and theoretically calculated parameters provided a good understanding on how dynamic parameters could result in reasonable structural analysis of rod-like whiskers.

Previously, the simulation techniques focused on the molecular mechanics (MM) approach to model microcrystalline cellulose structures and their interactions with other molecules, such as water (Mathews et al., 2006) They demonstrated that the surface of microcrystalline cellulose is highly structured with water. Their simulation also revealed that the primary mechanism for this structuring is direct hydrogen bonding. The first layer of cellulose localizes the water molecules that are hydrogen bonded to the cellulose surface. Other simulation methods use the Halpin-Kardos theoretical mean field mechanical model to predict the elastic modulus of short-fiber composites (Azizi et al., 2005). Despite this fact, very little parameter estimation techniques were adopted for the purpose of calculating the dimensions or dynamics of cellulose mycrocrystallites. Those parameters are of significant importance for the further processing of cellulose particularly, as reinforcing polymer matrices. Most of the recent publications focused on using microscopy techniques such as SEM and TEM for determining dimensional properties, and light scattering for dynamic properties. In our study we used built in MatLab functions having a specific optimization routine to attempt in calculating those parameters.

Chapter 3.0 Materials and Methodology

In this chapter, the detailed cationic polymerization adopted for synthesis of poly (2-alkyl 2-oxazoline) and its subsequent hydrolysis to poly (ethylenimine) is presented. The PEG-PAMAM dendrimers were used as previously synthesized by Lim using Michael addition synthesis approach (Lim, 2008). Later a brief theoretical background on experimental and instrumental characterization techniques is discussed followed by a description of the theoretical modeling and simulation methods utilized for the parameter estimation problem.

3.1 Materials

2-Methyl-2-oxazoline was purchased from Aldrich Co. and distilled over calcium hydride. Poly (2-ethyl-2-oxazoline) was supplied by Aldrich Co. and vacuumed distilled over calcium hydride using regular vacuum distillation apparatus. Methyl tosylate (MeOTs), α-CD and acetonitrile were purchased from Aldrich Co. Methyl Tosylate was recrystallized from n-hexanes. Organic solvents were purified by usual distillation methods. The other synthetic reagents were used as received without further purification. Deionized water was provided by Milipore Alpha-Q purification system equipped with a 0.22 micron filter.

3.2 PEI Synthesis

Homopolymeric PEI with NH_2 end groups and various molecular weights was synthesized following procedure as described elsewhere (Choi, et al. 2004). The variation of molecular weights can be achieved by changing the molar ratio of the initiator (MeOTs) to the monomer (2-alkyl 2-oxazoline).

PMOz and PEI synthesis

A representative example of the synthesis of poly (2-methyl-2-oxazoline) with molecular weight 3200 g/mol was performed according to the following protocols: In a 50ml dry schlenk flask, 2-methyl-2-oxazoline (0.25 g) and methyl tosylate (0.0074 g) were mixed. In another flask, acetonitrile (15 mL) was bubbled with argon for 10 minutes and transferred via a syringe to the 50 ml schlenk flask. The mixture was then heated to 70 °C under gentle stirring with initial argon purging for ~ 2 hrs. After 48 h, the reaction was cooled to 0 °C, and a methanol solution of ammonia (0.03 mol) was added to the reaction mixture under nitrogen, and the solution was stirred at room temperature for 3 h. This step insures the termination of the reaction and the insertion of NH_2 groups in the terminal chain of the polymer. Then the solvent was removed under reduced pressure, and the residue was dissolved in a mixture of distilled water (250 mL) and concentrated hydrochloric acid (400 mL). The reaction solution was precipitated into cold diethyl ether. The crude polymer was dissolved in methylene chloride, washed twice with a saturated aqueous $NaHCO_3$ (100 mL), and then washed with distilled water (100 mL) using liquid-liquid extraction method. After the organic layer was dried over anhydrous magnesium sulphate, the polymer was then isolated by precipitation into cold diethyl ether, and dried in a desiccator over night to yield yellow (brittle, and very hygroscopic) PMOz crystals. ^{1}H NMR ($CDCl_3$) (Fig. 3.3): ^{1}H NMR (D2O): δ 2.15 (m, -COCH3), 3.38 (s br,-CH_2CH_2- of OZ). The other peaks were assigned to solvent peaks which were removed after extensive dialysis, multiple precipitations, and placing the PMOz crystals in vacuum oven for 24 hrs.

Later, the PMOz product was dissolved in excess amount of water and concentrated hydrochloric acid. The mixture was refluxed for 48 h with vigorous stirring at ~ 100 ^{o}C. The solution was

then removed from the reactor flask and sodium hydroxide was added to the mixture at 0 °C until the solution became slightly basic. The resulting precipitates were collected by filtration and washed several times with water until the filtrate became neutral. The residue was dried in vacuum at 60 °C for 48 h to yield the homopolymeric PEI quantitatively. ^{1}H NMR (D_2O) (fig 3.4): δ 2.50 (s, -CH_2CH_2NH-). (Presat D_2O removes the D_2O peak). Figures 3.1 and 3.2 below shows a schematic diagram for the above synthesis.

Figure 3.1 Cationic polymerization of 2-methyl-2-oxazoline.

Figure 3.2 Acid Hydrolysis of PMOz yielding Homopolymeric PEI

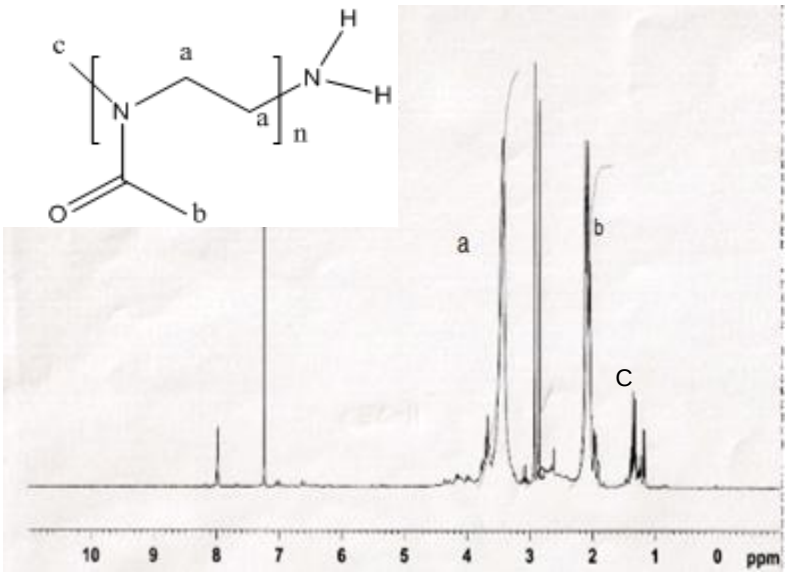

Figure 3.3 ^{1}H NMR of PMOz

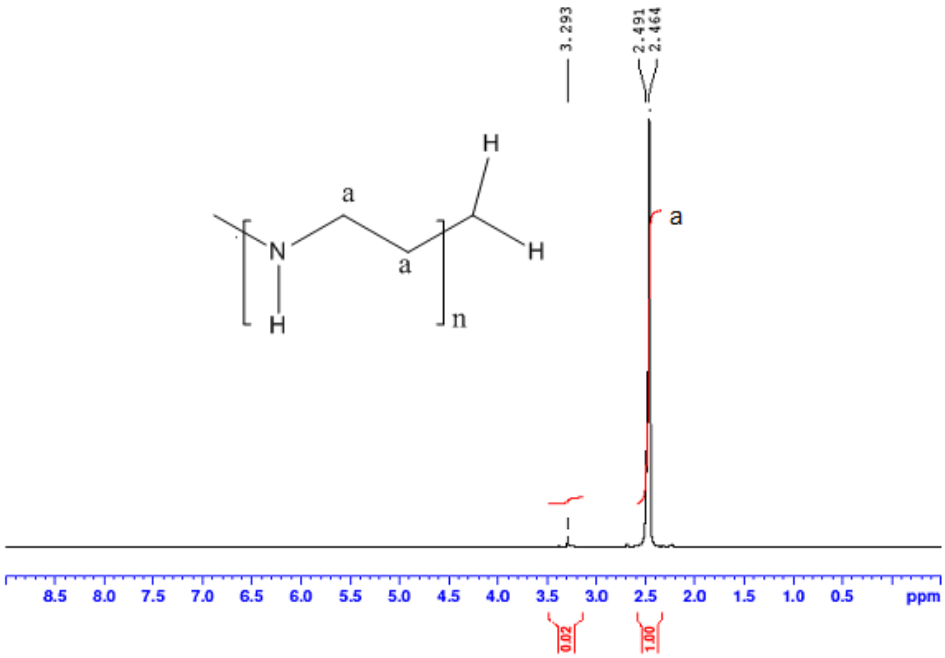

Figure 3.4 ^{1}H NMR of PEI

3.3 Synthesis of α-CD/polymer complexes

The synthesis of α-CD/polymer complexes involves direct mixing a prepared α-CD and polymer solution. For investigating the complexation between PEIs and α-CD, a solution of ~ 0.15 wt% of PEI was prepared in water at an initial basic pH (pH =10). Then predetermined amount of α-CD solutions (15-17 mM) were added slowly to the solution with initial stirring for 10 min. After consecutive heating and cooling, the solution turned turbid indicating the initiation of complexation. Then the pH of the mixtures was adjusted from 3.0 to 13.0 by adding HCl or NaOH solution, followed by stirring for another 60 min at 60 °C. At pH below 6, the solutions appeared clear even after consecutive heating and cooling. At pH values > 7, cooling the solutions to room temperature induce the formation of a turbid solution. Furthermore, the hydrogels produced were slowly heated again with continuous stirring. With gradual decrease in the solution temperature to 20 °C, the transparent mixtures turned turbid. Repeated heating and cooling processes induced further inclusion and precipitates in the end, which were collected by centrifugation and then washed with distilled water to remove the free PEIs and uncomplexed CDs. The resulting products were distilled to remove any impurities in the system and subsequently freeze dried to obtain pure powdered polypseudorotaxanes. A discussion and analysis of the turbidity and ITC result at different pH values will be presented in Chapter 4. The synthesis of PEGylated-PAMAM / α-CD complexes was done in a procedure similar to the one described above.

3.4 Background on Instrumental Characterizations

The characterization of the synthesized polymeric systems, and the binding between / α-CD and PEI & PEGylated PAMAM was performed using various analytical instruments including ^{1}H NMR, ITC, DLS/SLS, UV-VIS and zeta potential analyser. In this section we shall present the strategy adopted, the technique utilized and a brief background on the theory of these instruments.

3.4.1 Hydrogen Neutron Magnetic Resonance Spectroscopy (^{1}H NMR)

^{1}H NMR spectrum was characterized by chemical shifts ranging from +12 to -4 ppm and by spin-spin couplings between protons. The integration curve of each peak in the spectrum reflects the abundance of individual protons. Therefore, ^{1}H NMR spectrum is not only used to study the molecular structure of the synthesized polymer, but also to give a quantitative estimation of the molecular weight of the polymer chains. ^{1}H NMR spectrum was conducted on a Bruker Bio Spin 400 MHz spectrometer. Tetramethylsilane (TMS) was used as the reference compound. 0.1% weight percent of different samples were prepared and compared relative to internal $CHCL_3$ for $CDCL_3$ solution. Other proton chemical shifts were recorded relative to internal HOD for D_2O solution. These deuterated solutions were obtained from Sigma Aldrich with 99.9% purity. The chemical shifts of D_2O and $CDCL_3$ are 4.790 ppm and 7.260 ppm respectively.

To understand the theory behind NMR one has to look at the relation between energy of different states, the magnetic field applied and the frequency. The presence of an applied external magnetic field will induce nuclei that exist in two nuclear spin states of different energy. Slightly more than half of the nuclei exist in the lower energy state called alpha (α) than in the higher

energy state called beta (β). The external magnetic field Bo, which is homogeneous, is created with a large magnet, commonly a super-conducting solenoid (University Tutorial, 2003). The energy difference E between the spin states is proportional to the strength of Bo (figure 3.5). A typical Bo field is 7.05 T (Tesla) or 70,500 Gauss. NMR spectroscopy records transitions between these spin states induced by a radio frequency electromagnetic field called the B1 field. Figure 3.6 shows a typical NMR instrumental setup.

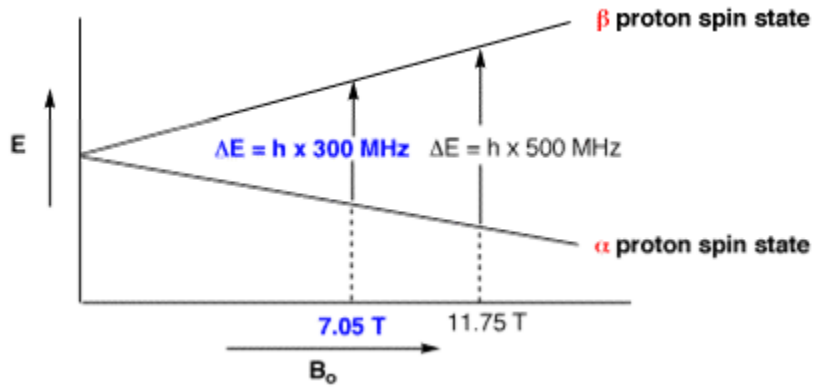

Figure 3.5 Relation between Bo (magnetic field) and frequency (v) or the energy ΔE = h ν (University Tutorial, 2003)

Figure 3.6 ^{1}H NMR set up (http://orgchem.colorado.edu/hndbksupport/nmrtheory/NMRtutorial.html)

3.4.2 Measurement of binding using ITC

Binding Isotherm

The calorimetric experiments were carried out using the Microcal isothermal titration calorimeter (Northampton, MA). This power compensation differential instrument was previously described in detail by Wiseman et al. (Wiseman, et al. 1989). It has a reference cell and a sample cell of approximately 1.45 mL, which are both insulated by an adiabatic shield. The titration was carried out by stepwise injections of different α-CD aqueous solution (20, 40, 60, 70, 80, 90 and 120mM) at various pH values from a 250 μL injection syringe into the sample cell filled with 0.1 wt % of PEGylated-PAMAM. Later, investigation on salt effect was carried out over a constant pH value and α-CD concentration. The syringe is tailor-made such that the tip acts as a blade-type stirrer to ensure an optimum mixing efficiency at 400 rpm. All measurements were carried out at a constant temperature of 25.0°C calorimetric data were processed by the computer program Origin for ITC.

ITC is a powerful technique since it directly measures the heat change associated with binding. ITC technique combines thermo-chemical and analytical applications. When substances interact, heat is either generated (exothermic) or absorbed (endothermic). The enthalpy change of a chemical reaction is a function of the amount of titrant added into the reaction cell. Measurement of this heat allows accurate determination of binding affinity (K), change in enthalpy (ΔH) and change in entropy (ΔS), thereby providing a complete thermodynamic profile of the molecular interaction in a single experiment:

$\Delta G = -RT \ln K = \Delta H - T\Delta S$ **Equation 3.1**

Figure 3.7 (b) shows a schematic drawing of ITC. Both the sample cell and the reaction cell are insulated by an adiabatic shield. A thermoelectric device measures the temperature difference, ΔT_1 and ΔT_2. Using the Cell Feedback system the instrument will be able to keep ΔT_1 constant

(baseline) by the addition or removal of heat from the sample cell. The integral of the power to maintain ΔT_1 constant over time is an indicated measurement of total heat resulting from the binding interaction (Figure 3.7a) (VP-ITC Instruction Manual. 2001). The top graph in Figure 3.7-a represents the heat released for each injection. After integrating of the area of each injection we obtain the complete binding isotherm as shown in the bottom panel.

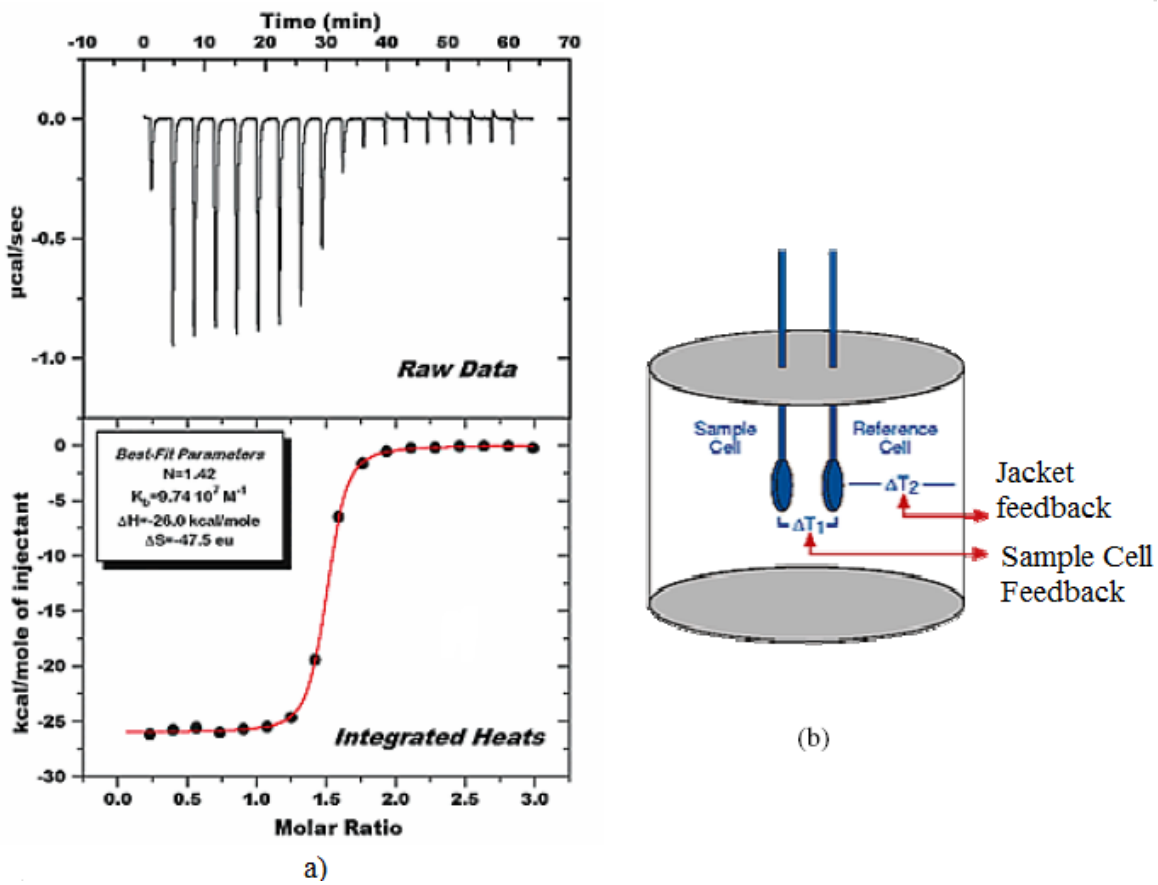

Figure 3.7 a) Heat evolved of an ITC data, b) ITC feedback system
(VP-ITC Instruction Manual. 2001)

One Binding Site Model

The ITC data were fitted with a one binding site model using MicroCal Origin analysis software. The equilibrium constant K defined by:

$K = \frac{[\text{dendrimer} \bullet \text{CD}]}{[CD][\text{dendrimer}]}$, where dendrimer represents the concentration of PEGylated PAMAM dendrimer, and CD is the concentration of α-CD (Zheng, et al. 2005).

The equilibrium constant K can be expressed as:

$$K = \frac{[\text{dendrimer}]_0 \Theta}{[\text{dendrimer}]_0 (1-\Theta)[CD]} = \frac{\Theta}{(1-\Theta)[CD]}$$

and **Equation 3.2**

$$\Theta = \frac{[\text{dendrimer} \bullet \text{CD}]}{[\text{dendrimer}_0]}$$

where Θ is the fraction of the dendrimer groups complexed with α-CD. From the mass balance equation of CD we obtain:

$$[\text{CD}] = [\text{CD}]_0 - [\text{dendrimer}]_0 n \Theta \quad \textbf{Equation 3.3}$$

where n is the molar number of binding sites in 1 mol of dendrimer groups.

Combining Equations 3.2 and 3.3 gives (Zheng, et al. 2005):

$$\Theta^2 - \Theta\left[1 + \frac{[CD]_0}{n[dendrimer]_0} + \frac{1}{nK[dendrimer]_0}\right] + \frac{[CD]_0}{nK[dendrimer]_0} = 0 \quad \textbf{Equation 3.4}$$

The total heat Q given off in the solution is expressed as:

$$Q = [dendrimer]_0 \Theta n V_0 \Delta H \quad \textbf{Equation 3.5}$$

where ΔH is the enthalpy change of the complexation, V_0 is the total volume of the solution. Solving the quadratic equation 3.4 for Θ and then substituting it into equation 3.4 gives:

$$Q = \frac{n[dendrimer]_0 \Delta H V_0}{2} \times \left[1 + \frac{[CD]_0}{n[dendrimer]_0} + \frac{1}{n K [dendrimer]} - \sqrt{\left(1 + \frac{[CD_0]}{n[dendrimer]_0} + \frac{1}{n K [dendrimer]_0} \right)^2 - \frac{4[CD]_0}{n[dendrimer]_0}} \right]$$

Equation 3.6

After correcting the displaced volume, the calculated heat effect for the i^{th} injection is given by equation 3.7:

$$\Delta Q_i = Q_i + \frac{dV_i}{V_0}\left[\frac{Q_i + Q_{i-1}}{2}\right] - Q_{i-1} \quad \textbf{Equation 3.7}$$

Finally, the degree of saturation is defined as:

$$y_i = \frac{\Delta[CD_i]_{bound}}{[dendrimer]_{tot}} \quad \textbf{Equation 3.8}$$

According to the above equations, non linear model-fitting ("one-type-of-sites") yields n, K *and* ΔH based on a titration experiment.

This fitting process of the experimental data is described as follows (Zheng, et al. 2005):

(1) Calculate ΔQ_i for each injection and compare these values with the measured heat for each corresponding injection.

(2) Improve the initial values of n, K *and* ΔH by the standard Marquardt method.

(3) Repeat the above procedures until no further significant improvement in the fitting can be achieved.

By normalizing the molar concentration to the standard state concentration of 1 mol/L, K will turn out to be dimensionless, and the ΔG binding can be obtained from the normalized K according to the expression: $\Delta G = -RT \ln K$ (Shechter, et al. 2010), where R is the gas constant (8.3145 J/K.mol), and T is in Kelvin.

3.4.3 Morphological study using DLS and SLS

Dynamic Light Scattering (DLS):

The microstructure of the sample solutions prepared at several pH values was examined using a Brookhaven Laser Light Scattering system, which consists of a BI-200SM goniometer and a BI-9000AT digital correlator. A 636 nm helium-neon diode laser was used as the light source. Firstly samples at pH =2 were prepared by adding 5, 20, 100, 170, and 300 μL of 150 mM α-CD onto 1.5 ml of 0.1 wt % of PEGylated-PAMAM to 0.5, 2, 9, 15, and 25 mM of α-CD. Secondly, to investigate the effect of pH, different solutions of various pH values were prepared at constant α-CD concentration of 8mM and the R_h was measured. Light scattering system is a well-known powerful technique used to obtain the particle size distribution in solution based on the scattering light intensity utilizing a monochromatic laser light as the light source. This time dependent intensity fluctuation correlates to the pro perties of the scattering objects. The scattering intensity of the light is obtained from DLS based on the correlation function of dynamic variables. The average intensities, I, long observation time, T, can be expressed by equation 3.9 (Brown, et al. 1992).

$$\langle I(\theta) \rangle = \frac{1}{T} \lim_{T \to 0} \left(\int_0^T I(\theta, T) dt \right) \quad \textbf{Equation 3.9}$$

At time, t, and a decay time, τ, the intensity-intensity autocorrelation function is the average < I (t) I (t + τ) > which is a function of t. Under the ergodic theory assumption, the autocorrelation function can be expressed by equation 3.9 such as:

The so called correlation function is a necessary requirement for a proper study of the dynamic properties of the scattering system. These functions can then be transformed using Fourier transformation techniques to yield appropriate scattering spectra that contain molecular information on the dynamics of the molecules. The autocorrelation function of scattered intensity is described by equation 3.10 (Brown, et al. 1992).

$$\langle I(t)I(t+\tau)\rangle = \frac{1}{T}\lim_{T\to 0}\left(\int_0^T I(t)I(t+\tau)dt\right)$$

$$G_2(t) = \langle I(t)I(t+\tau)\rangle \qquad \textbf{Equation 3.10}$$

The normalized version of equation 3.11 is obtained when dividing by $< [I (t)]^2 >$ such as:

$$g_2(t) = \frac{\langle I(t)I(t+\tau)\rangle}{\langle I(t)^2\rangle} \qquad \textbf{Equation 3.11}$$

Where I (t) is an average value of the product of the scattered intensity at an arbitrary observation time, τ, and I (t+ τ) is the intensity at decay time, t. The other two correlation functions: field autocorrelation function, G_1 (t), and normalized field autocorrelation function, g_1 (t), are shown in equations 3.12 and 3.13 (Brown, et al. 1992).

$$G_1(t) = (G_2(t) - B)^{1/2} \qquad \textbf{Equation 3.12}$$

$$g_1(t) = \sqrt{\frac{G_2(t) - B}{B\,\beta}} \qquad \textbf{Equation 3.13}$$

B is the baseline and b is the coherence factor that is normally considered an adjustable parameter in the data analysis procedure. The dynamic structure factor, S (q,c, τ), is defined as:

$$S(q,c,\tau) = \frac{1}{N^2} \sum_{i,j=1}^{N} \exp[i\, q\, (r_i(\tau) - r_j(0))] \qquad \textbf{Equation 3.14}$$

where r_i (τ) is the position of segment i at time difference, t. The angular bracket denotes an average over the space-time distance distribution. g_1 (t) is dependent on the relaxation function as expressed in equation 3.15:

$$g_1(t) = \frac{S(q,c,\tau)}{S(q,c,0)} \qquad \textbf{Equation 3.15}$$

For a system consisting of non-interacting, homogenous, mono-disperse, spherical particles, the normalized field autocorrelation function (equation 3.16):

$$g_1(t) = \exp(-\Gamma\, t) = \exp(-\frac{t}{\tau}) \qquad \textbf{Equation 3.16}$$

where τ is the time difference of the process and Γ =1/τ is the decay rate. This decay rate is related to the translational diffusion coefficient, D and the wave factor, q such as; $\Gamma = Dq^2$ where the translational diffusion coefficient, D depends on the wave factor, $q = (4\pi n / \lambda) \sin(\theta/2)$.The estimation of the hydrodynamic radius of the particles using Stokes-Einstein Law necessitates that the particles motion show good diffusivity (spherical particles) instead of rotational (non-spherical particles). The hydrodynamic radius, R_h, can then be determined from the diffusion coefficient through the Stokes-Einstein equation:

$$R_h = \frac{kTq^2}{6\pi\eta\Gamma} \qquad \textbf{Equation 3.17}$$

Static Light Scattering (SLS)

The study of size and morphology could be further investigated using static light scattering which is a powerful technique for determining the radius of gyration, R_g, of the particles under study. Using the same procedure described in DLS, several pHs values (2, 4,6,7,8 and 9) were prepared at constant [α-CD] ~8-10mM prior to use, and the radius was measured consequently. The measured R_g was then compared to the measured R_h from DLS.

Static light scattering the angular dependency of the time-mean-intensity of laser light scattered by the particles is measured. The course of the scattered intensity as a function of the detector angle depends on size and structure of the particles. According to Rayleigh, the intensity of the scattered light depends only on the size of the particles and not on their structure or the concentration. If the intensity of the scattered light is measured in a plane orthogonal to the polarization plane of the incident light, there will be no angular distribution of the scattered light (LLS Goniometer Instruction Manual. 2008). Rayleigh developed an expression which allows one to obtain the particle size, R according to (equation 3.18):

$$R_\theta = \frac{16\pi^4 R^6 \left(\frac{n^2 - 1}{n^2 + 2}^2 \right)}{\lambda^4} \qquad \textbf{Equation 3.18}$$

R_θ is the Rayleigh ratio, n is the relative refractive index of the solute and λ is the wavelength of the incident light.

When the concentration of the solution is dilute the particle form factor denoted *P(q)* can be written as the form given in equation 3.19:

$$P(qR_g) = \frac{I(q)}{I(0)} \approx 1 - \frac{q^2 R_g^2}{3} \qquad \textbf{Equation 3.19}$$

where q is the scattering vector magnitude, which is the *independent* variable in the experimentand R_g is the so-called radius of gyration (Van Zanten, et al.1991).

It is important to mention that the "particle form" factor is always ≤ 1. This factor is the ratio of the scattering intensity at some angle to that being measured. However, the denominator, *I (*0*)*, is usually obtained by extrapolation. For a sphere of radius *R* it can be shown that

$$R_g = \sqrt{\frac{3}{5}} R = 0.775R \qquad \textbf{Equation 3.20}$$

So in summary, we can determine the R_g by measuring the intensity as a function of q (which we can vary either by angle θ or by wavelength λ). One way to do this is by constructing the Guinier plot, which uses $\ln(I(q)) = \ln(I(0)) - \frac{q^2 R_g^2}{3}$. Another method is to use the slope/intercept method where one plots *I (q)* vs. q^2 and obtains R_g from some function of slope and intercept. In our case we use the Berry plot which is presented by equation 3.21

(LLS Goniometer Instruction Manual., 2008; Van Zanten, et al. 1991):

$$\sqrt{\frac{K_c}{R(q)}} = \sqrt{\frac{1}{M_w}} \left(1 + \frac{1}{6} \langle S^2 \rangle_z q^2 \pm .....\right) \qquad \textbf{Equation 3.21}$$

By extrapolating q $\rightarrow 0$, we can obtain the slope, $\langle S^2 \rangle_z$ and the ordinate section, M_w.

3.4.4 Measurement of phase separation using UV-Vis

The stability of the solution was determined based on the occurrence of phase separation in the solution by conducting a transmittance measurement using UV/Vis spectroscopy. Basically, this instrument measures the intensity of light passing through a sample (I), and compares it to the intensity of light before it passed through the sample (I_0). Initially the intensity of light (I_0) passing through a blank was measured. The blank was prepared in a cuvette using the same sample solvent, water and in the absence of solute particles. Then, the intensity of light (I) passing through the sample solution was measured and expressed as the ratio (I/I_0). This corresponds to the transmittance and is usually expressed as a percentage. UV/VIS spectroscopy involves the study on electromagnetic spectra within the visible, near-ultraviolet and near-infrared wavelengths. A spectrophotometer is used to measure the light intensity based on the function of color or wavelength of light. More light will be absorbed by the sample if the compound is more concentrated. The instrument operates by passing a beam of light through a sample and measuring the intensity of light reaching a detector. The beam of light consists of a stream of photons. When a photon encounters an analyte molecule (the analyte is the molecule being studied), there is a chance that the analyte will absorb the photon. This absorption reduces the number of photons in the beam of light, thereby reducing the intensity of the light beam. Using Beer-Lambert law, it is possible to relate the absorption of light to the properties of the material through which the light traverses. As shown in Equation 3.22 and Figure 3.8, the absorbance will vary linearly with concentration:

$$A = \alpha\, l\, \mathrm{c}$$

$$\mathrm{T} = I / I_o = 10^{-A} = 10^{-\frac{\alpha}{c}} \qquad \textbf{Equation 3.22}$$

α is the absorption coefficient of the absorber, l is the path length and c is the concentration of the sample.

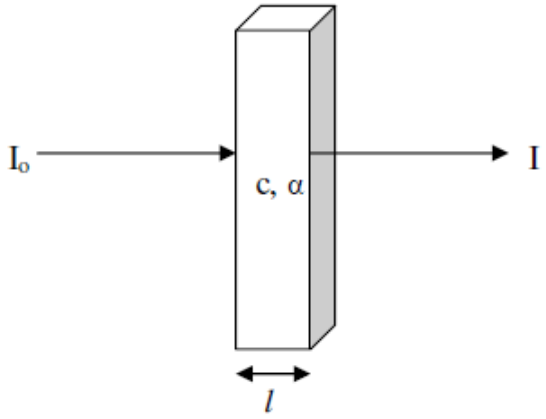

Figure 3.8 Schematic diagram showing absorption of sample in cuvette in UV-Vis spectroscopy.

For phase separation studies, the transmittance can be obtained my measuring the transmittance, T, instead of the absorbance A as seen from Equation 3.22.

3.4.5 Measurement of particle mobility using zeta potential

Zeta potential measurement was conducted with the Brookhaven Zeta PALS (phase analyzer light scattering), which measures the mobility of moving particles using the technique of laser Doppler anemometry. The zeta potential was estimated from the Smoluchowski model fitting of the mobility data. Experiment was conducted in a disposable cuvette consisting of 1.5 ml solution of 0.1 wt% of PEGylated PAMAM solution which was adjusted at various pH values. Zeta potential is the electrical potential of the slipping plane in the double layer as illustrated in figure 3.9.

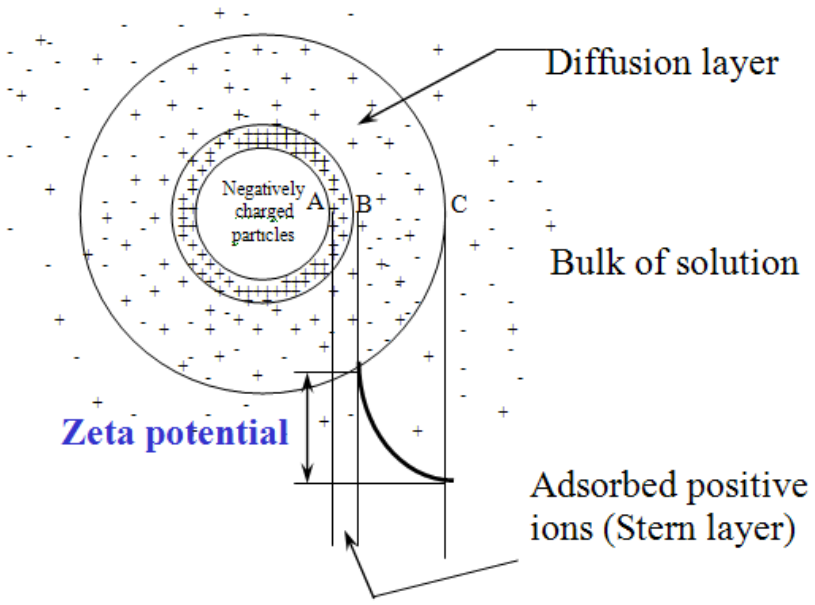

Figure 3.9 Double layer of a particle (Malvern 2008)

The inner layer is the stern layer, which is formed by oppositely charged ions that bind strongly on the surface of the particles while the second layer is the diffusive layer consisting of diffusive ions in the fluid (Malvern 2008). Generally, particles are said to carry a negative electrostatic surface charge. Positive ions in the solution are attracted to the negatively charged surface where they may be strongly adsorbed. The Stern layer and diffuse layer are called double layers. They are important in determining forces between colloidal particles. The Zeta Potential is the difference between the charge at the edge of the Stern layer and the bulk of the suspending liquid as shown in Figure 3.9. Zeta potential can be measured by tracking the moving rate of a negatively or positively charged particle across an electric field (Equation 3.23). Usually a value less than -15m V represents the onset of agglomeration. Values greater than -30mV generally signifies that there is sufficient mutual repulsion which result in colloidal stability (i.e. no aggloremation).

$$\nu = \mu_e E \qquad \textbf{Equation 3.23}$$

By using Smoluchowski and Huckel theories, the particle mobility is converted to zeta potential, ζ using equation 3.24:

$$\xi = \frac{3\eta\mu_e}{2\varepsilon f(ka)} \qquad \textbf{Equation 3.24}$$

where η is the dynamic viscosity of solvent (Pa.s), μ_e is the electrophoresis mobility ($m^2s^{-1}V^{-1}$), and ε, is the dielectric constant of dispersion medium. $f(ka)$, is the Henry's function, which itself is a function of k, the inverse of the Debye Length (thickness of the electric double layer), and a, is the particle radius. Thus, the product, ka, represents some properties of the electric double layer. When the electric double layer is thin (ka >1), the Smoluchowski approximation is used and Henry's function is taken as 1.5, thus simplifying the equation to $\xi = \frac{\eta\mu_e}{\varepsilon}$.

3.5 Modeling and Simulation of Rod like whiskers

The theoretical development to describe the dynamics of nan-orods was advanced by Broersma and co-workers (Broersma et al. 1960 and 1981) where the relationship between the translational and rotational diffusion coefficients were correlated to the dimensional parameters of nano-rods of a given aspect ratio (L/d). To understand these equations, we need to look at the atomic-level of the particles and to the forces that govern their movement within the aqueous media. Initially, O'Konski and Haltner were able to measure the rotational diffusion constant $D_{r,}$ of a monomeric unit of Tobacco Mosaic Virus (TMV) in water. Theoretically speaking, the rotational coefficient is related to the Burgers' torque constant of a cylinder given by:

$$T/\omega = \frac{8\pi\eta a^3}{3}\left[\log(2a/b) - 0.80\right], \qquad \textbf{Equation 3.25}$$

where ω the angular velocity, b is the half width of the particles, and η is the viscosity of the solvent·

From this equation, one can observe and infer that a proportional relationship exists between torque and angular velocity of a rotating sphere or cylinder shaped rod, and so it is consistent with the theory that the frictional viscous torque is proportional to the angular velocity to the first power. This ratio is directly related to the rotational diffusion coefficient D_r (with units of radians^2/s). It is given by the angular drift velocity $\Omega_d = (d\theta / dt)$ in response to an external torque Γ_θ i.e. T (assuming that the flow stays non-turbulent and that inertial effects can be neglected). The relationship between the rotational diffusion coefficient and the rotational frictional drag coefficient was derived by the Einstein relation (or Einstein–Smoluchowski relation):

$D_r = \frac{k_B T}{f_r}$ and $f_r = 8\pi\eta a^3$ f_r being the drag force, k_B as Boltzmann constant and T the absolute temperature.

The derivation of the translational diffusion coefficient is analogous to the above D_r equations. Therefore, using those equations, Broersma derived both the rotational and translational diffusion coefficients with the dimensions of any cylindrical macromolecule (rod-like particles) such as Equation 3.26 (Broersma; 1960, 1981):

$$\textit{Translational Diffusion: } D_t = \frac{k_b T}{3\pi\eta L}\left[\delta - \frac{1}{2}\gamma_{\mathrm{II}} - \frac{1}{2}\gamma_{\perp}\right] \text{ where } \delta = \ln(2L/d)$$

$$\gamma_{II} = 0.807 + \frac{0.15}{\delta} + \frac{13.5}{\delta^2} - \frac{37}{\delta^3} + \frac{22}{\delta^4}$$

$$\gamma_{\perp} = -0.193 + \frac{0.15}{\delta} + \frac{8.1}{\delta^2} - \frac{18}{\delta^3} + \frac{9}{\delta^4}$$

Equation 3.26

$$\textit{Rotational Diffusion: } \quad D_\theta = \Theta = \frac{3k_b T}{\pi\eta L^3}\left[\delta - \rho\right]$$

$$\rho = 1.140 + \frac{0.2}{\delta} + \frac{16}{\delta^2} - \frac{63}{\delta^3} + \frac{62}{\delta^4}$$

The adopted mathematical technique calculates the force distribution in a moving object that produces a certain velocity at its surface, so that once the force density is known, the torque can be calculated and thus the diffusion coefficient can be deduced. The high order polynomials come from the force expansion factor which is originally described by equation 3.27:

$$\upsilon(x) = \sum_{n=0,1}^{\infty}(x/a)^n \sum_{k=0,1}^{\infty}(c_n)(B_k) \qquad \textit{while having } \sigma = \ln(\frac{2a}{b})$$

$$\textit{resulting in coefficients } c_{kk} = 2\sigma + 1 - \sum_{l=1,2}^{k}\frac{2}{l}$$

Equation 3.27

$$c_{kn} = \frac{2}{k-n}$$

Table 1 shows the values of the coefficients as calculated by Broersma for a rod-like cylinder rotating or translating perpendicularly or parallel to the axis of the cylinder. Those factors are based on the theoretical calculation of the final version of the γ expansion given by:

$\gamma = \sum_k a_k \sigma^{-k}$ where $\sigma = \log\frac{2a}{b}$. They would provide more accuracy to the calculated force; however an analytical determination of polynomial to the fifth order becomes mathematically difficult.

	a_o	a_1	a_2	a_3	a_4
Rotational $\perp$	1.140	0.200	16	-63	62
Translational $\perp$	-0.193	0.15	8.1	-18	9
Translational $\uparrow\uparrow$	0.807	0.15	13.5	-37	22

Table 3.1 Translation and Diffusional Coefficients as calculated by Broersma Force expansion factors (De Souza et al, 2003).

Thus the final version of the expansion coefficients will be:

$$\gamma = a_0\sigma^{-1} + a_0\sigma^{-2} + a_0\sigma^{-3} + a_0\sigma^{-4} \qquad \textbf{Equation 3.28}$$

It has to be noted that the calculation of the rotational diffusion coefficient is less accurate than the translational coefficient because of the $1/L^3$ factor which produces a more sensitive θ measurement. As will become apparent, this may result in the instability of some of the calculated values produced by this specific function. Garcia et al. [16] calculated and developed alternative coefficients that possessed a second order polynomial instead of the fourth order. In addition, only one of the expansion factors is considered (Equation 3.29). Their model also serves to predict the translational diffusion coefficient, D_t, for rods with Brownian motion and a finite L/d. Unfortunately, the form of their equations produces significant instabilities in the calculated rotational diffusion coefficient (D_r / θ) values:

$$D_t = (k_bT)/(3\pi\eta L)\left[\delta + 0.312 + 0.565\lambda + 0.100\lambda^2\right]$$
$$D_r = \Theta = (3k_bT)/(\pi\eta L^3)\left[\delta - 0.662 + 0.917\lambda - 0.050\lambda^2\right] \qquad \textbf{Equation 3.29}$$
$$where \rightarrow \delta = \ln(\frac{2L}{d}) \; and \; \lambda = \frac{d}{L}$$

In this study, we adopted the Broersma's model since it yielded a more accurate and precise prediction of the dimensions of the rod-like cellulose whiskers. However, in both equations, we

noted the direct dependency between the two diffusion coefficients and the length and diameter of the rods, which imposes a non-linearity to the system. However, such non-linearity can be solved by several well-known methods of non-linear set of equations. The relationship between D and θ to its corresponding L and d should not be surprising as each rod has unique physical properties which can be measured by various instruments, such as light scattering, etc. Finally, it is vital to describe briefly the algorithm used for this purpose and the logic behind the programming language in MATLAB. The MATLAB "fminsearch" optimizer finds the minimum of a scalar function of several variables, starting at an initial estimate. This is generally referred to as unconstrained nonlinear optimization. As mentioned earlier, it uses the Nelder-Mead simplex algorithm as described in Lagarias et al (Lagarias et al, 1998). The Nelder-Mead algorithm is especially popular in the fields of chemical engineering, chemistry and medicine. The algorithm uses a simplex of $n + 1$ points for n-dimensional vectors x. I first makes a simplex around the initial guess x_0 (x_0 & y_o if 2 dimensional) by adding 5% of each component $x_0(i)$ to x_0, and using these n vectors as elements of the simplex in addition to x_0. One or more test points are computed, along with their function values, and the iteration terminates with bounded set values. The different processes of the algorithim are known as Reflect, Expand, Contract inside and Contract outside. Depending on the step used, the Nelder-Mead simplexes will result in a value either closer or further away from the predicted value.

The solution procedure adopted throughout this project is visualized in Fig.3.10.

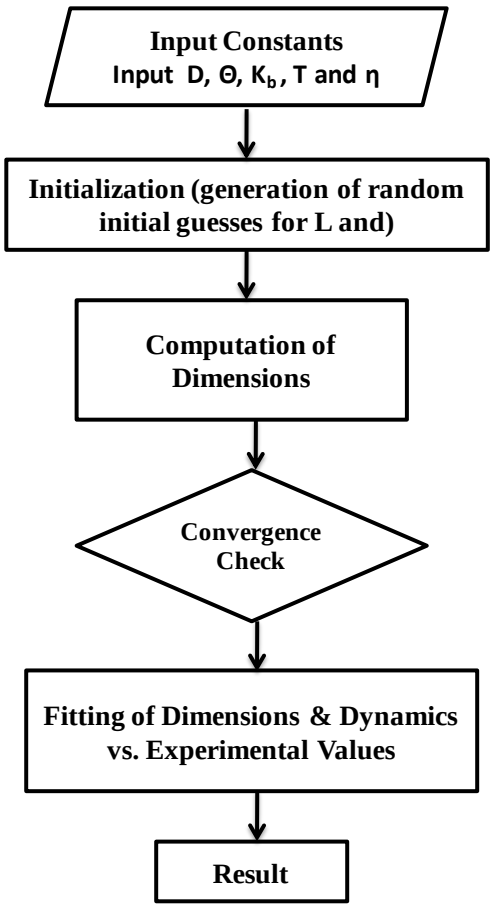

Figure 3.10 Solution Procedure

The adopted procedure starts by inputting the constant values: viscosity (η), Boltzmann constant (K_b), temperature (T), experimentally obtained translational diffusion coefficient (D_t) and rotational diffusion coefficient (Θ). Then the program is initialized by the using the generated random initial guessed values for length (L) and diameter (d) dimensions (L_o, d_o). Subsequently, L and d values can be calculated with an average $\bar{L}$ and $\bar{d}$ and error $\varepsilon_{\bar{L}}$ and $\varepsilon_{\bar{d}}$. Furthermore, a convergence of both functions presented in equation 2 is validated. Finally, all experimental dynamic and dimension values (obtained from different sources) are fitted and compared to their respective calculated values.

Chapter 4.0 Results and Discussion

4.1 Characterization of PEI and PEGylated PAMAM dendrimer with α-CD

Overview

Poly (ethylene glycol)-grafted-poly (amido amine) (PEGylated-PAMAM) dendrimers have attracted increasing interests due its improved stability, toxicity, and better particle drug leakage property. Initially, a brief investigation on a well known interaction between α-cyclodextrin (α-CD) and LPEI was conducted. Then, the complexation of α-CD with grafted PEG segments on the surface of PAMAM dendrimers were elucidated by light scattering and titration calorimetry. At high pH values, complexation between α -CD and PEGylated-PAMAM occurred once α -CD was titrated to the PAMAM solution. We observed for the first time a unique phenomenon at pH of 2, where no binding took place until a critical α-CD concentration (C*) of ~ 8.0 mM. At constant acidic pH value of 2, the size of the nanostructures increased from 6.7 nm to 57.6 nm when α-CD concentration was increased from 0.5 to 15 mM. Moreover, and at constant α-CD concentration of 8mM, the hydrodynamic radius (R_h) increased from 39.5 nm to 73.6 nm, and the radius of gyration (R_g) increased about 2.2 times from 36.4 nm to 80.4, at pH = 5 and pH = 8 respectively. The positive zeta potential measurements of the dendrimers, at low pHs, showed that they possessed positive charges as attributed to the protonation of primary amine groups on PAMAM chains that impart electrostatic repulsive forces to the system.

4.1.1 UV-Vis and ITC study of LPEI / α-CD complex

A linear polyethylenimines (LPEIs) having a amino end group and molecular weight of 3200 g/mol was synthesized for the purpose of studying its interaction and physical properties with α-CD. The polypseudrorotaxane formation was significantly dependent on the pH of the aqueous media. The maximum turbidity and yield of polypseudorotaxane precipitates was observed at pH 11.0, whereas very minimal complexation was observed in the pH range below 8.0 due to the protonation of secondary amine groups in LPEI backbones. The structure of LPEI was confirmed by using ^{1}H NMR as explained previously. The formation of the complexes was initially studied using UV-Vis through transmittance measurement and then by ITC via its binding isotherm.

UV-Vis Measurement:

One special interest of these poly-pseudorotaxanes is the an unexpected phenomenon of hydrogelation between cationic LPEI and α-CDs, and in addition, a spontaneous change of the physical state from hydrogel to crystalline precipitate during the process of poly-pseudorotaxane formation. Complex formation took place only at high pH values where the formation energy barrier can be reduced by increasing the temperature and then consecutive cooling that allows for further complexation.

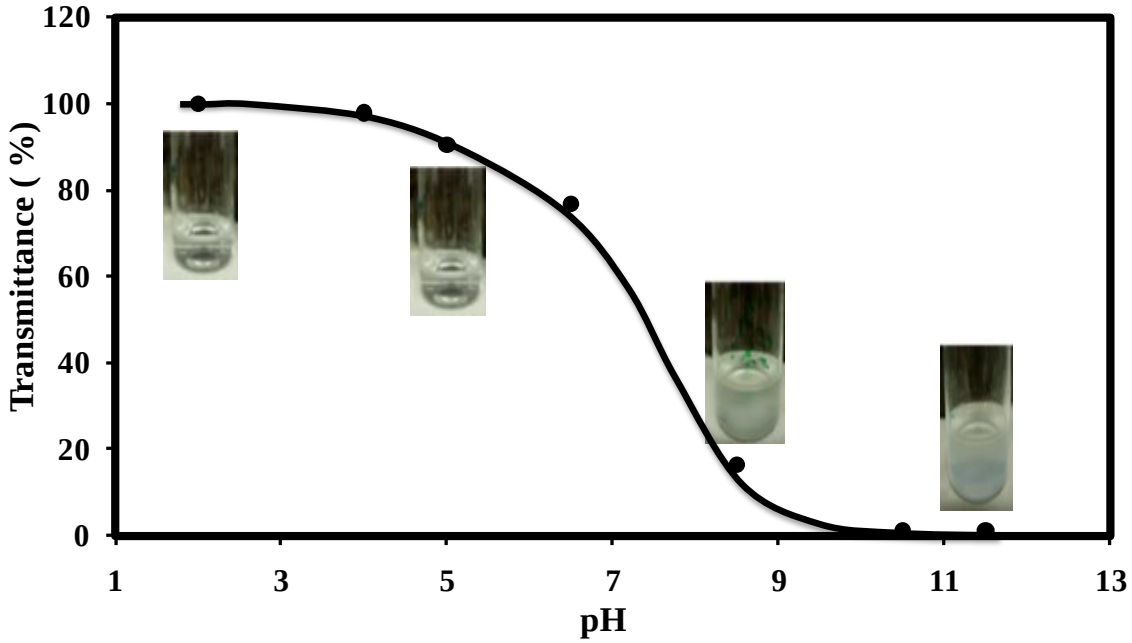

Figure 4.1 Transmittance measurements of α-CD/ PEI complexes at various pH values

As shown in Figure 4.1, the transmittance is well below 50 % for pH values > 7 of the α-CD/PEI complex solution (having 15 mM α-CD concentration). However, the transmittance of PAMAM solution decreased significantly as the pH was increased from 7 to 8, where it further decreased to zero at pH of 12, which coincides with the formation of the precipitates. This result agrees with previous studies reported by Choi et al. (Choi et al., 2004), in which the percent yield of α-CD/PEI complex were investigated at various pH values. They observed an increase of yield percent starting at pH = 8.5 reaching a maximum of 90% recovery at pH ~11. These findings are of significant importance since the precipitated gels could be used in drug delivery applications in a similar fashion to the PEG hydrogels. It is expected that the gelation results from physical links between the α-CD and PEI segments induced mainly via hydrogen bonding. The partially formed polypseudorotaxanes play a role in physical crosslinks to produce a network structure

(Choi et al., 2004). In addition, intermolecular hydrogen bonds between the hydrated LPEI chains and/or water might play a major role in the stabilization of the hydrogels, because almost all the secondary amines (pKa=8.9) are deprotonated at pH 11.0. It is important to note that at pH values beyond 12 the precipitates begin to disappear. This is because the hydroxyl group of α-CD will dissociate since their pKa is close to 12, resulting in deprotonated α-CD molecules.

ITC study

Because of the vital importance of pH responsive polymers, such as LPEI, we conducted a microcalorimetric study to investigate the interaction between α-CD and LPEI. Isothermal titration calorimetry (ITC) is a powerful tool to quantify the thermodynamic biding interactions between two different species. ITC measures the heat released or absorbed as the titrant is injected into the solution in the sample cell. In this case the binding isotherm of α-CD/PEI complexes was studied by titrating a 15mM α-CD solution into 0.125 wt% of PEI solution in the sample cell. The high sensitivity of ITC allows for the measurement of precise values corresponding to the enthalpy change when binding occurs. The enthalpy associated with α-CD/PEI interaction was determined by subtracting the heat contributed by α-CD /water from the heat resulted from α-CD/PEI.

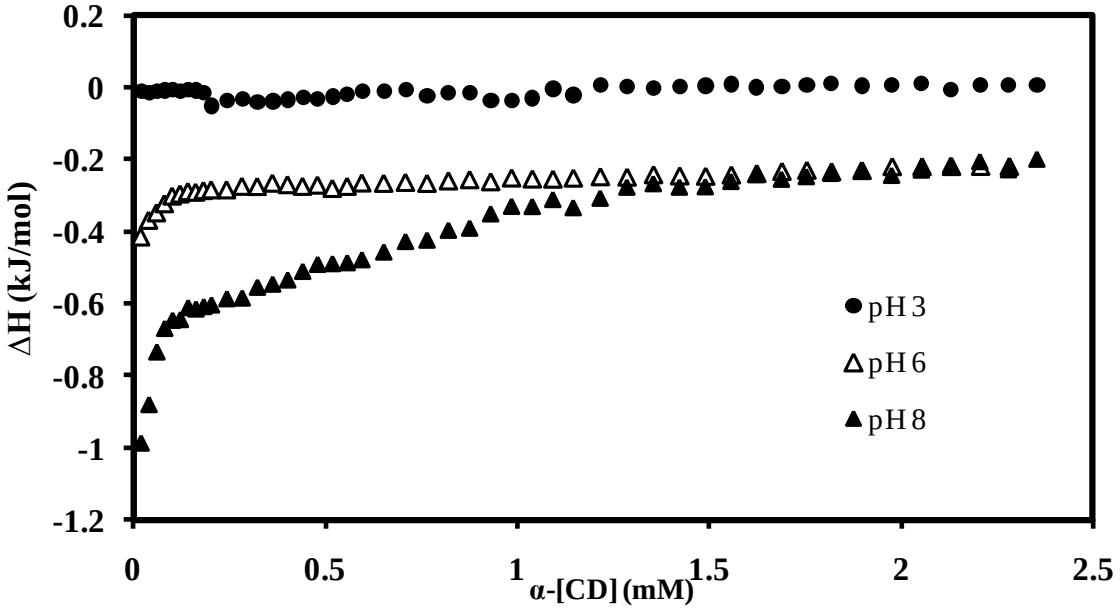

Figure 4.2 Differential enthalpy curve versus total α-CD obtained by titrating 15 mM of [α-CD] into 0.1 wt% of PEI solution at various pH values.

The binding process between α-CDs and PEI is generally described similar to the threading process between α-CDs onto PEG chains. As show in Figure 4.2, titrating the same amount ofα-CD concentration into PEI solutions at various pH values results in binding isotherms with different degree of interaction. The binding, at pH=10, occurred at the first injection of α-CD solution. At this pH, the PEI polymer was completely deprotonated and possessed negligible level of positive charges thereby permitting the threading of α-CD onto the polymeric segments. The same process can be attributed to the binding at pH 8. However, at this pH, the heat of enthalpy released during the interaction is lower than that observed at pH=10 since the NH_2 groups of the PEI repeating units are partially protonated, allowing for some electrostatic repulsion which are unfavorable for the threading process. This phenomenon is observed more clearly at pH values 6 and 3. The former produces a much lower interaction than at pH = 8 or 10 due to the fact that the PEI segments are increasing being protonated which reduces threading due to the increased electrostatic repulsion. The repulsion is mainly attributed to the hydrophobic

cavities of CDs which are energetically unfavorable to the protonated amino groups (Choi et al., 2004). The graph at pH 3 shows no interaction between α-CD molecules and PEI segments since at this pH all of the repeating units in the PEI chain are fully protonated. This result agree with the turbidity measurements shown in Figure 4.1, where the precipitates and turbid solutions were observed at pH values greater than 7-8, however complete dissolution was observed for pH values less than 6. Finally, and as expected, the full saturation of the PEI with α-CD molecules, at high pH values (10), necessitates an increasing α-CD concentration titrated into the sample cell.

4.1.2 Concentration effect in binding between α-CD and PEGylated-PAMAM dendrimers

Introduction

The design of polyrotoxanes is one of the most active fields in supramolecular inclusion complexation. To date, a diverse number of polymeric inclusion complexation (PIC) structures via host guest interaction between CDs and various polymeric systems have been reported (Ceccato, Lo Nostro, & Baglioni, 1997; Choi et al., 2004; Huh et al., 2002; Lee, Choi, Ooya, & Yui, 2004; Liu, Sondjaja, & Tam, 2007; Ni, Cheng, & Li, 2009; Okada, Kawaguchi, Okumura, Kamachi, & Harada, 2000; Zheng, Wang, Hu, Tam, & Li, 2005).

CDs are cyclic molecules comprising of six (α), seven (β), or eight (γ) glucose units linked through α-1-4-glycosidic linkages (Challa, Ahuja, Ali, & Khar, 2005). The average diameters of the cavities of α -, β - and γ - CD are 4.5, 7.0, and 8.5 Å, respectively, while the height of each CD's torus is ca. 7.8 Å (Bender, 1978; Okumura, Okada, Kawaguchi, & Harada, 2000; Sabadini, Cosgrove, & Taweepreda, 2003). They are readily soluble in water, with solubility ranging from 130 to 146 g/l, and are capable of selective inclusion of a wide range of guest molecules (Harada, 1997, 2001; Wenz, 1994). The four most important driving forces for the formation of ICs are hydrophobic interactions between host (CD) and guest molecules; Van Der Waals forces,; geometrical compatibility between the host and guest; and hydrogen bonding between the hydroxyl groups of CD and the guest molecule (Ceccato et al., 1997; He, Huang, Chen, & Liu, 2005; Lee et al., 2004; Loethen, Ooya, Choi, Yui, & Thompson, 2006). Harada and co-workers were the first to report on the formation of a PIC between α-CD and poly (ethylene glycol) (PEG) (Harada, Li, & Kamachi, 1992; Harada, 1996, 1996; Harada, Nishiyama, Kawaguchi, Okada, & Kamachi, 1997) . When PEG was added to a saturated α-CD solution, white crystalline precipitates in high yield were produced. The complexation was confirmed by NMR with a stoichiometric ratio of α-

CD:PEG = 2:1; i.e two α-CDs are needed to complex with one ethylene oxide (EO) unit (Harada et al., 1992; Harada, 1996; Harada, 1996). The formation of the complexes is thought to be promoted by hydrogen bond formation between neighbouring cyclodextrins, while adopting head-to head or tail-to-tail arrangements (Harada, 2001). Similar complexation was observed for other biodegradable polymers and copolymer systems, which may find interesting applications. Tam et al. reported on the formation of vesicular structures when α-CD complexed with PEO-b-PAA at high pH (pH=11) (Liu et al., 2007). The solution remained clear; however it became turbid when the pH was reduced to 3. They studied the thermodynamics and morphology of the nanostructures using ITC and light scattering techniques. In another study, Yui et al. (Lee et al., 2004) reported the formation of a pH-dependent polyrotoxatanes formed by the complexation of α-CD and a triblock PEI-*b*-PEG-*b*-PEI, where a reduction in pH induced repulsion between the cationic polymer chains and α-CDs that hinder the threading of α-CD. Because of the possible uses of CDs in various applications, such as controlled drug delivery (Loethen, Kim, & Thompson, 2007; Luo, Haverstick, Belcheva, Han, & Saltzman, 2002), food processing (Szejtli, 1982, 1984, 1998; Ishiwata & Kamiya, 2000), environmental protection (Ishiwata & Kamiya, 2000), and pharmaceutical formulations (Duchane & Wouessidjewe, 1990) , the study and formation of these supramolecular structures are of significant importance.

Most of the investigations on CD ICs concentrated on well-defined co-polymeric systems that are designed and synthesized using techniques, such as ATRP, cationic/anionic polymerization etc. In this study we examined a PEG grafted dendritic structure that was previously prepared by the Michael addition reaction. The synthesis of PEGylated PAMAM dendrimers is generally based on a condensation reaction between PEG and PAMAM as previously reported in several communications (Kim, Klutz, & Jacobson, 2008; Luo et al., 2002; Yang, Morris, & Lopina, 2004).

Modified PAMAM dendrimers can be used as drug carrier (Kojima, Kono, Maruyama, & Takagishi, 2000; Kolhe, Misra, Kannan, Kannan, & Lieh-Lai, 2003), gene carriers (Baek & Roy, 2002), antiviral agents(Wiener et al., 1996), contrast agents(D. A. Tomalia & Dvornic, 1994), and nanoscale catalysts for industrial processes (Klajnert & Bryszewska, 2001). The uniqueness of dendrimer stems from the fact that they are robust, well-defined, and highly branched globular structures making them flexible systems for various applications..

PAMAM dendrimers possesses primary, secondary and tertiary amines, where the pK_a value of 1^o amine groups ranges from 7-9, whereas that of 3^o amine are 3-6. At low pH (e.g. pH < 2), PAMAM would swell and entrap more molecules within the cavity of the core since all of the amine groups are fully protonated. At neutral pHs (7-8) studies showed that only the amines at surface of PAMAM are protonated, whereas the ones in the core are deprotonated due to the fact that their pKa values (3-6) are lower than the pH [8]. (D. A. Tomalia, 1994; Wang, Wyn-Jones, Sidhu, & Tam, 2007; Zheng et al., 2005) (Figure 4.3).

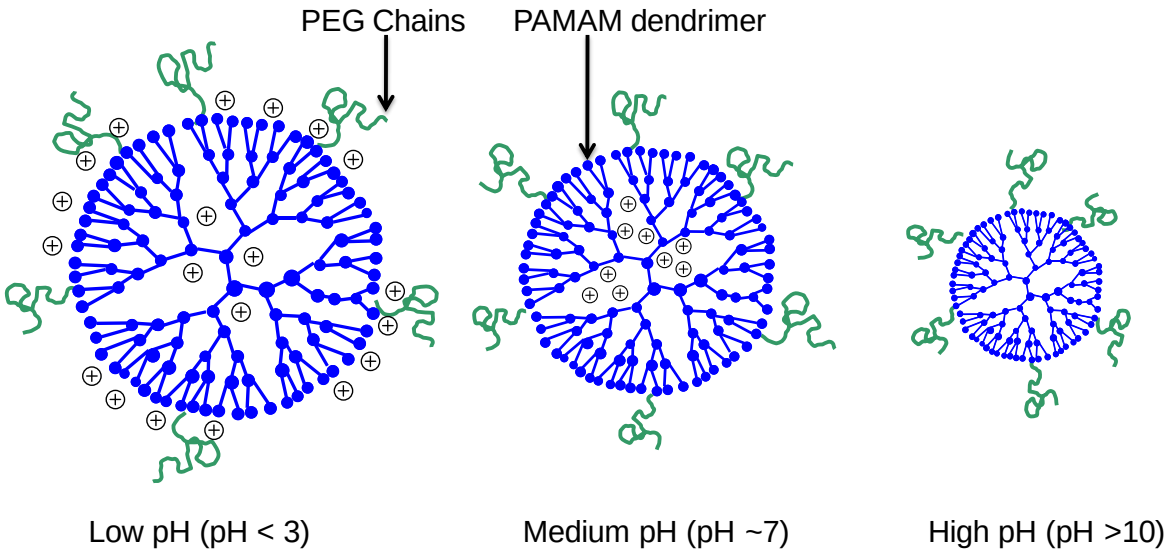

Figure 4.3 PEGylated-PAMAM dendrimer at various pH conditions

In this study, we investigated the complexation of PEGylated-PAMAM dendritic system with α-CD at two extreme pH conditions. The difference in the ionic strength and the pH values has a strong impact on the threading of CD into the PEGylated-PAMAM resulting in formation of different microstructures.

Materials and Methods

The polymeric materials were used from previously synthesized protocols with molecular weight ≈ 9000 g/mol (M.W of PEG = 2000g/mol, PAMAM Generation 3 with M.W= 6909 g/mol) (LIM, 2008). The amine- terminated generation 3 PAMAM dendrimers were purchased from Sigma-Aldrich Chemical Co. (> 99% purity) and used without further purification.

G3-[EDA]-PAMAM-NH_2 (M_w = 6909 g/mol) has 32 primary amines on the surface and 90 tertiary amines at the branch points within the core. The synthesized PEG conjugated PAMAM has average mol ratio of MPEG to PAMAM equal to 32. It is fully protonated and unprotonated at pH ~ 2 and ~ 10 respectively, and in the pH range of 7 to 8, only the primary amines on the outer most surface are protonated. α-CD (M.W =972 g/mol) with 99% purity was purchased from Sigma Aldrich. All the solutions were prepared using Millipore water at neutral pH (~7).

Isothermal Titration Calorimetry (ITC): The calorimetric experiments were carried out using the Microcal isothermal titration calorimeter (VP-ITC, Northampton, MA). This power compensation differential instrument was previously described in detail by Wiseman et al.(Wiseman, Williston, Brandts, & Lin, 1989). It has a reference cell and a sample cell of 1.35 mL, which are both insulated by an adiabatic shield. The titration was carried out by stepwise injections of different α-CD aqueous solution (40, 70, 80, 90 and 120 mM) at pH = 2 and 10

from a 250 μL injection syringe into the sample cell filled with 0.1 wt % of PEGylated-PAMAM at pH = 2 and 10. The syringe is tailor-made such that the tip acts as a blade-type stirrer to ensure an optimum mixing efficiency at 400 rpm(Wiseman et al., 1989). All measurements were carried out at a constant temperature of 25.0°C, and the calorimetric data were processed by the Origin software supplied with the ITC.

Dynamic Light Scattering (DLS): The microstructure of the sample solutions prepared at pH ~ 2 was examined using a Brookhaven Laser Light Scattering system, which consists of a BI-200SM goniometer and a BI-9000AT digital correlator. A 636 nm vertically polarized argon ion laser was used as the light source. Samples were prepared by adding 5, 20, 100, 170, and 300 μL of 150 mM α-CD onto 1.5 ml of 0.1 wt % of PEGylated-PAMAM to create 0.5, 2, 9, 15, and 25 mM of α-CD.

Results & Discussion

The raw cell feedback signals for titrating 40 and 80 mM of α-CD into the PEG-PAMAM dendrimers at pH of 2 and 10 are shown in Figures 4.4 (a to d). Different injection volumes were used, ranging from 2 to 10 μL. Integrating the raw heat under each of the thermogram yielded the enthalpy of interaction between α-CD and the dendrimers. Figure 4.5 (a & b) shows the integrated heat signals showing the binding isotherms for the titration of 40 and 80 mM α-CD into 0.1 wt % PEGlyated-PAMAM at pH of 2 and 10 respectively.

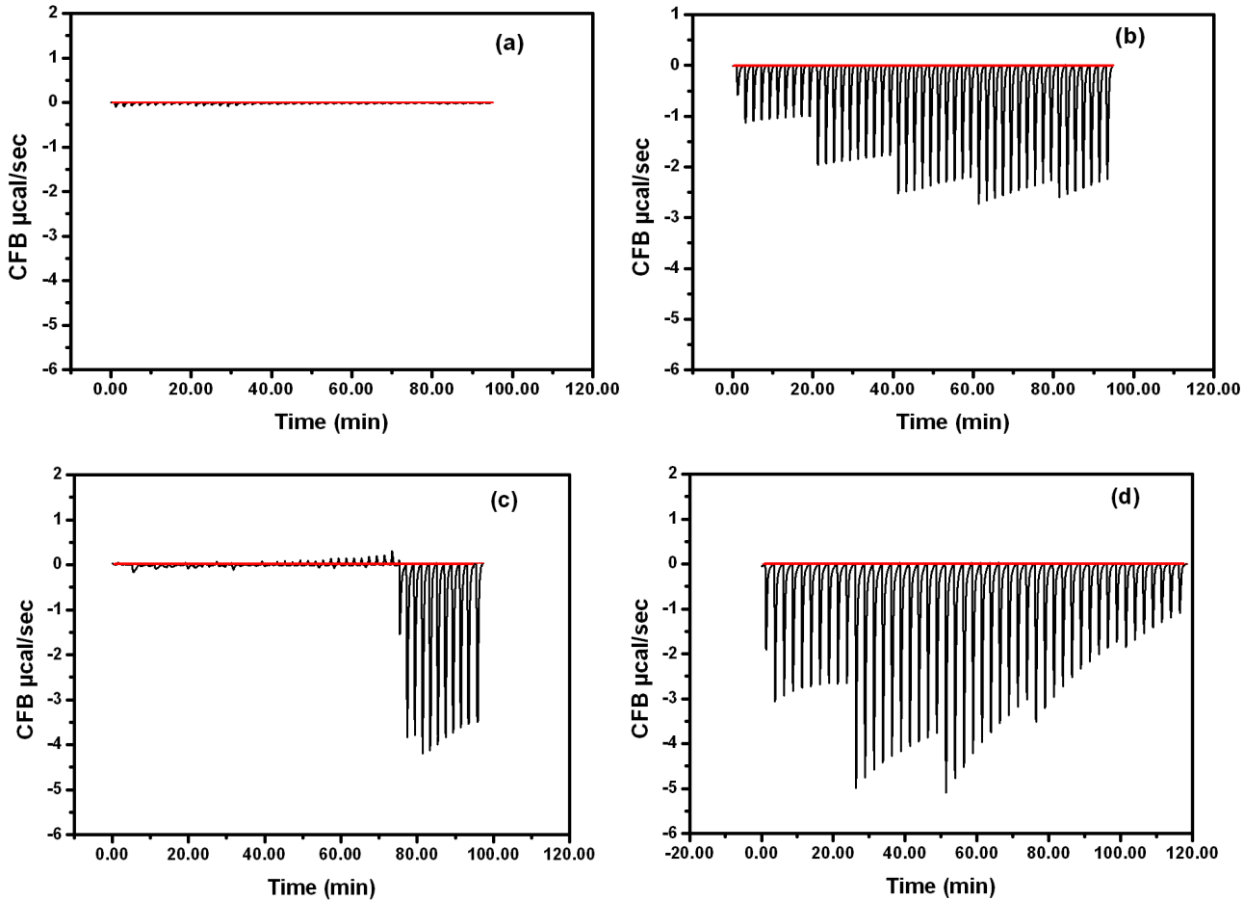

Figure 4.4 Thermograms showing Cell Feedback (CFB) for (a) pH=2, [α-CD] =40 mM; (b) pH=10, [α-CD]=40 mM; (c) pH=2, [α-CD]=80 mM; (d) pH=10, [α-CD]=80 mM.

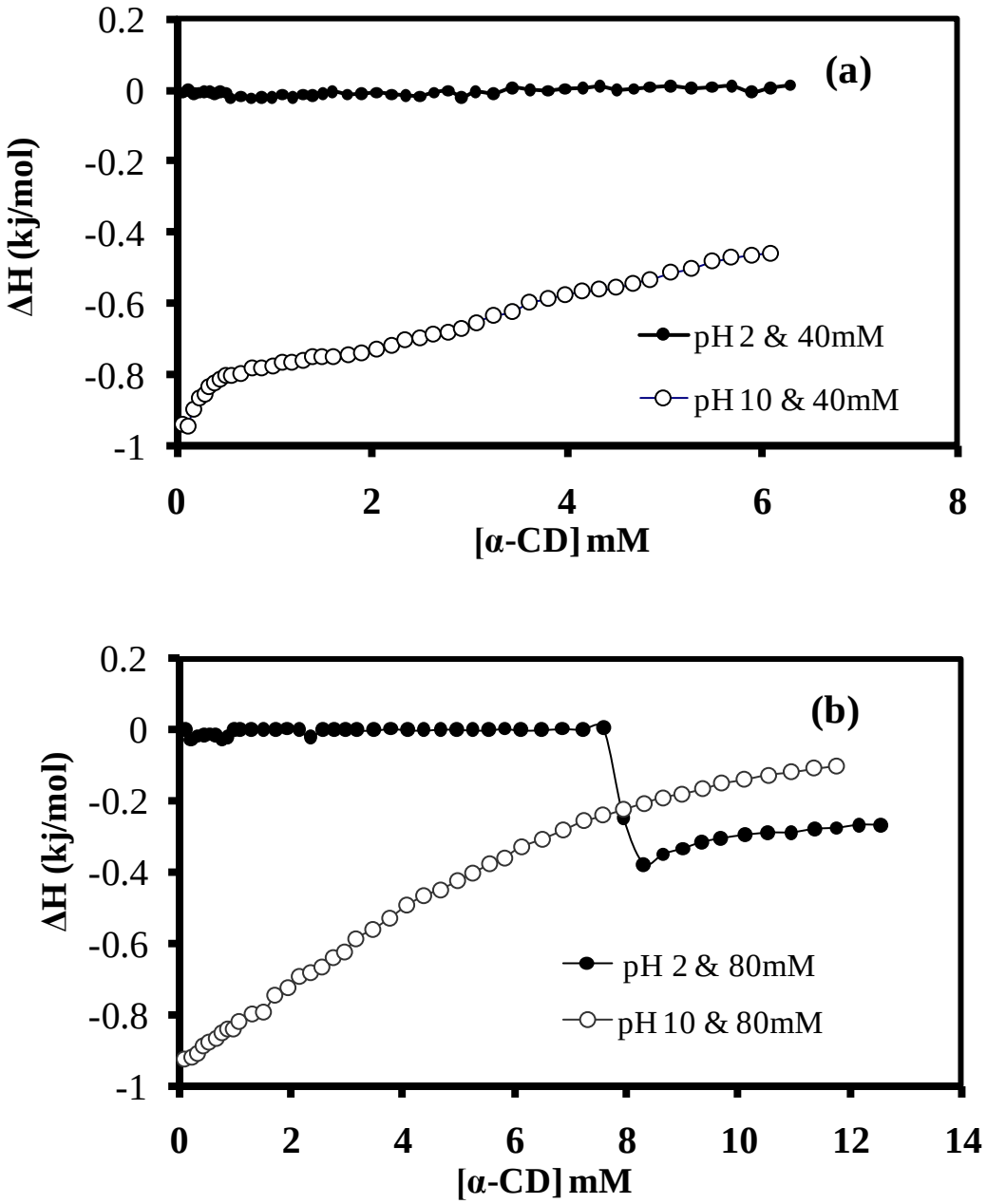

Figure 4.5 Differential enthalpy curve versus total α-CD obtained by titrating [α-CD] on 0.1wt% solution of PEGylated –PAMAM: a) [α-CD] =40mM and b) [α-CD] =80mM

As the titration of α-CD to water produced negligible heat change (Zheng et al., 2005), it is apparent that negligible heat was produced for the titration of α-CD to 40 mM of PEGylated-PAMAM at pH of 2 (filled circles - Figure 4.5a). Thus, the observed binding enthalpies for the

40 and 80 mM PEGylated –PAMAM at pH 10 were attributed to the complexation of α-CD and PEG segments on the PEGylated-PAMAM dendrimer (unfilled circles of Figures 4.5a and 4.5b). The threading of α-CDs onto PEG chains for the 40 and 80 mM PEGylated-PAMAM solutions at pH=10 occurred at the first injection of α-CD solution. At this pH, PAMAM dendrimers are completely deprotonated and possessed negligible level of positive charges, thereby permitting the threading of α-CD onto PEG segments. On the other hand, at a low pH of 2, where the PAMAM dendrimers are protonated, threading of α-CD only occurred when the α-CD concentration exceeded 8.0 mM as shown in Figure 4.5b (filled circles). The results revealed the profound effect of electrostatic repulsion of positive charges on the PAMAM on the threading of α-CD on PEG chains.

In both cases, the threading process was exothermic, indicating that the complex formation between PEGylated-PAMAM and α-CD was energetically favourable. The impact of α-CD concentration on the binding between α-CD and PEG at pH of ~ 2 can be seen more clearly when the binding thermograms for the titration of different α-CD concentrations into PAMAM dendrimers are compared as shown in Figures 4.6a and 4.6b. The titration of 40, 70, 80 and 120mM, of α-CD into PEGylated-PAMAM at pH = 2 showed no interaction until the α-CD concentration of 8.0 mM was reached. At this point, sufficient α-CD molecules are present to induce the threading process, where the cumulative hydrogen bond interactions between the α-CD molecules exceed the electrostatic repulsive forces of the positive charges on the surface and core of the dendritic structure.

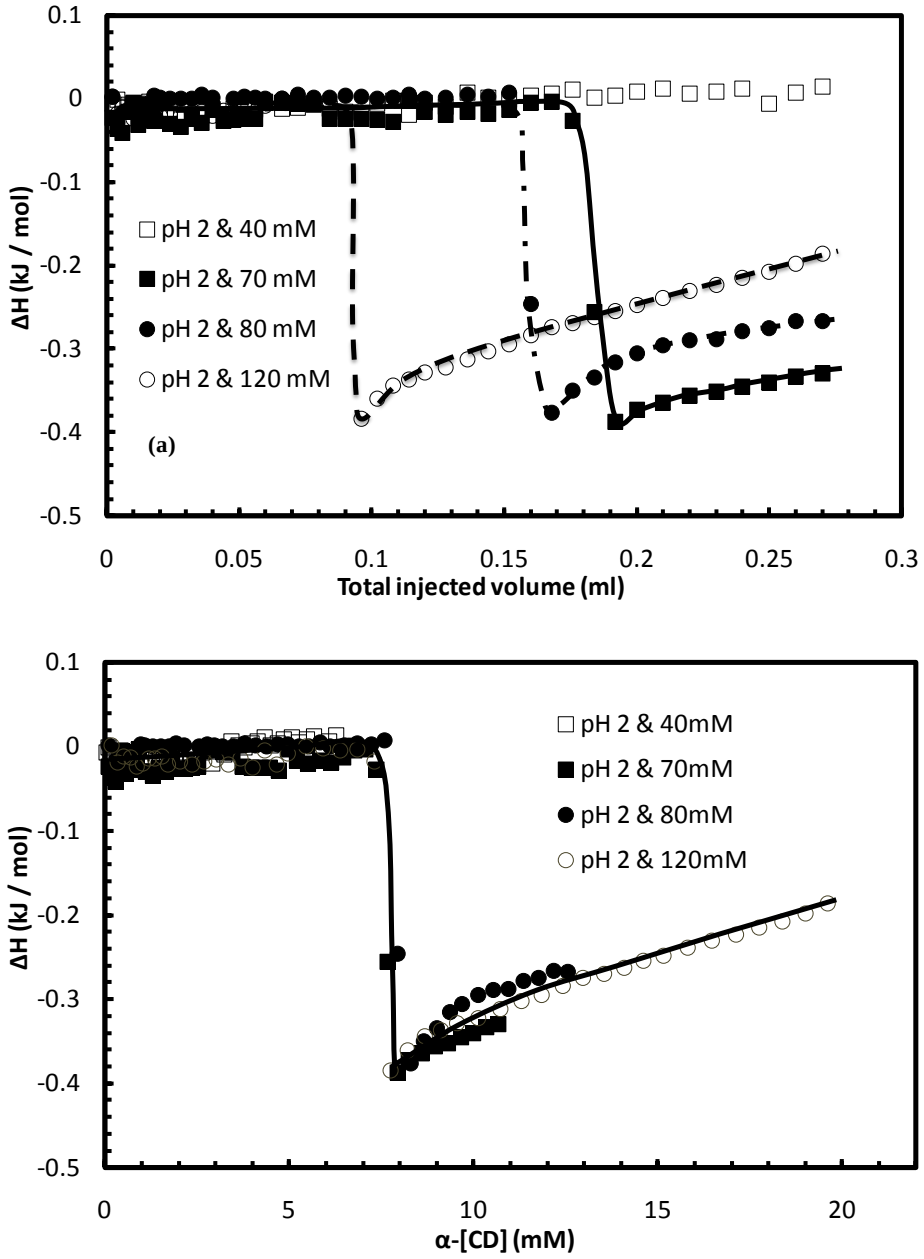

Figure 4.6 Calorimetric Titration of α-CD into 0.1 wt% solution of PEGylated -PAMAM at pH 2 (a) ΔH curve vs. Total injected volume; (b) ΔH curve vs. the α -CD concentration.

As shown in Figure 4.6a, titrating 120 mM requires lower volume of titrant to initiate binding compared to 70 mM, as the former has 1.71 times more α-CD molecules, thereby requiring less amount of injected volume, and thus resulting a shift in the graph to lower volume. When the

data in Figure 4.6a were replotted with a-CD concentration on the x-axis, all the data collapsed onto a single master curve with a critical observable transition at 8 mM (Figure 4.6b).

Six solutions at pH = 2 were prepared with increasing concentrations of α-CD, using the method outlined above, and the microstructure was examined using the Brookhaven DLS system. Figures 4.7 and 4.8 shows the decay rate and distribution functions for several scattering angles for low (2 mM) and high (15 mM) α-CD concentration. From previous studies, the size of PEGylated-PAMAM was found to be around 6.7 nm(Luo et al., 2002). The decay mode of the PEGylated dendrimer was contributed by the translational diffusion of the scattering objects in solution.

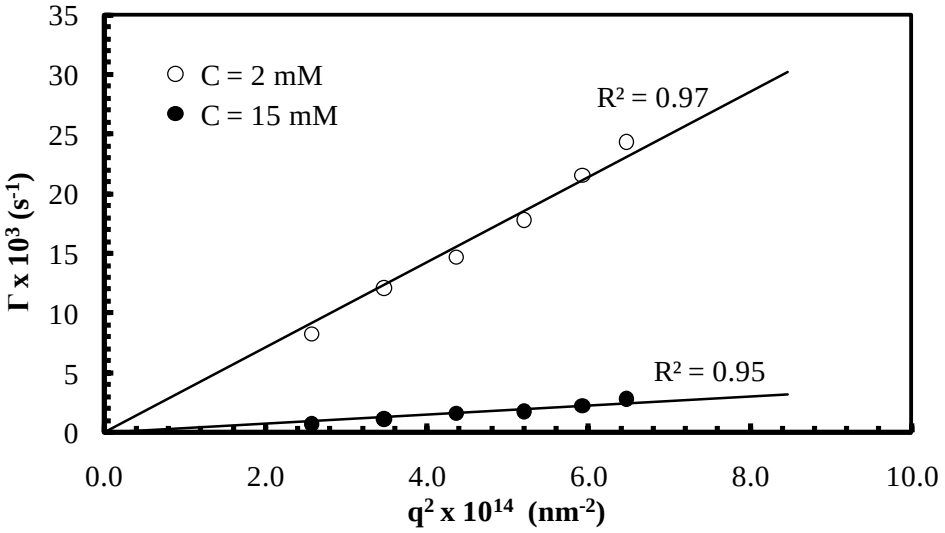

Figure 4.7 The dependence of the decay rate Γ on the square of scattering vector, q2 , at a) [α-CD] =2mM, b) [α-CD] =15mM

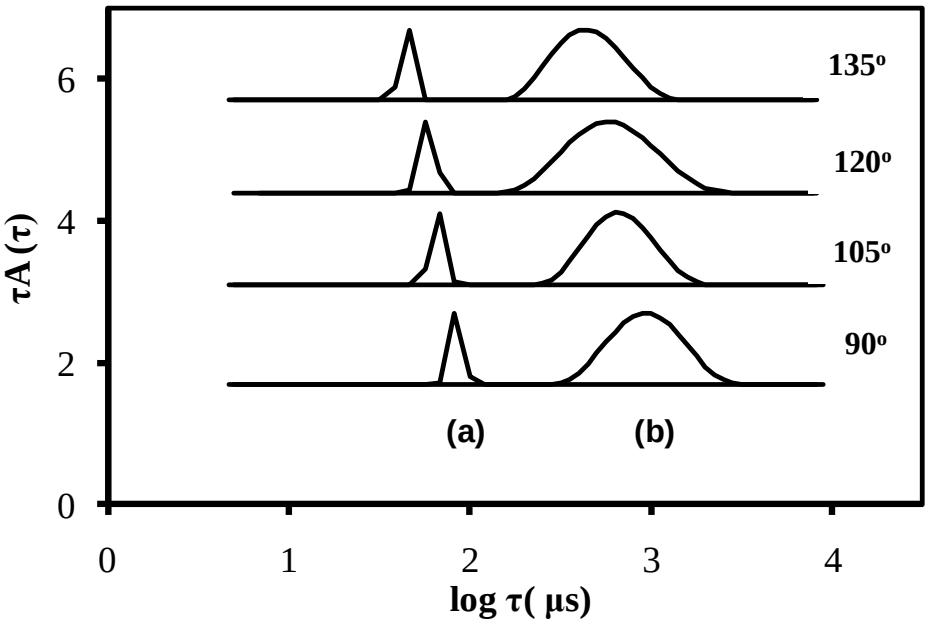

Figure 4.8 Relaxation distribution functions obtained from DLS measurement at a) [α-CD] =2mM, b) [α-CD] =15mM

The graph showed a linear relationship between the decay mode, Γ**,** and wave vector, q^2 with R^2 = 0.97 and 0.95 for [α-CD] = 15 mM and 2 mM respectively (Fig. 4.7). By using the Stokes-Einstein equation, $R_h = \frac{kTq^2}{6\pi\eta\Gamma}$ (k is the Boltzmann constant, T is the absolute temperature, η is the solvent viscosity and R_h is the hydrodynamic radius) we can estimate the hydrodynamic radius at both α-CD concentrations. When [α-CD] = 2mM, the R_h was 6.7 nm (which is identical to size of individual PEGylated PAMAM dendrimer. The size of the PEGylated PAMAM/CD complex increased to 57.6 nm when [α-CD] was increased from 2 to 15 mM. This increase suggests the impact of threading of α-CD on the PEG chains that induces the bridging and association of PEGylated PAMAM/CD complexes.

A plot showing the dependence of hydrodynamic radius (R_h) and radius of gyration (R_g) on α-CD content for 0.1 wt% PEGylated PAMAM dendrimers in varying α-CD concentrations is shown in Figures 4.9a and 4.9b.

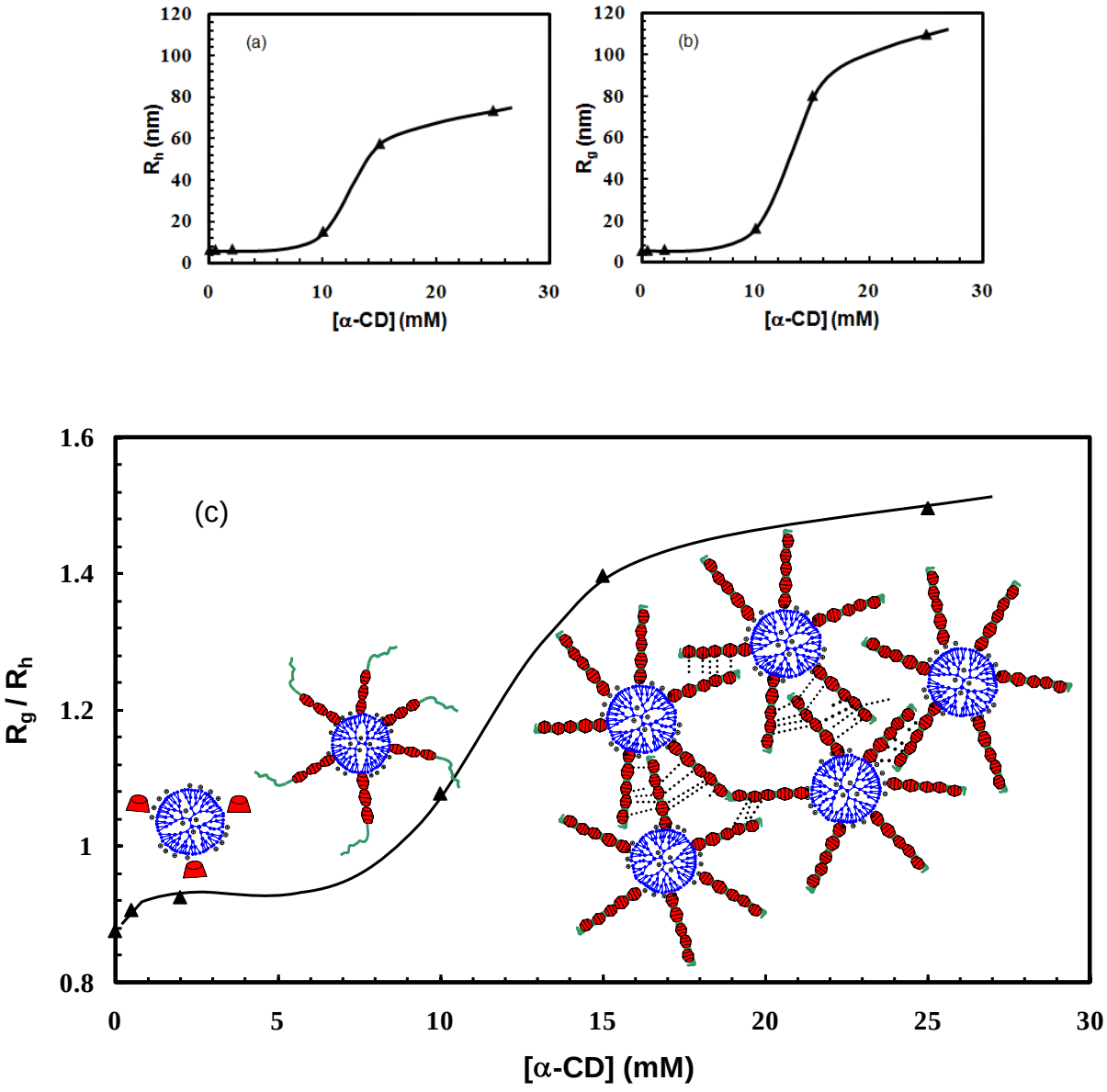

Figure 4.9 Particle size of PEGylated PAMAM at increasing [α-CD] (mM) a) R_h, b) R_g, c) R_g/R_h

The results revealed a significant increase in the particle size with increasing α-CD concentration, which is associated with favourable and stable PEG/α-CD inclusion complexes. As mentioned earlier, we believe that at low α-CD concentration, the threading of α-CD is inhibited by the strong electrostatic repulsion from the positive charges on the PEGylated-PAMAM dendrimers. Hence, isolated dendrimers are observed with a size of approximately 6.7 nm. However, when the α-CD concentration was increased from 2 to 25 mM, exceeding the critical concentration of 8.0 mM, threading of α-CD onto the PEG chains occurred as evident from the ITC thermogram. Beyond this concentration, the hydrodynamic radius increased by 8 times from 6.7 to 57.6 nm when the α-CD concentration was increased from 2 to 15 mM. The size of the aggregate increased further to 73.5 nm at [α-CD] = 25mM since more α-CD molecules are threaded onto the PEG chains resulting in the bridging of more PEGylated-PAMAM dendrimers. The morphological transformation of the dendrimer and the dendrimer/CD complexes can be elucidated from the R_g/R_h data as shown in Figure 4.9c. The parameter, ρ, (R_g/R_h) commonly used to examine the morphology of the microstructure of aggregates. In the absence of α-CD, the R_g/R_h possessed a value of 0.87, which corresponds to a dendritic core with dangling PEG chains. It remained approximately at this value until the critical α-CD concentration of 8 mM, where it increased sharply to approximately 1.49 at high α-CD concentration. This value is very close to the theoretical values of a Gaussian chain (1.50), confirming that at [α-CD] = 25 mM, inter-particle association of α-CD threaded PEG segments resulting in the formation of a larger aggregate with a Gaussian distribution of the polymeric chains.

As illustrated by other researchers [41], the zeta-potential determined for the PEGylated-PAMAM dendrimers at pH 2.2 was + 6.7 mV, which confirmed the presence of positive charges at pH

values ≤ 3 as most of the amine groups are protonated (Figure 4.3). With decreasing pH values, the surface of the dendrimer becomes more positive as the core and surface amine groups of PAMAM are increasingly being protonated. Figure 4.10 illustrate the complete dissolution of the PEGylated-PAMAM/ α-CD complex at pH value of 2 as compared to a turbid solution at pH of 10.

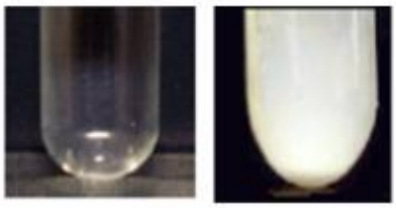

a) pH=2 **b) pH=10**

Figure 4.10 PEGylated-PAMAM / α-CD complex obtained at a) pH 2 (clear solution) and b) pH 10 (turbid solution) at [α-CD] = 20mM.

At pH = 2, stable PEGylated-PAMAM/ α-CD aggregates with size less than 100 nm are produced, induced by the balance of electrostatic repulsive forces on the dendrimers and hydrogen bond/hydrophobic forces of the PEG/α-CD chains (Scheme 4.1). On the other hand, at pH=10 the dendrimers are neutral, and the hydrogen bonds between the amine and ether groups of the threaded α-CDs results in the formation of larger insoluble aggregates as revealed by the white precipitates. The mechanism that summarises the threading and association of the PEGylated-PAMAM/α-CD complex at pH of 2 is illustrated in Scheme 4.1. At C < C* (~8 mM), threading of α-CD is absent, and individual dendrimers are present in solution (Scheme 4.1a). When the critical concentration C* is exceeded, threading of α-CD on the PEG occurs (Scheme 4.1b). Further increase in the concentration results in the bridging and the formation of larger

aggregates as illustrated in Scheme 4.1c. The aggregates continue to associate to form larger particles (Scheme 4.1d) as confirmed by light scattering results. Studies are underway to investigate and confirm the morphology of PEGylated-PAMAM / α-CD at different pH values.

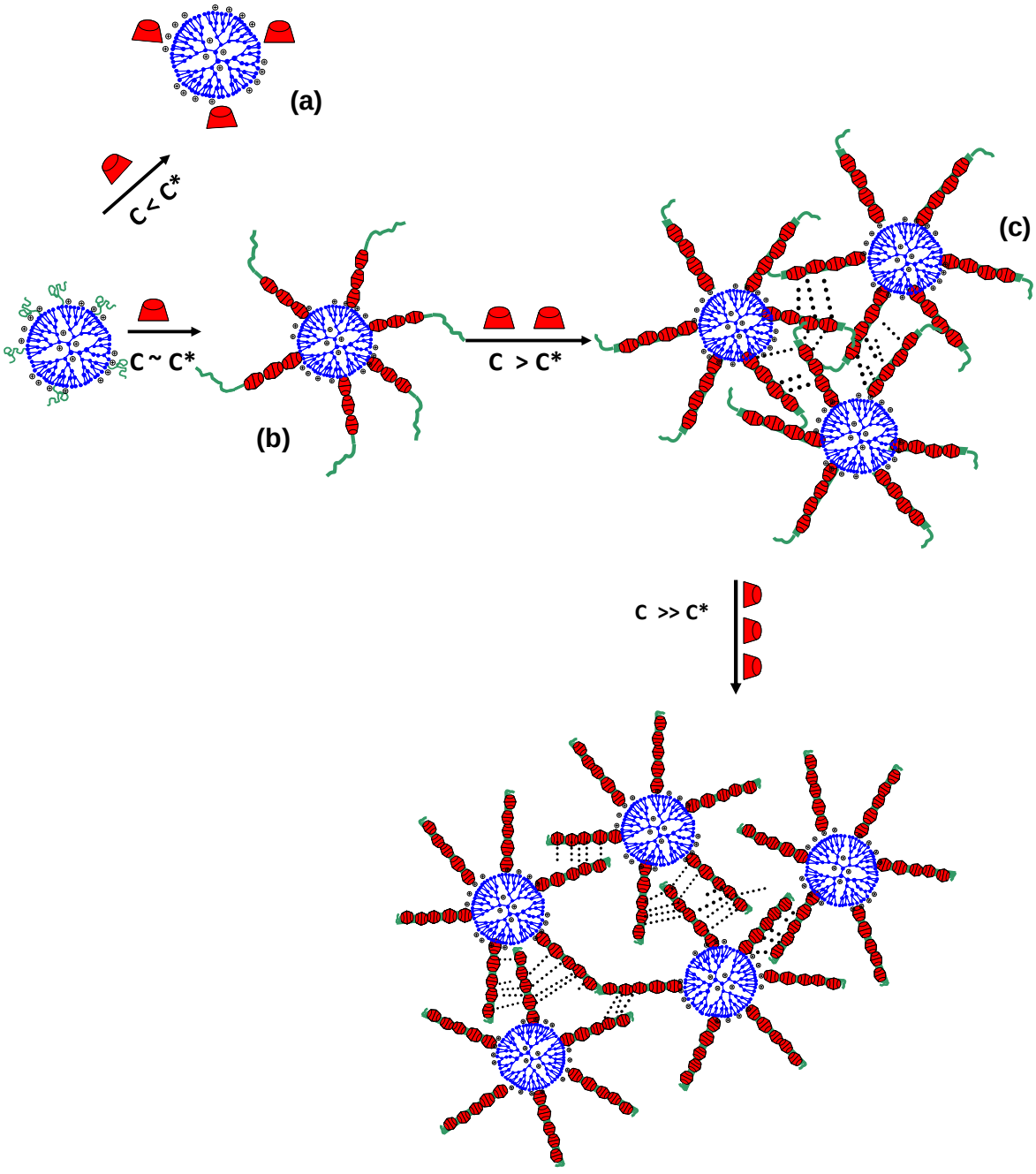

Scheme 4.1 Schematic diagram showing the mechanism nanostructures at pH 2 Induced by the Complexation between PEO Segments and α-CD

4.1.3 pH and ionic effect in binding between α-CD and PEGylated PAMAM dendrimers

After examining the concentration dependence of α-CD complexation on PEG segments in of the PEGylated-PAMAM dendrimers, in this section we shall present both pH and ionic effect of PAMAM on the binding process. This was conducted using UV-Vis, zeta potential, titration calorimetry, and light scattering measurements.

Turbidity and Zeta potential measurement:

Turbidity measurement was conducted to investigate any occurrence of phase separation of PEGylated PAMAM dendrimers complexed with α-CD molecule at different pH values. In addition, the zeta potential was measured to examine the surface charge of PEGylated-PAMAM dendrimers. Figure 4.11 shows the combined results of both zeta potential and percent transmittance. At low pH values, the positive charges on the PAMAM dendrimer (zeta potential ~ 6.7mV) will impart electrostatic repulsive forces to the system preventing the binding between α-CD and PEG, and thus no precipitation was observed (percent transmittance ~ 85-100%). At a pH of 7, the transmittance decreases significantly to about 18% indicating that complexation has already commenced. This is also observed from the decrease in zeta potential to +1.0 mV, demonstrating the reduced electrostatic repulsion effect on the threading of α-CD and on PEG. Finally, clear precipitates were formed at basic pH values (> 9) where the α-CD molecules fully threaded on the PEG segments. This is demonstrated from the percent transmittance and zeta potential values approaching 0% and 0 mV respectively. Similar to the concentration effect seen earlier, we believe that the lack of positive charges on PAMAM at high pH values will induce strong hydrogen bonding between the amine and ether groups of the threaded α-CDs, resulting in the formation of larger insoluble precipitates as revealed by the turbid solution.

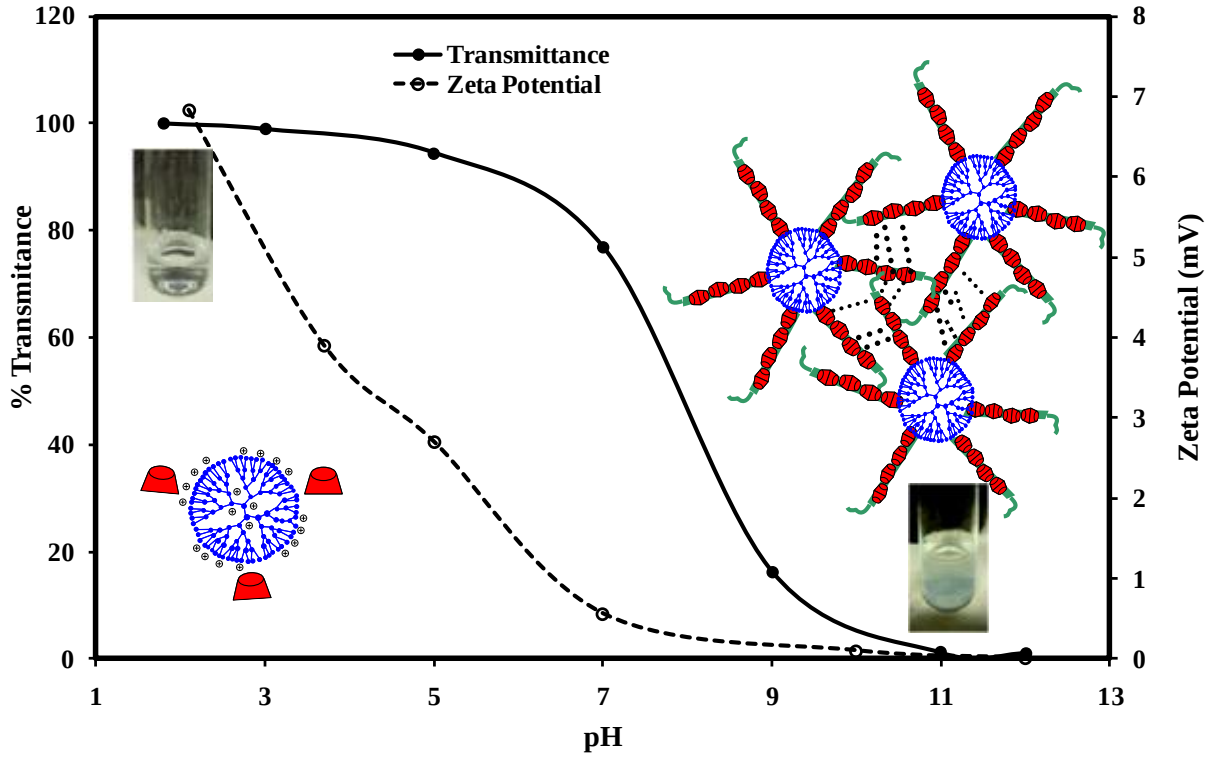

Figure 4.11 a) Transmittance of PEGylated-PAMAM / α-CD complexes with [α-CD] = 20mM (●) b) Mobility measurement of 0.15 wt % PEGylated PAMAM dendrimer at different pH values (○).

ITC Study

pH effect: As all chemical reactions involve a change in enthalpy, the thermodynamics for the binding of α-CD to PEGylated PAMAM could be detected by the heat released or absorbed in the system. The high sensitivity of ITC allows precise values in the change of enthalpy to be measured when binding occurs. The titration of 55mM of α-CD concentration into 0.1 wt % of PEGlyated-PAMAM dendrimers at various pH values is shown in Figure 4.12. As discussed earlier, the observed binding enthalpies were attributed to the complexation of α-CD and PEG segments on the PEGylated-PAMAM dendrimers. However, the degree of binding depends on the pH due to the different degree of protonation of the PAMAM dendrimer. As expected, at low

pH value of 2, the fully protonated PAMAM dendrimers resulted in no binding between α-CD and the PEG segment, suggesting the strong electrostatic repulsion effect that PAMAM has on the complexation process. This effect, however, will slightly diminish as we increased the pH value to 4, where the onset of complexation occurred. However, the binding was somewhat impeded, since, at this pH value, the primary amines on the outer most surface and some of the secondary amines in the core of the PAMAM dendrimers were protonated, imparting some electropositive repulsion on the PEG segment. The binding isotherms at both basic pH values showed larger extent of complexation between the α-CD and PEG segment since the PAMAM possesses less positive charges as seen from the scheme in Figure 4.3 and also from the zeta potential results shown in Figure 4.11. As expected, the binding enthalpy at pH 12 was larger than at pH 8 since the former was fully deprotonated, and thus, possessed no positive charges, and the threading of α-CD to PEG was enhanced.

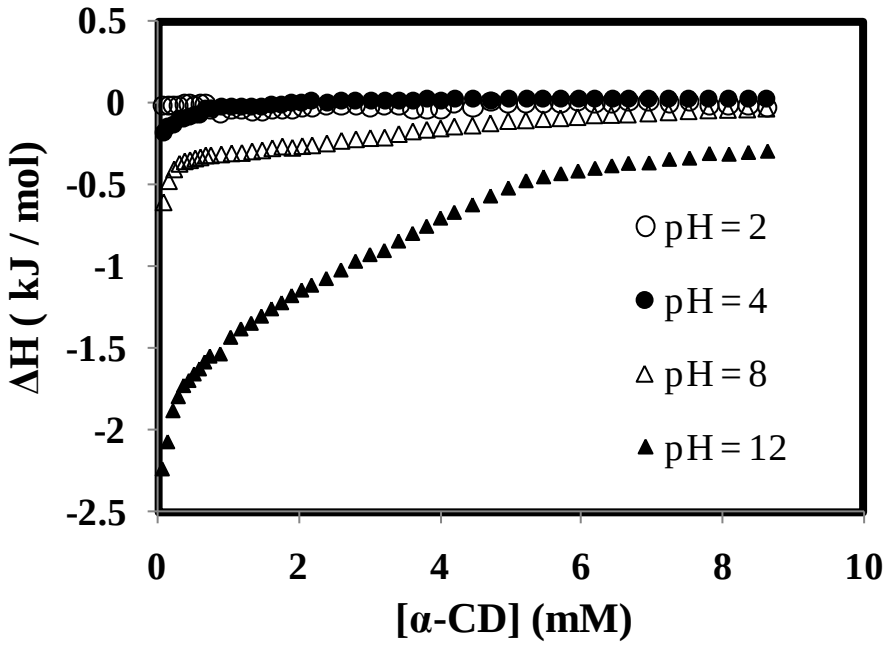

Figure 4.12 Differential enthalpy curves versus total α-CD obtained by titrating [α-CD] on 0.1wt% solution of PEGylated –PAMAM at different pHs:
pH=2 (○), pH = 4 (●), pH = 8 (Δ), pH=12 (▲)

Salt Effect: The ionic effect of PAMAM dendrimers on the complexation between α-CD and PEG was also studied by titrating a constant amount of 40 mM α-CD concentration into a PEGylated-PAMAM solution having different sodium chloride (NaCl) salt concentration. To reveal the effect of the salt on the binding process the titration was carried out at a constant pH of 4, where the primary amines on the outer most surface and part of the secondary amines in the core of the PAMAM dendrimers were protonated.

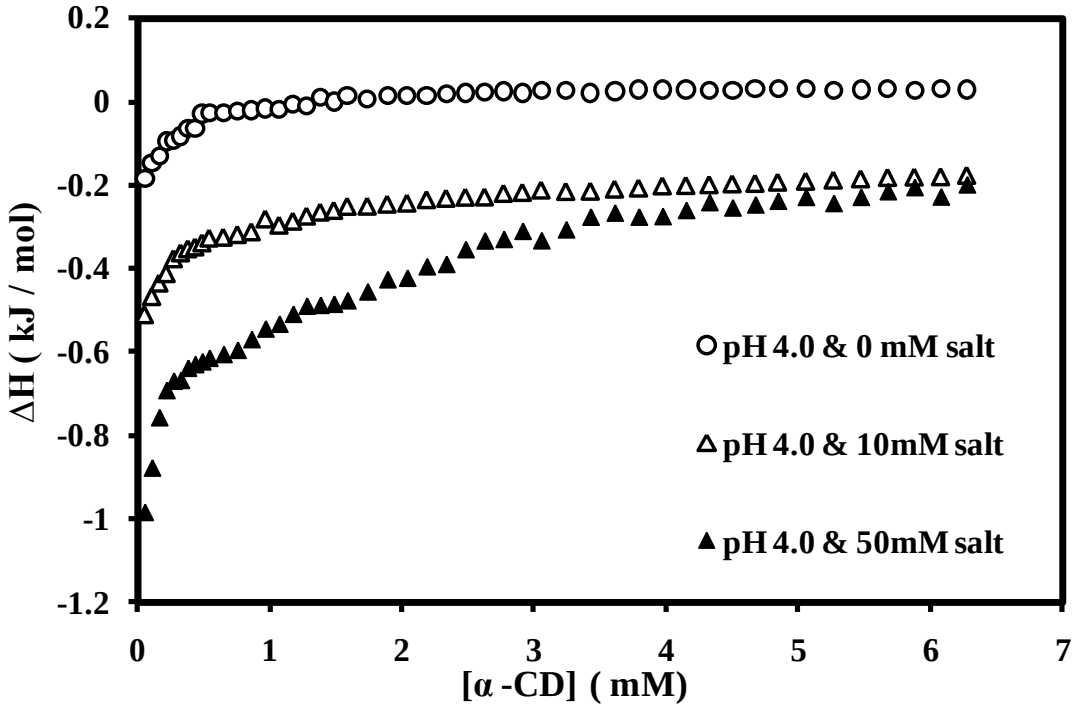

Figure 4.13 Differential enthalpy curves versus total α-CD obtained by titrating [α-CD] on 0.1wt% solution of PEGylated –PAMAM at pH=4 and different salt concentration: 0mM (○), 10mM (Δ), 50mM (▲)

As anticipated, increasing salt concentration resulted in a higher degree of binding between the α-CD and PEG chain (Figure 4.13). This is because a higher salt concentration would shield the positive charges present on the PAMAM dendrimers, facilitating the threading of α-CD on the

PEG segment. In some systems, electrostatic interactions are the main contributors for binding, and thus the presence of increasing salt concentration is expected to decrease the binding between the host and guest molecules. Previous studies conducted by Tam and coworkers (Wang et al., 2007) , showed that the addition of salt weakens the interaction of drug and polymer interactions by charge shielding effect on the carboxylate groups on the polymer, and the ionized amino groups on the drug. In our study, since the nature of binding is based on hydrogen bonding and hydrophobic effect, the shielding of positive charges by salt will enhance the binding between the host (α-CD) and the guest (PEG repeating units).

One binding site Model: A one-site binding model described was used to fit the binding isotherms at pH 8 and pH 12. The process of this fitting, along with the mathematical equations was previously described in section 3.4.2. Figure 4.14 shows the nonlinear fitting of the enthalpy curves. It can be seen that the fitting curves (solid red lines) show good agreement with the experimental data expressed by the closed symbols, indicating that the fitting model is appropriate and the thermodynamic parameters derived from the fitting curves are reliable. The thermodynamic parameters extracted from the model fitting are summarized in Table 4.1. The stoichiometric number, *n*, was found to be dependent on the pH value; where it increased from 0.38 to 1.29 upon increasing the pH from 8 to 12. As described by Harada and coworkers (Harada et al., 1992, 1996, 1997), the full threading of α-CD molecules on PEO takes place in a 2:1 ratio. In other words, each ethylene glycol (EG) repeating unit on PEG, binds exactly with two α - CD molecules. Therefore, at pH 8 only approximately 20 % of the total α -CD groups is bound to the PEG segments in the PEGylated-PAMAM dendrimers. On the other hand, at pH = 12, binding increases to approximately 70% reaching a stoichiometric number of 1.29. As shown in Table 4.1, a large negative enthalpy change (ΔH) was observed for both pH values,

suggesting that the inclusion complexation is enthalpy driven. The equilibrium constant, K, increased when the pH was increased to 12, and consequently the Gibbs free energy, ΔG also increased, suggesting a strong binding between α-CD and the PEG segments. This is consistent with the previous discussion that the absence of any electrostatic repulsion at very high pH values will facilitate the formation of inclusion complexes between α-CD and PEGylated-PAMAM dendrimers.

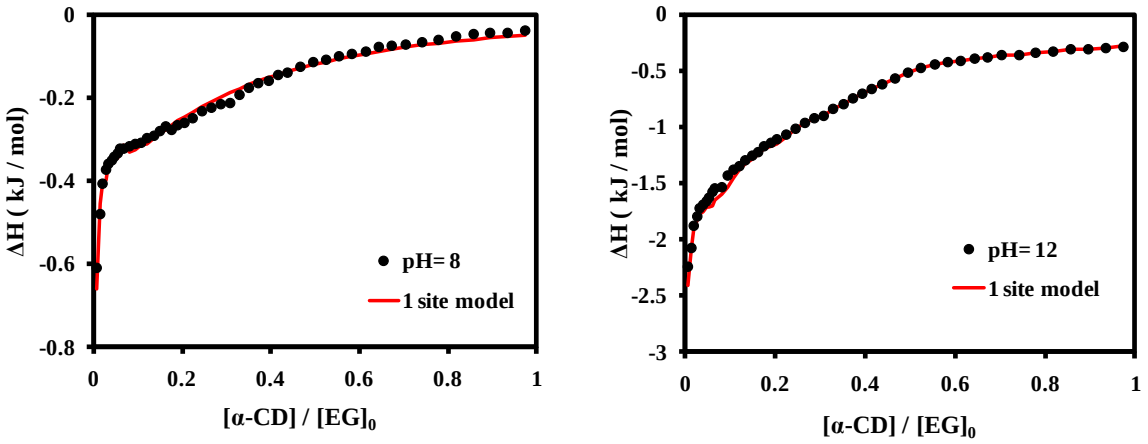

Figure 4.14 Nonlinear fitting curves of ΔH vs [α-CD]/ $[EG]_0$.

Table 4.1 Thermodynamic Parameters of the biding between α-CD and PEGylated-PAMAM dendrimers in aqueous solutions at 298 K

pH	*n*	K (mol^{-1}.L)	ΔH (kJ/mol)	ΔG (kJ/mol)	ΔS (J/mol.K)
8	0.38 ± 0.068	252 ± 75.1	-295.21 ± 34.1	-298.19	10.00
12	1.29 ± 0.021	474 ± 95.1	-1014.12 ± 110.3	-1017.35	10.84

Size and morphology: The size and morphology of the PEGylated-PAMAM / α-CD complexes at different pH values was studied using laser light scattering technique. Several solutions were prepared with increasing pH values and at a constant α-CD concentration (~ 7- 8 mM), and the microstructure was examined using the Brookhaven DLS system. Figures 4.15 and 4.16 show the distribution functions for several scattering angles and the decay rate at those angles at three pH values (2, 5, and 8), respectively. The hydrodynamic radius R_h, was calculated using the Stokes-Einstein equation, $R_h = \frac{kTq^2}{6\pi\eta\Gamma}$ (k is the Boltzmann constant, T is the absolute temperature, η is the solvent viscosity and R_h is the hydrodynamic radius). The size of the α-CD / PEGylated-PAMAM complex at pH =2 was the lowest with a R_h value of 6.8 nm, which corresponds to the individual PEGylated-PAMAM particles (Luo et al., 2002). Increasing the pH value to 5 (at constant [α-CD]) resulted in the size increase to around 40 nm. This increase suggests that the binding between α-CD and PEG segments has commenced, and that some bridging between individual PEGylated PAMAM / α-CD complexes had occurred. Further increase in the pH to 8, will induce more bridging between the complexes and thus a larger R_h value of 73nm was observed. This is a very similar observation to the one previously described in concentration effect, where the increase in α-CD concentration at a fixed low pH value of 2 was believed to result in the size increase of PEGylated PAMAM/CD particles.

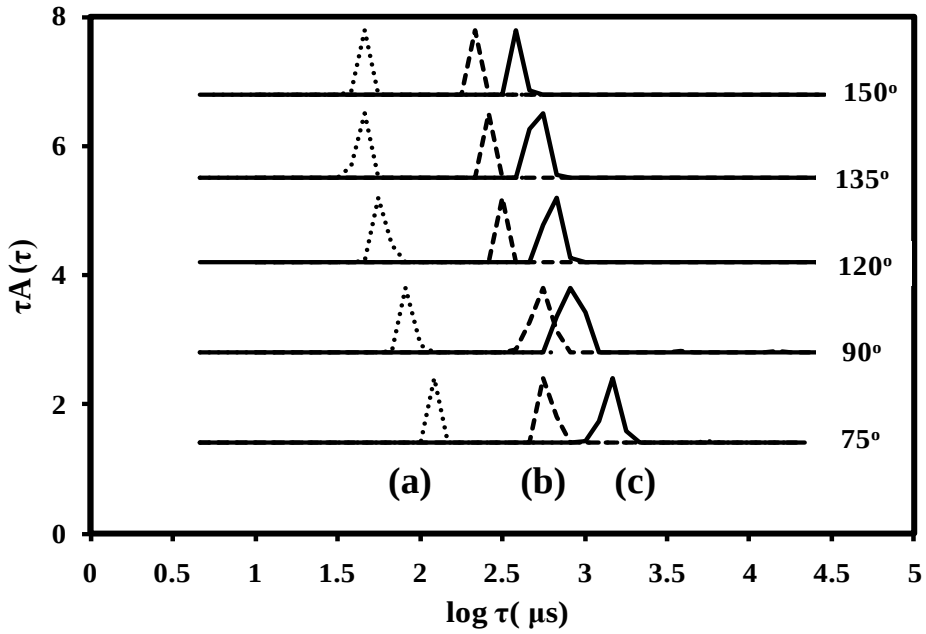

Figure 4.15 Relaxation distribution functions obtained from DLS measurement at [α-CD] ~ 8mM a) pH = 2, b) pH = 5, c) pH = 8

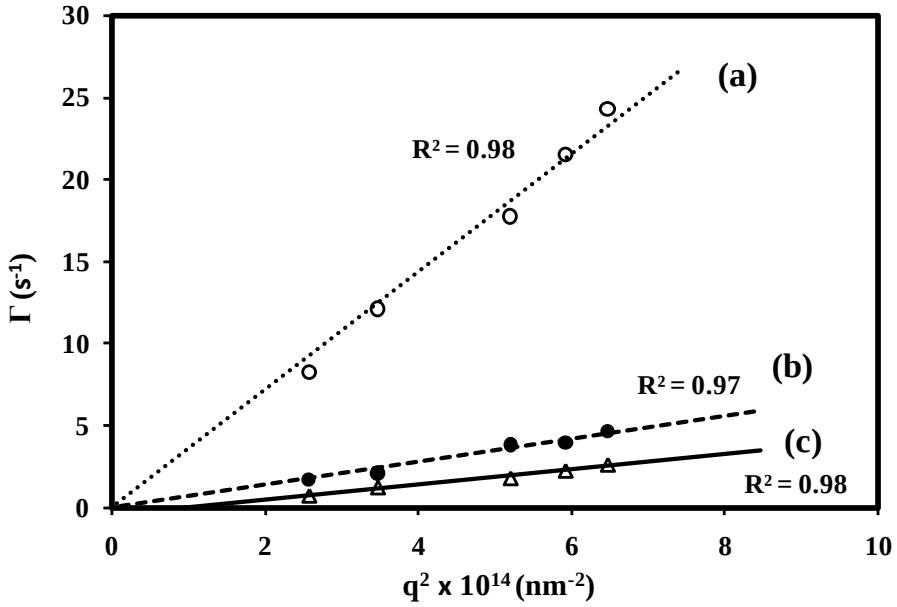

Figure 4.16 The dependence of the decay rate Γ on the square of scattering vector, q^2 , at (a) pH = 2 , (b) pH = 5, (c) pH = 8

A plot showing the dependence of hydrodynamic radius (R_h) and radius of gyration (R_g) on pH values at a constant α-CD concentration is shown in Figures 4.17 (a and b). At low pH values (< 5) the R_g and R_h values were similar, showing a slight increase from the normal size of isolated PEGylated-PAMAM dendrimers at approximately 6.7 nm. However, with increasing pH (≥ 5), the hydrodynamic radius (R_h) increased by about 1.8 times from 39.5 nm to 73.6 nm, and the radius of gyration (R_g) increased about 2.2 times from 36.4 nm to 80.4, at pH = 5 and pH = 8 respectively. We believe that at higher pH values, the electrostatic repulsion from the positive charges on the PAMAM dendrimers will be reduced significantly allowing for additional complexation between α-CD and PEG segments and thus a further size increase of the complexes. The morphological transformation of the dendrimer and the dendrimers/CD complexes was also observed, similar to section 4.12, as shown from the R_g/R_h data in Figure 4.17 (c). With increasing pH values, a gradual increase was observed for R_g/R_h starting at 0.86 at pH = 2 and increased to 1.49 at pH = 12. This value is very close to the theoretical Gaussian chain (1.50), also suggesting a similar observation as the one described in section 4.1.2, where the inter-particle association between the complexes result in the formation of a larger aggregate with a Gaussian distribution of the polymeric chains.

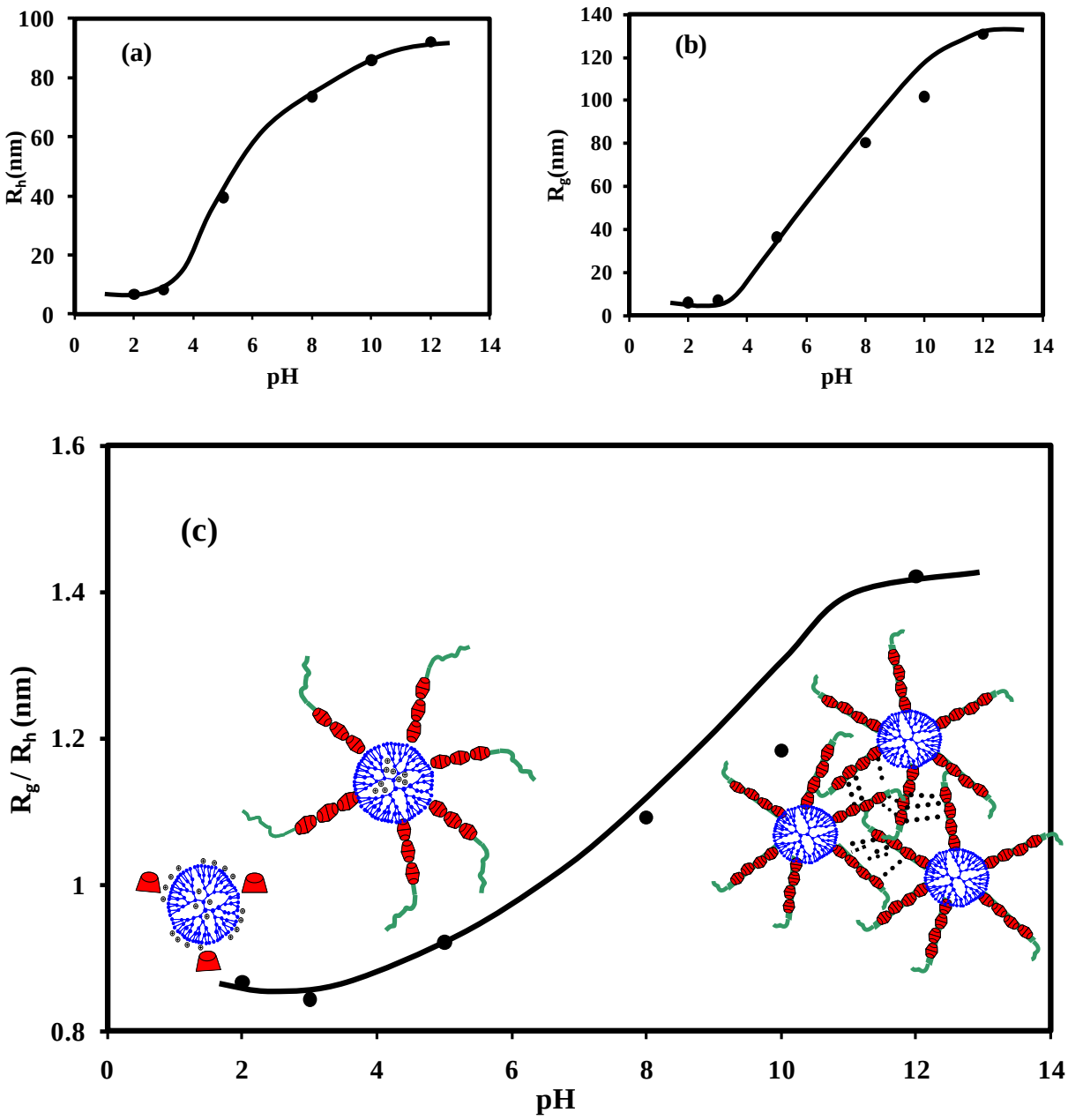

Figure 4.17 Particle size of PEGylated PAMAM at increasing pH values with constant [α-CD] ~ 7-8 mM) a) R_h, b) R_g , c) R_g/R_h

The mechanism that summarizes the threading and association of the PEGylated-PAMAM/α-CD complex at increasing pHs is illustrated in Scheme 4.2. At pH < 4 no threading of α-CD on PEG segments took place. However, threading was initiated as the pH increased from 5 to 8, at a

constant concentration of α-CD. Further increase in the pH results in the bridging and the formation of larger aggregates as previously observed in the concentration effect.

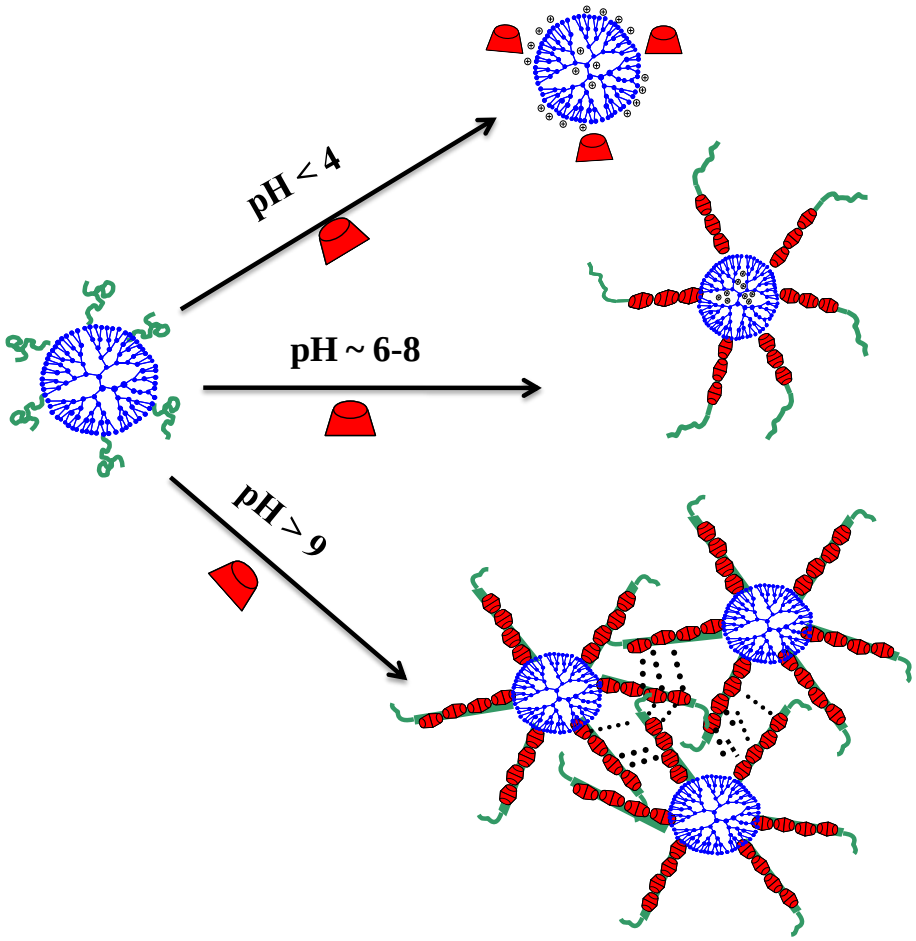

Scheme 4.2 Schematic diagrams showing α-CD complexation on PEGylated-PAMAM dendrimers at different pHs (at [α-CD]=7-8 mM)

Conclusions

We report on the pH and concentration dependence for the binding of α-CD and PEGylated-PAMAM dendrimers. Both pH and α-CD content play a vital role in the binding process, where a critical α-CD concentration is required to induce the threading of α-CD onto PEG chains at low pH. The size and morphology of the PEGylated-PAMAM dendrimers transformed from a star-like to a Gaussian-like aggregate with increasing pH and α-CD concentration. Because the polymers used in this work (LPEI and PAMAM) have a unique responsive character, this study provides insightful information on host guest interaction particularly with cyclic sugar like molecules such as α-CD

.

4.2 Determination and Prediction of Physical Properties of Cellulose Whiskers

Overview:

Nanocrystalline cellulose has attracted increasing interest due to their biocompatibility, rigidity, and potential applications in biomedicine and cosmetics. In this communication, we used a parameter estimation technique to calculate both the average dimension of cellulose whiskers with different aspect ratios, and their dynamic physical parameters denoted by the translational (D_t) and rotational diffusion (Θ) coefficients. For rod with L/d ratio equal to 17, the experimental D_t and Θ values produced calculated length (L) and diameter (d) values showing close resemblance to experimental results as determined from microscopy techniques with a significant decrease in percent error approaching 0.22 and 0.27% for L and d after 1000 iterations, respectively. The calculated translational and rotational coefficients converged to a minimum value of 5.048×10^{-12} $m^2.s^{-1}$ and 551.9 s^{-1} with the latter requiring larger number of iterations to reach convergence. Close resemblance was shown between experimentally obtained and calculated of dimensions and dynamics (L, d, D_t , and Θ) of various nano-crystalline rods as obtained from various sources. By combining the theoretical model formulated by Broersma and the computational method utilizing a Nelder-Mead simplex direct search algorithm, reliable prediction of the average sizes of our own nano-crystalline cellulose (NCC) from light scattering data was obtained; resulting in an average L = 305.6 and average d = 15.1 nm. The proposed approach provides a suitable and simple method to determine the length and diameter of rod-like nanoparticles, such as nanocrystalline cellulose.

Introduction:

Inspired by the growing environmental issues, there is a major interest in finding new materials that are biodegradable and environmental friendly (Azizi Samir, et al., 2005). Materials derived from natural resources have attracted increasing interest from the industrial and scientific communities. Of particular importance, the preparation of novel bio-nanocomposites, based on biopolymers such as nanocrystalline cellulose, has drawn specific attention. It is expected that these types of nanoparticles will open new areas for medical, packaging and electronic applications. The main advantages of cellulose in these applications are: 1) renewable source in nature, 2) wide variety of fillers available throughout the world, 3) non-food agricultural based economy, 4) low energy consumption, 5) low cost, 6) low density, 7) high specific strength and modulus (Favier, et al., 1997), 8) high sound attenuation of lingo-cellulosic based composites (Azizi Samir, et al., 2005), 9) comparatively easy processability due to their nonabrasive nature (Siqueira, et al., 2009, Sanchez-Garcia and Lagaron, 2010), which allows high filling levels, resulting in significant cost savings, 10) relatively reactive surface, which can be used for grafting specific groups (Azizi Samir, et al., 2005).

The crystallinity and dimensions of cellulose depend on the origin of these fibers. For the cotton whiskers, electron microscopy gave averaged dimensions of about 10-15 nm in diameter and 250-300 nm in length, and about 15 nm in diameter and 2000 nm in length for tunicate (De and Borsali, 2002). Cellulose rod-like whiskers are known to possess anisotropic character, that is, they are directionally dependent in both shape and optical properties, which makes them good candidates for study by dynamic depolarized light scattering (DDLS). This technique is quite powerful in determining the dynamic properties of the microcrystallites, namely the translational and rotational diffusion coefficients (D_t in m^2/s and Θ in s^{-1} respectively). However,

characterization of cellulose dimensions is not an easy task because the aspect ratio (Length / diameter) of the rods is generally large. The dimension of a cellulose nano-whisker is also difficult to characterize since the dimensions are usually not very robust because of the low stiffness of the whiskers. Characterization techniques, such as microscopy gives an estimate of the aspect ratio (Habibi, et al., 2010, Kvien I., Tanem B.S. and Oksman K., 2005). However, it is pertinent that accurate dimension of the whisker should be determined as they are important parameters for mechanical modeling where cellulose is used as a reinforcing phase in polymeric matrix composites (Terech, et al., 1999). Terech and co-workers (Terech, et al., 1999) have carried out experimental measurements on cellulose microcrystalline rods with an average length of 1 μm using small-angle scattering technique (neutron and X-rays). The cross-sectional morphology was found to have a radius of 88 A^{o}. Their neutron scattering intensity vector, Q, was also measured and was found to have negligible influence on the shape of the scattering curves, even at low Q, hence there is no significant concentration-dependence on the aggregation process. Van Der Zande et al. (Van, et al., 2000) carried out the characterization of gold nano-rods using dynamic light scattering and electrophoresis techniques. These researchers found that the average length of the gold particles ranged between 390 and 730 nm, and the diameter was approximately 17 nm. The experimental and theoretically calculated dynamics of these gold nano-rods (using modified version of Broersma models showed better agreement when poly (vinyl pyrrolidone) (PVP) adsorption layer was included in the theoretical calculations. One significant aspect of their work is that comparisons were made between experimental and theoretical values that suggested that theoretical modeling can provide good insight on the characteristics of the nanostructures. However, no detailed explanation on the theoretical prediction technique of the model was provided. Soon after, De Souza et al. (De and Borsali,

2002, De, et al., 2003) used similar techniques to determine the dynamic properties of fractionated microcrystal cellulose "whiskers" utilizing elastic and quasi-elastic light scattering techniques. It was noted that effective diffusion coefficient ($D_t = \Gamma (q)/q^2$) was inversely proportional to the structure factor S (q), which is directly related to the dimensions of the cellulose. In addition, the results showed that the mobility M (q) is independent of q (scattering vector) according to the general Ferrel-Kawasaki expression for the apparent diffusion coefficient. This result has often been seen in other whiskers where the mobility has minimal dependency to the scattering angle since at high q values the diffusion is dominated by D_t and D_{rot} (Θ) which are the only motions capable of modulating the intensity when the rods are oriented nearly perpendicular to q (De and Borsali, 2002). The same group also conducted a study on the dynamics and dimensions of cellulose whiskers using similar techniques in addition to using electric birefringence (TEB). Using their experimentally calculated dynamics with $D_t = 5.5 \times 10^{-8}$ cm^2/s, $\Theta_{DDLS} = 552$ s^{-1}, and $\Theta_{TEB} = 536$/s (De, et al., 2003) and the full version of Broersma's relations (Broersma, 1960a, Broersma, 1981), the rotational and translational diffusion coefficients produced dimensional values with length equal to 255 nm and cross-section diameter of 15 nm. These values along with other calculated experimental and theoretical parameters gave good understanding on how dynamic parameters could result in reasonable structural analysis of rodlike whiskers (De and Borsali, 2002, De, et al., 2003) . Thus, most of the current work focused on the experimental determination of the dimensions and dynamics properties of cellulose whiskers, but very few studies have focused on determining these values theoretically.

Previously, the simulation techniques focused on Molecular Mechanics (MM) approach to model microcrystalline cellulose structures and their interactions with other molecules, such as water.

Mathews et al. (Matthews, et al., 2006) demonstrated that the surface of microcrystalline cellulose surfaces highly structure the water solution in contact with them. They also showed that the primary mechanism for this structuring is direct hydrogen bonding with the first layer of cellulose that localizes the water molecules that are hydrogen bonded to the cellulose surface. Other simulation methods use the Halpin-Kardos theoretical mean field mechanical model to predict the elastic modulus of short-fiber composites (Azizi Samir, et al., 2005).

In this paper, we use an optimized simulation technique to solve a parameter estimation problem for the purpose of calculating both the dynamics (D_t and Θ) and dimensions (L and d) of several cellulose whiskers of different aspect ratios. The method utilizes an optimization routine with built-in MatLab function to solve a model developed by Broersma (Broersma, 1960a, 1960b, 1981). The syntax runs over several iterations for a range of generated initial guessed values. One major significance of our work stems from the fact that computing the dimensions of cellulose by theoretically fitting D_t and Θ values obtained from light scattering data, yield more representative information on the size of nanocrystals since large number of particles are sampled as compared to TEM or other microscopic techniques. In addition, the sample preparation and time required to acquire such information is significantly shorter and simpler. When comparing our calculated values and the previously obtained experimental values from literature we noted very close resemblance. In addition, we observed an expected inverse proportional relation between dynamics and dimensions.

Mathematical Models and Methods:

The theoretical development describing the dynamics of nano-rods was advanced by Broersma and co-workers, (Broersma, 1960a, 1960b, 1981) where the relationship between the translational and rotational diffusion coefficients were correlated with the dimensional parameters of nano-rods of a given aspect ratio (L/d). In order to understand the governing equations, it is indispensible to observe the atomic-level of the particles and the forces that govern their movement within the aqueous media. Initially, O'Konski and Haltner were able to measure the rotational diffusion constant D_r (Θ), of a monomeric unit of Tobacco Mosaic Virus (TMV) in water. Theoretically, the rotational coefficient is related to the Burgers' torque constant of a cylinder:

$$T/\omega = \frac{8\pi\eta a^3}{3}\left[\log(2a/b) - 0.80\right] \qquad (4.1)$$

where ω is the angular velocity, b is the half width of the particles, and η is the viscosity of the solvent. (Broersma, 1960b)

From Equation (4.1), it is obvious that a proportional relationship exists between torque and angular velocity of a rotating sphere or cylinder shaped rod. Moreover, it is consistent with the theory that the frictional viscous torque is proportional to the angular velocity to the first power. This ratio is directly related to the rotational diffusion coefficient (Θ) (with units of radians^2/s). It is given by the angular drift velocity $\Omega_d = (d\theta / dt)$ in response to an external torque Γ_θ i.e. T (assuming that the flow stays non-turbulent and that inertial effects can be neglected) (Garcia de and Carrasco, 1998). The relationship between the rotational diffusion coefficient and the rotational frictional drag coefficient was derived by the Einstein relation (or Einstein–Smoluchowski relation):

$D_r = \Theta = \frac{k_B T}{f_r}$ and $f_r = 8\pi\eta a^3$ f_r being the drag force, k_B as Boltzmann constant and T the absolute temperature.

The derivation of the translational diffusion coefficient is analogous to the above expressions for Θ.

Therefore, using these equations, Broersma derived both the rotational and translational diffusion coefficients with the dimensions of any cylindrical macromolecule (rod-like particles) as shown in Equation (4.2) (Broersma, 1960b, Broersma, 1981):

$$\textit{Translational Diffusion: } D_t = (k_b T / 3\pi\eta L)\left[\delta - \frac{1}{2}\gamma_{\text{II}} - \frac{1}{2}\gamma_{\perp}\right] \text{ where } \delta = \ln(2L/d)$$

$$\gamma_{II} = 0.807 + \frac{0.15}{\delta} + \frac{13.5}{\delta^2} - \frac{37}{\delta^3} + \frac{22}{\delta^4}$$

$$\gamma_{\perp} = -0.193 + \frac{0.15}{\delta} + \frac{8.1}{\delta^2} - \frac{18}{\delta^3} + \frac{9}{\delta^4} \qquad (4.2)$$

$$\textit{Rotational Diffusion: } D_r = \Theta = (3k_b T)/(\pi\eta L^3)[\delta - \rho]$$

$$\rho = 1.140 + \frac{0.2}{\delta} + \frac{16}{\delta^2} - \frac{63}{\delta^3} + \frac{62}{\delta^4}$$

The adopted mathematical model calculates the force distribution in a moving object that produces a certain velocity at its surface. Once the force density is known, the torque can be calculated and the diffusion coefficient can be deduced from the above correlation. The high order polynomials come from the force expansion factor, which is originally described by the following equation 4.3 (Broersma, 1960a):

$$\upsilon(x) = \sum_{n=0,1}^{\infty} (x/a)^n \sum_{k=0,1}^{\infty} (c_n)(B_k) \qquad \textit{while having } \sigma = \ln\left(\frac{2a}{b}\right)$$

$$\textit{resulting in coefficients } c_{kk} = 2\sigma + 1 - \sum_{l=1,2}^{k} \frac{2}{l} \qquad (4.3)$$

$$c_{kn} = \frac{2}{k-n}$$

Table 3.1 shows the values of the coefficients as calculated by Broersma for a rod-like cylinder rotating or translating perpendicularly or parallel to the axis of the cylinder. These factors are based on the theoretical calculation of the final version of the γ expansion given by:

$\gamma = \sum_k a_k \sigma^{-k}$ where $\sigma = \log \frac{2a}{b}$, which is expected to provide more accuracy to the calculated force; however an analytical determination of polynomial to the fifth order becomes mathematically difficult to obtain.

Thus the final version of the expansion coefficients will be:

$$\gamma = a_0\sigma^{-1} + a_0\sigma^{-2} + a_0\sigma^{-3} + a_0\sigma^{-4} \tag{4.4}$$

It is to be noted that the calculation of the rotational diffusional coefficient is less accurate than the translational one because of the $1/L^3$ factor which produces a more sensitive Θ measurement. It is apparent that, this may result in instability of the calculated Θ values produced by this specific function. Garcia et al. (Garcia de and Carrasco, 1998) calculated and developed alternative coefficients that possessed a second order polynomial instead of the fourth order. Their model also predicts the translational diffusion coefficient, D_t, for rods with Brownian motion and a finite L/d ratio (Equation (4.5)) (Garcia de la Torre, J. & Bloomfield, V. A., 1981). Unfortunately, the form of their equations produces significant discrepancies in the calculated rotational diffusion coefficient (D_r or Θ) values:

$$\begin{aligned} D_t &= (k_b T)/(3\pi\eta L)\left[\delta + 0.312 + 0.565\lambda + 0.100\lambda^2\right] \\ D_r &= \Theta = (3k_b T)/(\pi\eta L^3)\left[\delta \quad 0.662 + 0.917\lambda \quad 0.050\lambda^2\right] \\ \text{where} \rightarrow\ & \delta = \ln\left(\frac{2L}{d}\right) \text{ and } \lambda = \frac{d}{L} \end{aligned} \tag{4.5}$$

In this study, the model developed by Broersma's was adopted since it yielded a more accurate and precise prediction of the dimensions of the rod-like cellulose whiskers. However, in both

equations (4.2 and 4.5), direct dependency between the two diffusion coefficients and the length and diameter of the rods were noted, which imposes both, non-linearity to the system and sensitivity to initial guesses. However, such non-linearity can be solved by several well-known optimization methods. The non linear relationship between D_t and Θ to its corresponding L and d should not be surprising since each rod has unique dynamic physical properties which can be measured by various instruments, such as light scattering, etc.

Finally, it is vital to describe briefly the solution technique used for this purpose. The MATLAB "fminsearch" optimizer finds the minimum of a scalar function of several variables, starting at an initial estimate. This is generally referred to as unconstrained nonlinear optimization. As mentioned earlier, it uses the Nelder-Mead simplex algorithm as described by Lagarias et al. (Jeffrey C.L. et al., 1998). The Nelder-Mead algorithm is especially popular in the fields of chemical engineering, chemistry and medicine. The algorithm uses a simplex of $n + 1$ points for n-dimensional vectors x. It first makes a simplex around the initial guess x_0 (x_0 & y_o if 2 dimensional) by adding 5% of each component $x_0(i)$ to x_0, and using these n vectors as elements of the simplex in addition to x_0. One or more test points were computed, along with their functional values, and the iteration terminates when it satisfies the preset tolerance limit. The different processes of the algorithim are known as Reflect, Expand, Contract inside and Contract outside (Jeffrey C.L. et al., 1998). Depending on the step used, the Nelder-Mead simplexes will result in a value either closer or further away from the predicted value. The solution procedure adopted throughout this project is visualized in Figure 3.10

The adopted procedure starts by inputting the constant values: viscosity (η), Boltzmann constant (K_b), temperature (T), experimentally obtained translational diffusion coefficient (D_t) and rotational diffusion coefficient (Θ). Then the program is initialized by the using the generated random initial guessed values for length (L) and diameter (d) dimensions (L_o, d_o). Subsequently, L and d values can be calculated with an average $\bar{L}$ and $\bar{d}$ and error $\varepsilon_{\bar{L}}$ and $\varepsilon_{\bar{d}}$. Furthermore, a convergence of both functions presented in equation 4.2 is validated. Finally, all experimental dynamic and dimension values (obtained from different sources) are fitted and compared to their respective calculated values.

Results and Discussion:

Calculations

Usually, experimental values of dimensional parameters (i.e. Length (L) and diameter (d)) are obtained using microscopic techniques such as TEM, SEM and AFM. On the other hand, dynamic parameters (D_t and Θ) could be obtained from light scattering techniques, in which the intensity average autocorrelation function (IACF) is fitted to single exponentials including a second cumulant *(c* (*k*)) to account for polydispersity as given by Equation (4.6) (Van, et al., 2000):

$$y = \alpha + \beta \exp(-b(k)t + c(k)t^2) \tag{4.6}$$

In the Vertical-Vertical (V-V) polarization mode the decay exponent (*b* (*k*)) corresponds to:

$$b(k) = 2D_t k^2 \tag{4.7}$$

and in the Vertical-Horizontal polarization (V-H) mode to:

$$b(k) = 2D_t k^2 + 12\Theta \tag{4.8}$$

The rotational diffusion coefficients are determined from the intercept of the linear fit obtained in the V-H mode (De, et al., 2003, Van, et al., 2000). The translational diffusion coefficient, D_t, and rotational diffusion coefficient, Θ, values can now be used in the model described above to calculate the length and diameter of the rod- like particle, which subsequently could be compared to their respective experimental values, L^* and d^*. However, due to the non linear nature of the model (Eq. 4.2), different initial guessed values often yield results that do not agree with experimentally measured values. In addressing this problem, random initial guesses were generated (covering a wide range of values) and used to solve the functions in Eq. (4.2) to obtain L and d. Each of the calculated variables (L and d) has an absolute error of:

$$\varepsilon_{\bar{L}} = \left| \frac{L^* - \bar{L}}{L^*} \right| x\,100 \qquad \varepsilon_{\bar{d}} = \left| \frac{d^* - \bar{d}}{d^*} \right| x\,100 \tag{4.9}$$

Since the initial guesses are not biased, predicted values, estimated as a function of these guesses, are more reliable. By adopting this approach, one can demonstrate the impact of initial guesses on predicted and derived parameters as compared to the experimental ones. In addition, the random generation of initial guesses allows us to perform many iterations over several realizations, using $[\,i = 1 : n\,]$ where n is the desired number of guessed values. In other words, $d_o(i)$ and $L_o(i)$ are the initial guesses and they produce the predicted values $d(i)$ and $L(i)$. The flow chart summarizing this explanation is this shown in Figure 4.18:

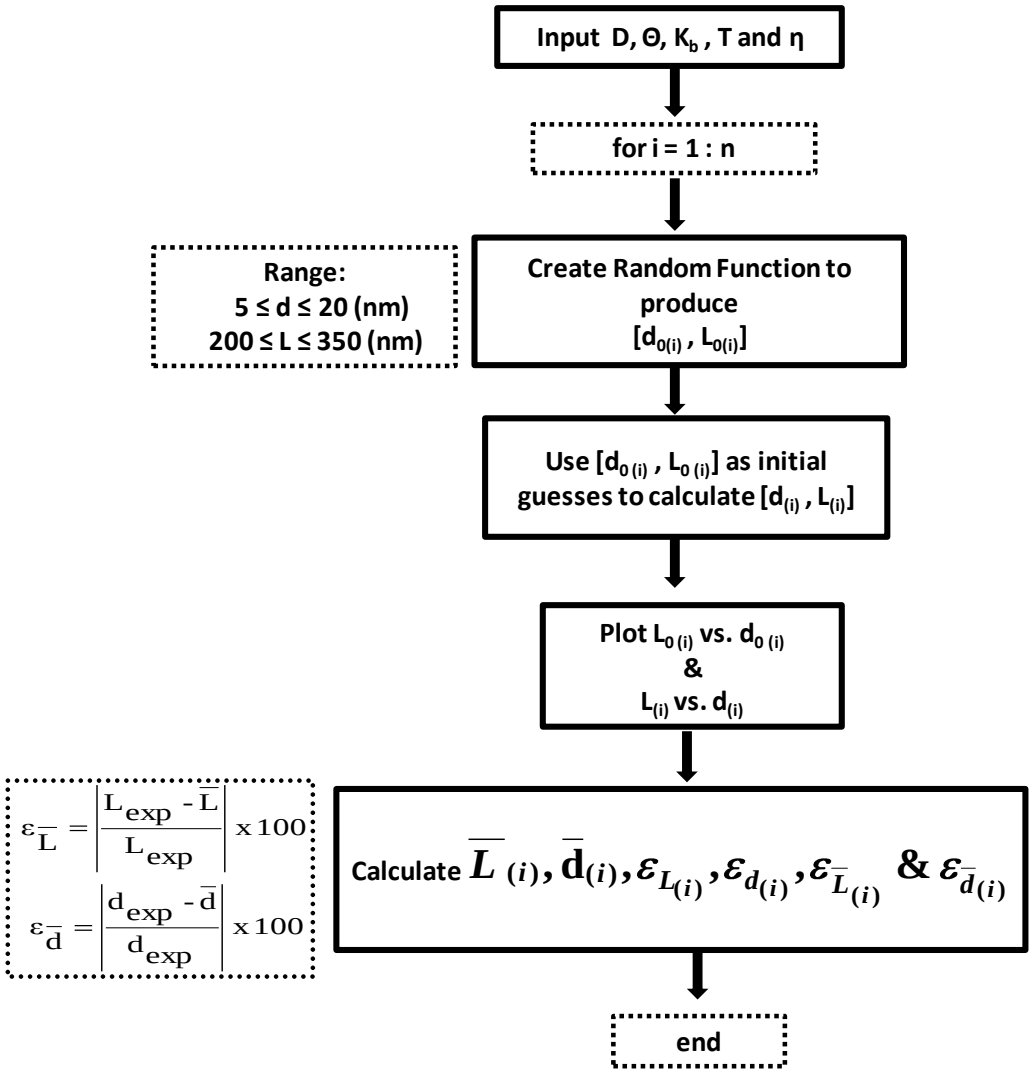

Figure 4.18. Flow chart summarizing the method adopted for calculating dimensional properties (n is number of iterations)

Validity of Model (Eq. 4.2) (Dimensions)

ROD 17 (Aspect ratio L/d=17): The average experimental L and d values as determined by TEM for these rods was L^{*} = 255 and d^{*} = 15nm respectively (De, et al., 2003, Lima and Borsali, 2004, Dufresne, et al., 1999). Table 4.2 shows the guessed and predicted values for ROD 17, and Figure 3 (a and b) shows a plot of the L vs. d as guessed values and, as output parameters (predicted values) at $i = 5$. The range of initial guesses for L and d was kept constant over the course of the simulations: $200\text{nm} \le \text{L} \le 350\text{nm},\ 5\text{nm} \le \text{d} \le 20\text{nm}$. This range is acceptable based on the range of experimental values obtained by TEM (De and Borsali, 2002 , De, et al., 2003, Lima and Borsali, 2004).

From Figure 4.19a we observe that the guessed values for L and d are randomly distributed over the range of initial guesses. Each of these values yielded predicted results as shown in Figure 4.19b. The experimental (red triangle) deviates from the average predicted value (green square) by 2.3% and 11.8 % for L and d respectively. This result is expected, since over a "division" of 5 points, the percent error of both predicted parameters (L and d) should be relatively high. Despite the large errors, all predicted points lie within a distinct region (L and d) as compared to the random scatter of points produced by the random function. Interestingly, this distinct region represents a straight line and is composed of linear combination of all predicted L and d values. The best fit straight line fit line is given by $y = a\,x + b$ where:

y is L, x is d, $\text{a} = -3.396$ and $\text{b} = 0.3059$. From Table 4.2 it has to be noted that the standard deviation, σ_{stand}, of the diameter dimension varies less than the standard deviation for the length dimension. This indicates that they are clustered closely around the mean value, represented by the calculated average shown in Figure 3b. However; it does not mean that the predicted values constitute a better estimate to the experimental one, since we note the relatively high percent

errors for all the diameters. This result provides an indication that there exists a smaller uncertainty of the repeated measurements in each of the calculated diameter parameters as compared to the length. As discussed earlier, this could be a result of the smaller range of initial guessed values for the diameter compared to a much larger one for the length.

Table 4.2 Length (L), diameter (d), and percent error values as obtained from random function compared to calculated value.

		Experimental L^{*} x 10^{-9}(m)	Experimental d^{*} x 10^{-9}(m)	Percent Error (%)	
		255	15		
Guessed L x 10^{-9}(m)	Guessed dx10^{-9} (m)	Calculated L x 10^{-9}(m)	Calculated d x 10^{-9}(m)	Error on L (%)	Error on d (%)
342.1	5.8	263.3	12.5	3.2	16.6
272.1	11.9	265.0	12.1	3.9	19.3
289.4	17.2	260.4	13.4	2.1	10.6
209.5	12.1	259.2	13.7	1.6	8.6
242.4	10.8	257.1	14.4	0.8	4.0
Average Calculated		**261.0**	**13.2**	**2.3**	**11.8**
Standard deviation		**3.160**	**0.925**		

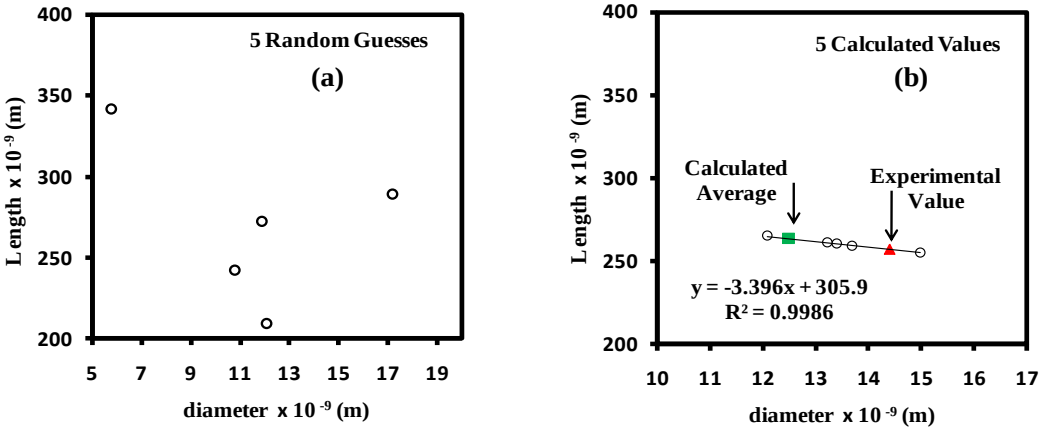

Figure 4.19. Plot of Length (L) vs. diameter (d) for 5 guesses

a) Initial guessed values as obtained by random function for 5 iterations

b) Calculated values as calculated by model for 5 iterations

Experimental value (▲) and Calculated Average (■)

We also note a high discrepancy between the percentage errors of each of the value for the predicted length and diameter. The reason behind this could be explained by the physical characteristics of the NCCs as the length is generally longer and more uniform (200-400 nm) compared to a shorted and irregular shaped diameter of 10-20 nm. The relatively small dimension of the diameter could contribute to additional numerical discrepancies at each of the iterations performed resulting in about 5.5 times higher percent error compared to the length. This is in agreement with the predicted results reported previously (Van, et al., 2000), and experimentally ones determined from microscopic techniques (Van, et al., 2000)' (De, et al., 2003). We anticipate that a better fit and smaller error would be obtained by increasing the number of iterations. Figure 4.20 shows the distribution of initial guesses and the predicted values for L and d with 1000 iterations.

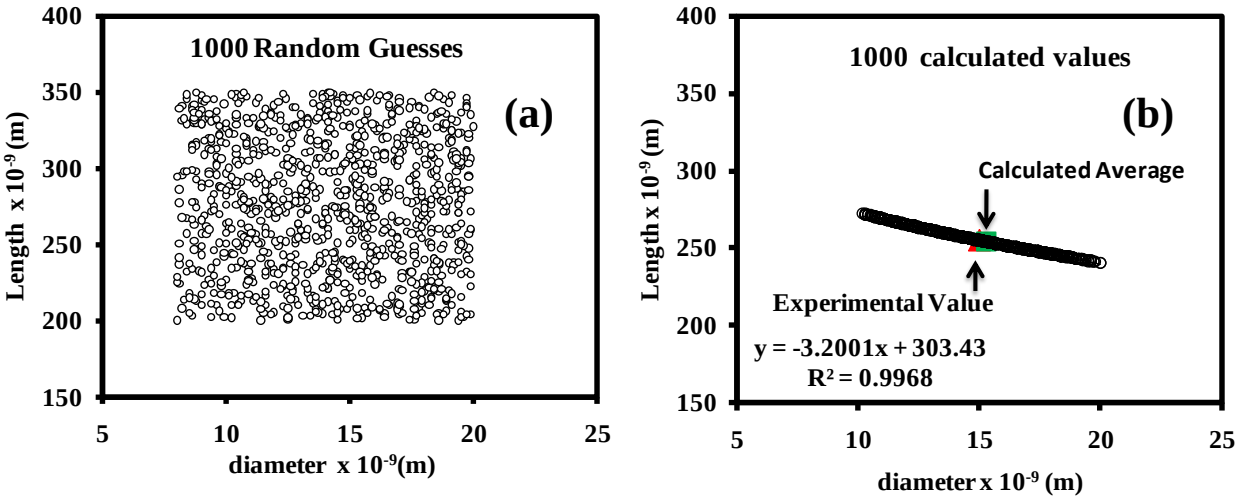

Figure 4.20 Plot of Length (L) vs. diameter (d):
a) Initial guessed values as obtained by random function for 1000 iterations
b) Calculated values as calculated by model for 1000 iterations
Experimental value (▲) and Calculated Average (■)

The calculated average value becomes much closer to the experimental result with an error approaching 0.22 % and 0.26% (compared to 2.3 and 11.8% for 5 iterations) for the length and diameter respectively. Therefore, with increasing number of iterations the percent error decreased for both L and d since both numbers approached that experimentally measured value. Figure 4.21 shows the relationship between L and d predicted from the model at various iterations. As the number of guesses / iterations was increased, the percent error decreased significantly, until the predicted values nearly coincides with the experimental one at $i = 1000$. In statistical terms, as we increase the number of iterations, governed by the range of initial guesses, the probability of our average calculated values for length and diameter to approach the experimental value would be much higher.

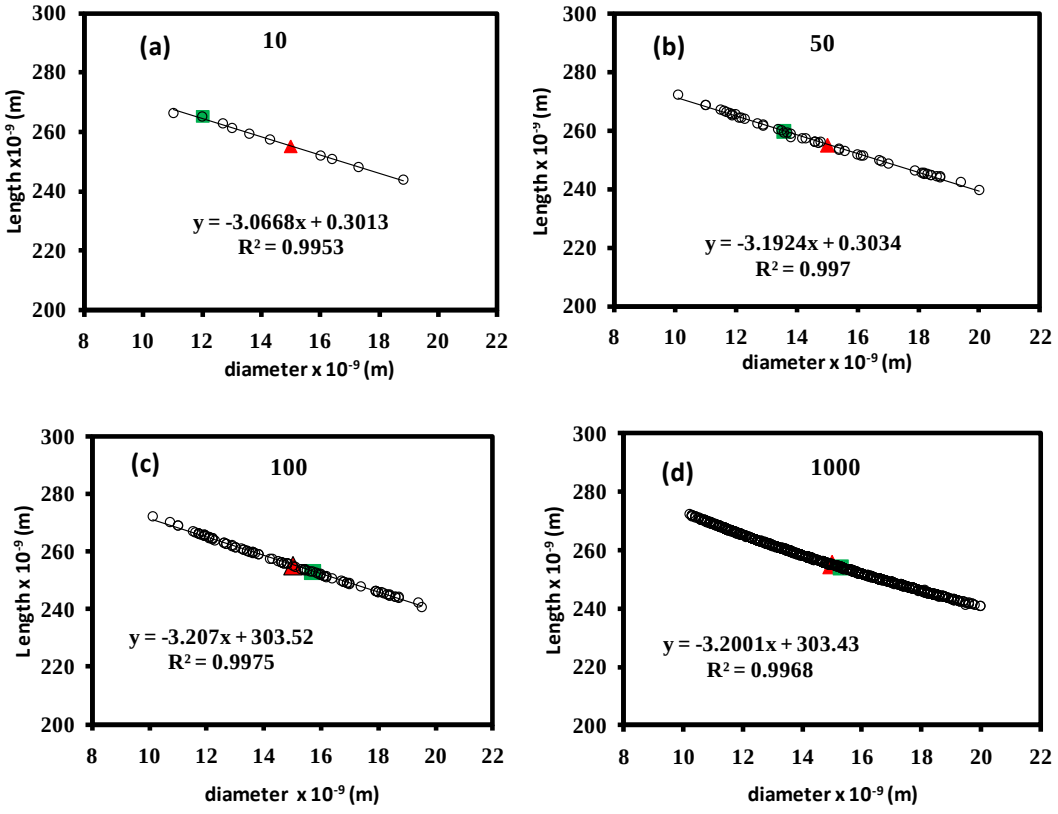

Figure 4.21. Plot of Length (L) vs. diameter (d) at: i=10 (a), i=50 (b), i=100 (c), and i=1000 (d)
***i* is number of iterations denoted by number of guesses**

As discussed before, we noted that all predicted L and d values were linearly dependent as demonstrated by the best fit straight line (Figure 4.21). This could be explained by a simple mathematical analysis of Equation 4.2, by examining on the factor $\delta = \ln \frac{2L}{d}$. In order to solve this non-linear equation, it is necessary to compute the critical points of D_t and Θ functions as represented by their 1st order optimality conditions. To do this, one has to calculate the partial derivatives of each of the functions with respect to L and d and equate them to zero:

$$\frac{\partial \mathrm{D_t}}{\partial \mathrm{d}} = \frac{\partial \mathrm{D_t}}{\partial \mathrm{L}} = 0 \text{ and } \frac{\partial \Theta}{\partial \mathrm{d}} = \frac{\partial \Theta}{\partial \mathrm{L}} = 0$$

We note that the result would be a linear dependency between these two variables L and d having a slope a and an intercept b i.e. $L = a \times (d) + b$

Both researchers, Broersma and Burgers infer that both dimensional parameters are non-linearly dependent on the dynamics (D and Θ) of the rod as observed from the measurement of the torque of a cylinder (Broersma, 1981). The adopted model can be linearized into a linear equation once we solved and took the first derivative of the two functions with respect to their independent variables, L and d. Furthermore, one understands the physical dependency between L and d by observing the shape of the cellulose fibers, which is usually considered as a long cylindrical rod that maintains an optimized surface area, hence increasing length will result in a corresponding reduction in the diameter. From the best fit line over the chosen region, one would be able to calculate the length or diameter via extrapolation. The percent error at various numbers of guesses is shown in Figure 4.22. The calculated values decreases significantly after the 20th iteration where it approached a value of 0.22 and 0.27 % at 1000 guesses for the length and diameter dimensions respectively.

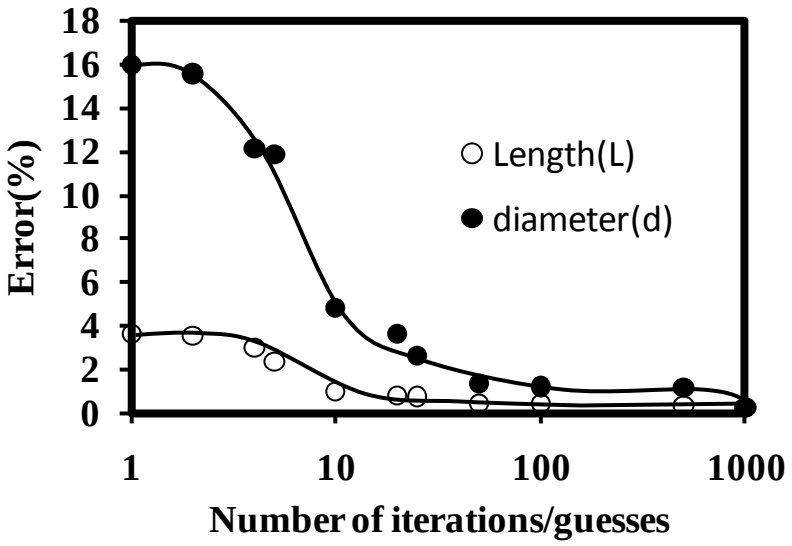

Figure 4.22 Plot of length and diameter error percent at increasing number of iterations

Stability test: It is important to test the effectiveness of Equation (4.2) by performing a simple stability test on the two functions, D and Θ. This could be done by identifying the converged value of D and Θ corresponding to the minimum value of the optimized function at several iterations of calculated L and d. The main motivation of doing this is to monitor how both functions vary with increasing number of guesses at various dimensional values (L and d). As shown in Figure 4.23, after the 50^{th} iteration, the calculated translational diffusion coefficient, D_t, reached a converge minimum value of 5.048 $x10^{-12}$ m^2/sec. The calculated Θ required greater number of iterations (after 200 guesses) to reach its final converged value at 551.889 s^{-1}. As noted by Broersma, the third power dependence of L introduces greater sensitivity to Θ, as reflected by the convergence results (Broersma, 1981) .

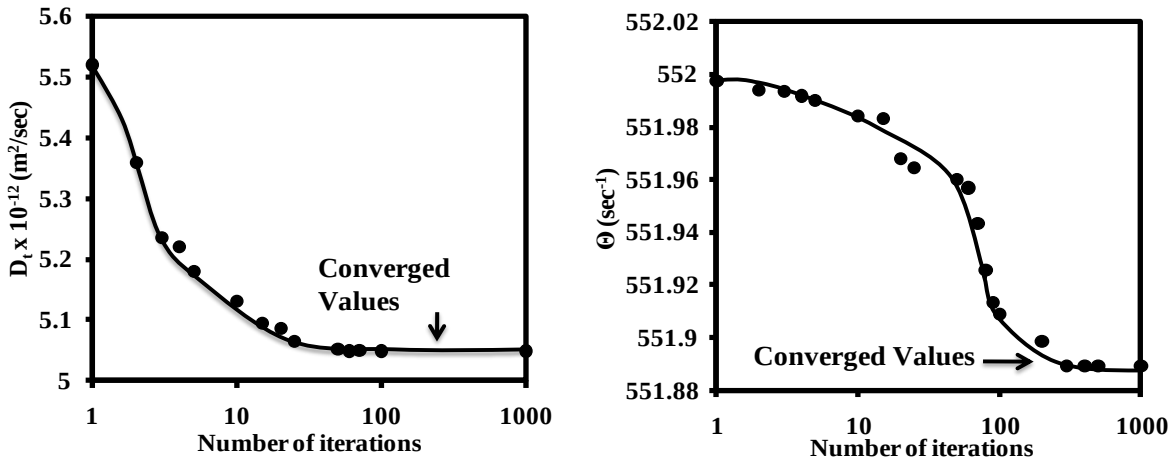

Figure 4.23 Stability: Plot of the calculated translational D_t and rotational Θ diffusion coefficient D_t and Θ values at the minimum value of the optimized function

Dynamics vs. Dimensions

The dimensional parameters are not the only important properties to be studied in rod-like cellulose whiskers, but dynamics also play a vital role to fully understand how they behave in aqueous media. The measured dynamic or dimension values for rods with $8.5 \le \frac{L}{d} \le 72.5$ can be fitted using the functions developed for smooth cylinders. This allows us to compare between predicted and experimental values for each of the dynamic and dimension properties of the nanocrystalline cellulose. Table 4.3 shows the calculated results of D_t from experimental L and d, and Table 4.4 shows the calculated values of L and d from experimental diffusion coefficients (D_t and Θ). Finally a comparison between all experimental and calculated dimensions / dynamics is summarized in Table 4.5. The calculated values agree quite well with those obtained from experiments, except for ROD 14.5 and 48.6 which might be due to experimental error. All experimental D_t and Θ were obtained from other sources having error estimates of about $\pm 10\%$ (Table 4.4). Standard deviation values were used as calculated by Van der Zande et al. (Van, et

al., 2000), whereas percent error for the calculated L and d were approximated using Equation (4.6). It is important to note that in parameter estimation problems of this kind, differences between the model and the actual behaviour will always arise, as a result of deficiencies in the optimized functions and other approximations employed in the simulations (Matthews, et al., 2006). However, it must be remembered that the experimental values obtained from instruments (light scattering or microscopy), could also contain experimental errors, as has often been the case in previous studies (Kvien, et al., 2005, Van, et al., 2000).

Table 4.3 Calculated D_t values fitted from equation 2 using experimental L and d values as obtained by TEM elsewhere (Kvien, et al., 2005, Van, et al., 2000) **.**

System (ROD)(exp)	Length (nm) (exp)	σ(nm)	diameter (nm) (exp)	σ (nm)	D_t x10^{-12}(m^2/s) (cal)
8.6	146.0	37.0	17.0	3.0	7.0
14.5	240.0	40.0	16.0	3.0	5.6
17.0	255.0	30.0	15.0	3.0	5.4
17.2	259.0	60.0	15.0	2.0	5.3
17.4	279.0	68.0	16.0	3.0	5.0
44.0	660.0	68.0	15.0	3.0	2.2
48.6	729.0	20.0	15.0	3.0	1.9
72.5	1160.0	25.0	16.0	2.0	1.8
12.6	189.0	24.0	15.0	3.0	6.8
2.6	39.0	10.0	15.0	3.0	20.0

Table 4.4 Calculated Length and diameter as fitted from equation 4.2 using experimental D_t and Θ obtained by Light Scattering elsewhere (Van, et al., 2000) **.**

System (ROD) (cal)	Length (nm) (cal)	ε %	diameter (nm) (cal)	ε %	D_t x10^{-12}(m^2/s) (exp)	Θ (s^{-1}) (exp)
10.3	200.2	37.1	19.4	13.9	6.0	306.0
13.7	231.5	3.5	16.9	5.4	18.0	687.0
17.1	255.5	0.2	15.0	0.3	5.5	550.0
17.6	252.9	2.3	14.4	3.9	4.0	187.0
17.6	247.1	11.4	14.0	12.4	3.8	175.0
60.6	990.5	50.1	16.4	9.0	1.2	13.7
43.3	725.1	0.5	16.7	11.5	0.7	35.7
67.1	1102.2	5.0	16.4	2.6	1.5	11.0
15.1	300.6	59.1	19.9	32.9	4.9	281.0
10.3	200.2	37.1	19.4	13.9	6.0	ND

Table 4.5 Comparison between experimental and calculated Dimensions as well as experimental and calculated Translational Diffusion Coefficients

System (ROD)	Length (nm) (exp)	Length (nm) (cal)	diameter (nm) (exp)	diameter (nm) (cal)	D_t x10^{-12}(m^2/s) (exp)	D_t x10^{-12}(m^2/s) (cal)
8.6	146.0	200.2	17.0	19.4	6.0	7.0
14.5	240.0	231.5	16.0	16.9	18.0	5.6
17.0	255.0	255.5	15.0	15.0	5.5	5.4
17.2	259.0	252.9	15.0	14.4	4.0	5.3
17.4	279.0	247.1	16.0	14.0	3.5	5.0
44.0	660.0	990.5	15.0	16.4	1.2	2.2
48.6	729.0	725.1	15.0	16.7	0.7	1.9
72.5	1160.0	1102.2	16.0	16.4	1.5	1.8
12.6	189.0	300.6	15.0	19.9	4.9	6.8
2.6	39.0	ND	15.0	ND	ND	20.0

We can use the values obtained in the above tables to plot the translational diffusion coefficient (D_t) vs. the length and aspect ratio (L/d). Figure 4.24 shows a comparison between the calculated and experimental values. Previously, Van der Zande et al. (Van, et al., 2000) plotted the D_t values vs. 1/L and $1/L^3$ and they showed a clear 1/L dependence on the experimental D_t which agrees

qualitatively with the calculated value. This result is also evident from the plots shown in Figure 4.24, but instead we use length and aspect ratio as independent variables. The graphs show the expected inverse proportionality between the dynamic and dimension properties of cellulose, i.e. as dimensions become larger, the diffusional properties of cellulose in aqueous media are reduced. We also note small variations between the experimental and calculated D_t values for most of the non-crystalline rods as plotted in Figure 4.24. We focused on the translational diffusion measurements and not the rotational ones since, as described earlier; the Θ parameter is a more sensitive measurement because of its $1/L^3$ dependence. Furthermore, we focus on the length parameter since changes in D_t will induce a profound change in length, whereas relatively minimal change in diameter as shown in Table 4.3, 4.4 and 4.5.

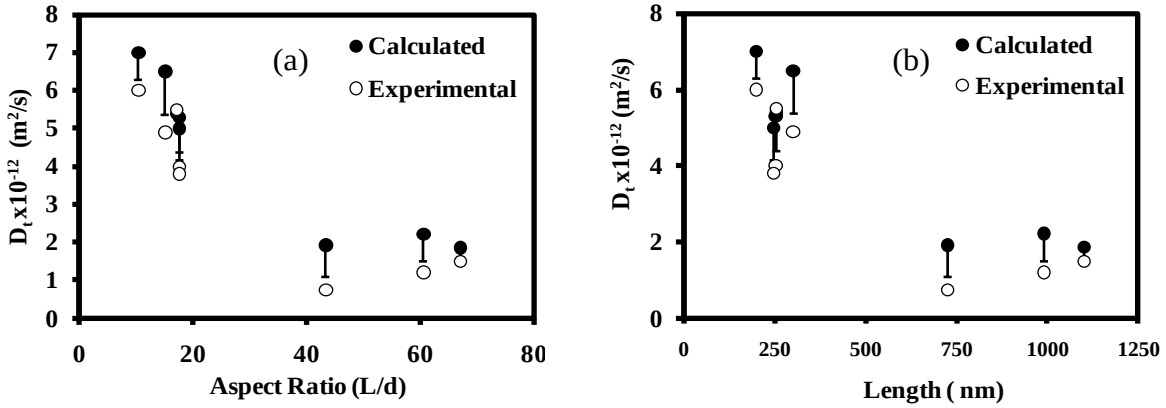

Figure 4.24 Plot of Calculated and experimental translation diffusion coefficient (D_t) vs. (a) L/d and (b) Length

A plot of the translational diffusion coefficient, D_t, versus the calculated aspect ratio or length is shown in Figure 4.25. This significance of this plot is that it allows us to obtain the desired dimensional properties (aspect ratio or length) from experimentally obtained D_t values. As expected, the graph shows a universal inverse proportionality trend as represented by the relationship between D_t and the dimensions of the nanocrystalline cellulose.

Moreover, the effect of the diameter can be demonstrated by comparing the graphs for aspect ratio (Figure 4.25a) and that of the length (Figure 4.25b). We noted that the ratio L/d produced a better plot and fit of the experimental values. This indicates the importance of using aspect ratio measurements in the characterization of nanocrystalline cellulose, and that this normalized value is a good approximate of the dimensions of the NCC.

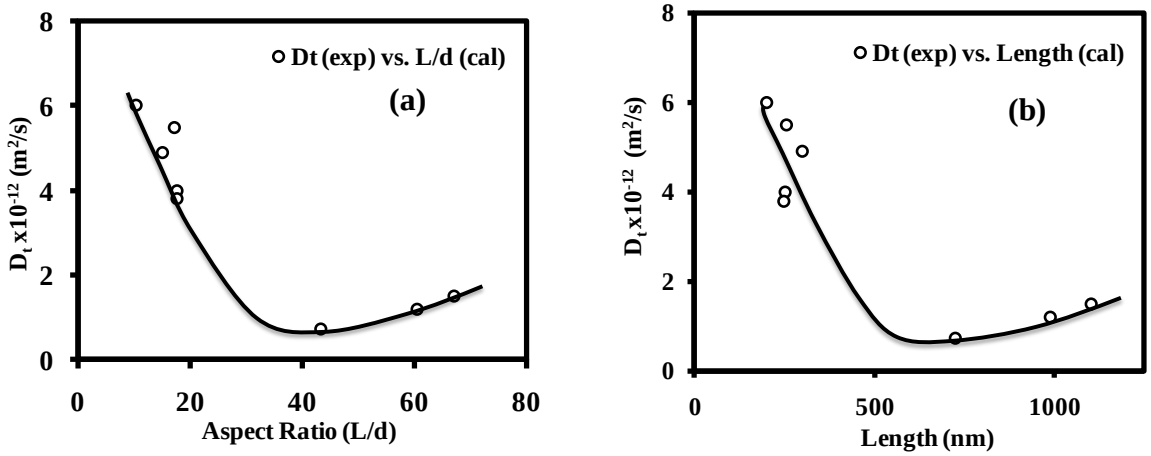

Figure 4.25 Variation of experimental translation diffusion coefficient (D_t) vs. (a) Aspect ratio and (b) length

The main objective for plotting dynamics vs. dimensions is to use an empirical best fit line to calculate specific L/d or length values from experimentally obtained D_t values. It is hard to do so over a wide range of lengths, since the inverse proportionality graph between D_t and L (or L/d) is not linear, however it is attainable at small range of lengths and diameter:

200.0 nm $\leq$ Length $\leq$ 300.0, 16.0 nm $\leq$ diameter $\leq$ 20.0 nm, and 10.0 nm $\leq$ L /d $\leq$ 18.0 nm.

The plot D_t (exp) and D_t (cal) vs. L/d is shown in Figure 4.26, and the fitted straight line from both plots allows us to extrapolate some points using experimental D_t values.

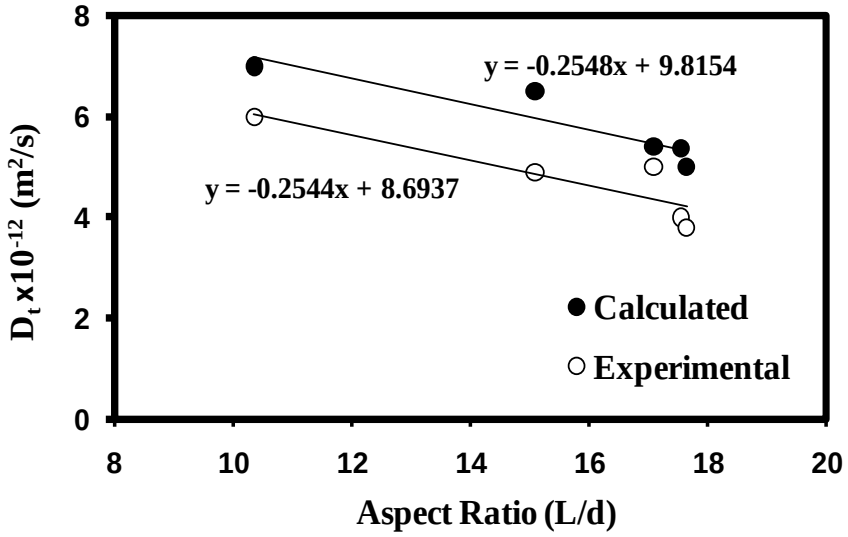

Figure 4.26 Best fit of straight line of experimental translation diffusion coefficient (D_t) vs. Aspect Ratio (L/d) at range $10 \leq L/d \leq 18$

Table 4.6 shows an illustration of the calculated extrapolated aspect ratio values using experimental D_t (De and Borsali, 2002, De, et al., 2003, Rodriguez-Fernandez, et al., 2007, Van, et al., 2000) values while using the equation of the best fit straight line in Figure 4.26. The extrapolated points show a close resemblance to both, the experimental and calculated values, and so for a certain confidence level ($\sim 8 \leq L/d \leq \sim 20$) we can use these equations to calculate the aspect ratio of cylindrically shaped cellulose rods.

Table 4.6 Extrapolation of Aspect Ratio using experimental D_t and equations in Fig. 4.26

Experimental D_t x 10^{-12} (m^2/s)	Experimental L/d *(table3)*	Extrapolated L/d	Calculated L/d *(table 4)*
4.0	17.2	y = 4.0 = (-0.2544) x + 8.6937 x = L/d = 18.45	17.6
4.9	12.6	y = 4.9 = (-0.2544) x +8.6937 x = L/d =14.8	15.1
6.0	8.9	y = 6.0 = (-0.2544) x +8.6937 x = L/d =10.0	10.3

Determination of another NCC dimensions from DLS

Finally, the dimensions of our own rod like nano crystalline cellulose (NCC) were calculated using the same approach presented above. Initially, the IACF for the dispersion for rods was fitted with Equation 4.6 and subsequently the translational and rotational diffusion coefficients were determined. The equations of the polarized (I_{VV}) and depolarized (I_{VH}) first–order time correlation functions in dilute solution were used as presented by De Souza et al. (De, et al., 2003, Lima and Borsali, 2004) according:

$$I_{vv}(q,t) = < N > \alpha_{iso}{}^2 \exp(- q^2 D_t \times t) + \frac{4}{45} < N > \alpha_{iso}{}^2 \exp[-(q^2 D_t + 6\Theta)t]$$

$$I_{VH}(q,t) = \frac{1}{15} < N > \alpha_{aniso}{}^2 \exp[-(q^2 D_t + 6\Theta)t] \qquad (4.10)$$

where <N> is the average number of particles in the scattering volume, α_{iso} is the isotropic part of the polarizability tensor, and α_{aniso} is the molecular optical anisotropy.

The procedure for the sample preparation was adopted as summarized elsewhere (De, et al., 2003, Lima and Borsali, 2004). Figure 4.27 (a and b) shows the relaxation distribution functions and the variation of the extracted frequencies (Γ) as a function of the scattering vector (q^2) for the cotton whiskers at a concentration of 0.2 wt %.

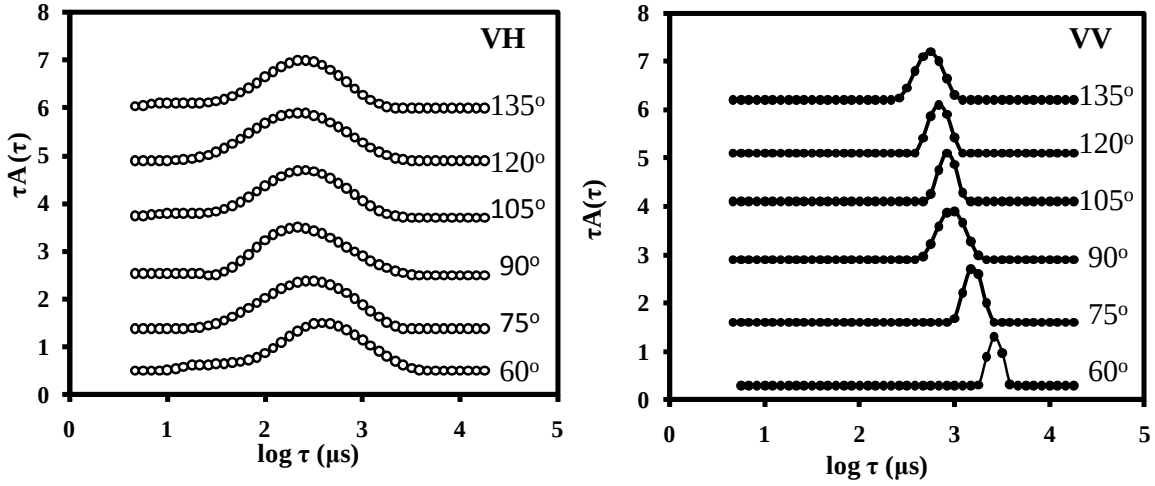

Figure 4.27-a Relaxation distribution functions obtained from DLS measurement at VH (○) and VV mode (●)

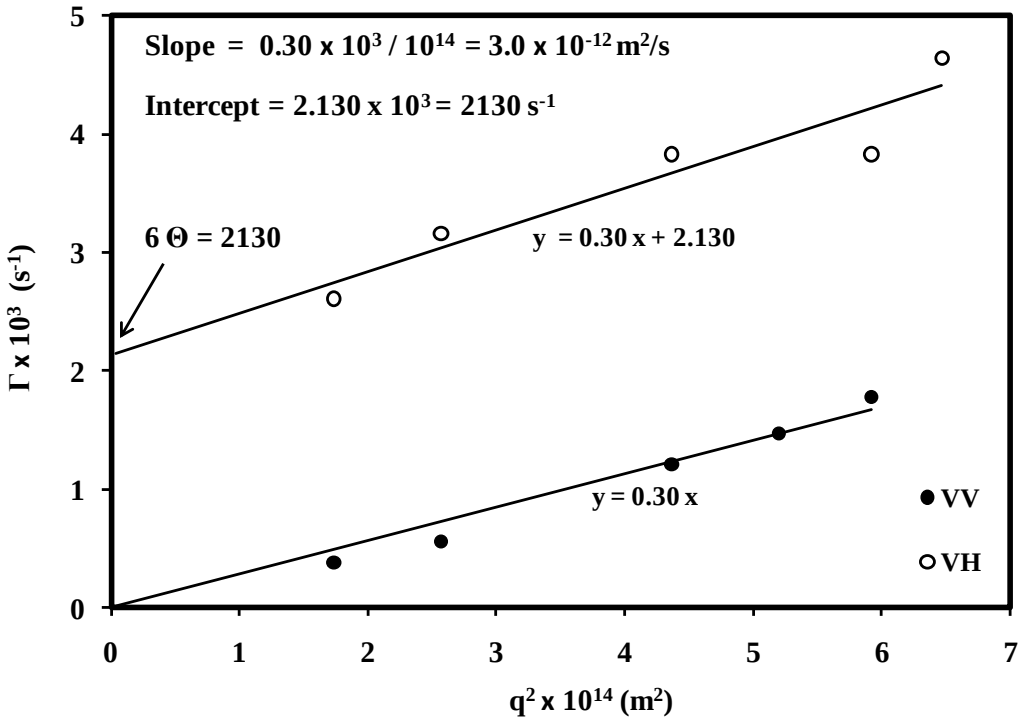

Figure 4.27-b The dependence of the decay rate Γ on the square of scattering vector, q^2 obtained for the VV (●) and VH mode (○)

The translational diffusion coefficient (D_t) and the rotational diffusion coefficient (Θ) are determined from the slope of the VV and VH mode, and the intercept of the VH mode, respectively. These values are: $D_t = 3.0 \times 10^{-12}$ m^2/s and $\Theta = 355$ s^{-1}. Table 4.7 shows the average predicted dimension values (Length and diameter) as calculated by the method described earlier for 5 guesses. The dimensions correspond approximately to the average size of NCC as measured by scanning and tunnelling electron microscopy (Zhao, et al., 2007, Habibi, et al., 2010, Siqueira, et al., 2009). As before, it is expected that increasing the number of guesses will produce a more accurate L and d values, however here we only focus on the averaged value obtained for i = 5 .

Table 4.7 Predicted average values of dimensions of rod like NCC

	Experimental $D_t \times 10^{-12}$ (m^2/s)	**Experimental Θ (s^{-1})**	
	3.0	355.0	
Guessed L x 10^{-9}(m)	**Guessed d x 10^{-9} (m)**	**Calculated L x 10^{-9}(m)**	**Calculated d x 10^{-9}(m)**
326.2	10.4	322.1	10.7
241.1	12.3	287.3	20.6
280.8	17.6	295.1	18
200.3	13.9	306.2	14.7
214.5	11.6	317.3	11.8
Calculated Average		**305.6**	**15.1**
Standard Deviation		14.2	4.2

Chapter 5.0 Conclusion

5.1 Properties of binding between α-CD and pH responsive polymers

From the first study, it was found that the threading of α-CD upon PEG segments of the PEGylated-PAMAM dendrimers was pH and concentration dependent. Both pH and α-CD concentration play an important and mutually dependent role in the binding process. The first is characterized by a critical α-CD concentration (C^*) required to induce the threading of α-CD onto PEG chains at very low pHs. Whereas the second, is related to the binding enthalpies of interaction between α-CD and PEGylated PAMAM dendrimer. This binding showed a profound increase while moving from an acidic pH range to a basic one. This suggests that electrostatic effect of PAMAM has significant effect on the threading process. The size and morphology of the PEGylated-PAMAM dendrimers transformed from a star-like to a Gaussian-like aggregate while increasing both α-CD concentration and pH values. This behavior sheds lights on the importance of studying non covalent interactions mainly electrostatics, hydrogen bond and hydrophobic forces on the behavior of PEGylated-PAMAM dendrimers in the presence of α-CD.

5.2 Physical properties of cellulose nano-crystallites

The prediction of dynamics and dimensions of cellulose is of particular importance for the future processing and industrial uses of these nanocomposites. Using a parameter estimation technique the length, diameter, translational and rotational diffusion coefficients were calculated for various samples, while showing close resemblance to the experimental L^* and d^* values. The percent error between experimental and calculated dimensions showed significant reduction with increasing number of guesses. The predicted results also revealed a universal inverse

proportionality relationship between the diffusional coefficients and dimension factors. Generally, the parameter estimation problems using built-in optimized functions in Matlab are good approximate to solve complex non-linear equations. It is expected that these calculations will contain some error similar to the inaccuracies observed in experimentally obtained values. However, the method used will constitute a versatile model system for calculating the dimensions and dynamics of rigid rod like particles.

Chapter 6.0 Recommendation for Future Studies

Due to the wide uses of dendrimers and α-CD in the fields of drug delivery, gene therapy, personal care products and nano-catalysis, it is of particular importance to conduct further research on host guest systems of this type to have a good understanding on the interaction between branched polymers and cyclic molecules. Further research could be conducted using larger molecular weights of PEG or by grafting homopolymers other than PEG (such as LPEI) capable of threading with α-CD. More studies could also be investigated while using larger generations of PAMAM dendrimer. Crucial issues to be addressed in the study of the binding between responsive polymers such as PEGylated- PAMAM dendrimers and cyclic molecules (α-CD) include:

a) The extent of threading process under various conditions other than concentration and pH including: surface modification, temperature effect, nature of solvent, effect of urea on hydrogen bonding etc.;

b) The binding capabilities of PAMAM dendrimers and α-CD with different type of molecules including surface encapsulation of small or large molecules;

c) The application of pH responsive systems in the loading and controlled release of different types of molecules for uses in the field cosmetics and pharmaceutics.

An important future step in this study would be the investigation of α-CD/ PEGylated-PAMAM complexes for the release of sample molecules at acidic pH ranges.

Finally, much study could be conducted (experimentally and theoretically) for determining the physical properties of rod like cellulose. Modification of surface functional groups of cellulose with PEG and the coating of NCC with surfactant are expected to result in a change in these physical properties. The study of these variations will be vital for the future commercialization of cellulose products.

References

Alexei A.Fedortchenko. 1997. Stabilization of transition of Organic Reactions by Cyclodextrin, Micelles and dendrimers, Master of Science Thesis at Concordia University

Araki, J., & Ito, K. (2007). Recent advances in the preparation of cyclodextrin-based polyrotaxanes and their applications to soft materials. *Soft Matter, 3*(12), 1456-1473.

Avny, Y., & Porath, D. (1976). Polyethylenimine-"Poly(vinyl chloride) crosslinked polymers and their use in adsorption of mercuric and cupric salts.*10*(6), 1193-1203.

Azizi Samir, M.,Ahmed Said, Alloin, F., & Dufresne, A. (2005). Review of recent research into cellulosic whiskers, their properties and their application in nanocomposite field. *Biomacromolecules, 6*(2), 612-626.

Azizi Samir, M.,Ahmed Said, Alloin, F., & Dufresne, A. (2005). Review of recent research into cellulosic whiskers, their properties and their application in nanocomposite field. *Biomacromolecules, 6*(2), 612-626.

Baek, M., & Roy, R. (2002). Synthesis and protein binding properties of T-antigen containing GlycoPAMAM dendrimers. *Bioorganic & Medicinal Chemistry, 10*(1), 11-17.

Basaran, O. A., Burban, P. M., & Auvil, S. R. (1989). Facilitated transport with unequal carrier and complex diffusivities. *Industrial and Engineering Chemistry Research, 28*(1), 108-119.

Battista, O. A., Coppick, S., & Howsmon, J. A. (1956). Sisson,level-off degree of polymerization: Relation to polyphase structure of cellulose fibers.*48,* 333-335.

Bender, M. L., 1924-. (1978). In Komiyama M. (Ed.), *Cyclodextrin chemistry*. Berlin ; New York: Berlin ; New York : Springer-Verlag.

Bielinska, A. U., Chen, C., Johnson, J., & Baker, J. R. (1999). DNA complexing with polyamidoamine dendrimers: Implications for transfection. *Bioconjugate Chemistry, 10*(5), 843-850.

Boas, U., & Heegaard, P. M. H. (2004). Dendrimers in drug research. *ChemInform, 35*(16)

Bonini, C. A., Heux, L., Cavailla, J., Lindner, P., Dewhurst, C., & Terech, P. (2002). Rodlike cellulose whiskers coated with surfactant: A small-angle neutron scattering characterization. *Langmuir, 18*(8), 3311-3314.

Boussif, O., Lezoualc'h, F., Zanta, M. A., Mergny, M. D., Scherman, D., Demeneix, B., et al. (1995). A versatile vector for gene and oligonucleotide transfer into cells in culture and in vivo: Polyethylenimine. *Proc Natl Acad Sci U S A, 92*, 7297-7301.

Braun, C. S., Vetro, J. A., Tomalia, D. A., Koe, G. S., Koe, J. G., & Middaugh, C. R. (2005). Structure/function relationships of polyamidoamine/DNA dendrimers as gene delivery vehicles. *Journal of Pharmaceutical Sciences, 94*(2), 423-436.

Broersma, S. (1960). Rotational diffusion constant of a cylindrical particle.*32*(6), 1632.

Broersma, S. (1960). Rotational diffusion constant of a cylindrical particle.*32*(6), 1626.

Broersma, S. (1981). Viscous force and torque constants for a cylinder.*74*(12), 6990.

Brown, W., Fundin, J., & Miguel, M. d. G. (1992). Poly(ethylene oxide)-sodium dodecyl sulfate interactions studied using static and dynamic light scattering. *Macromolecules, 25*(26), 7192-7198.

Buschmann, H. -., Denter, U., Knittel, D., & Schollmeyer, E. (1998). The use of cyclodextrins in textile processes: An overview. *Journal of the Textile Institute, 89*(3), 554-561.

Buschmann, H. -., Knittel, D., & Schollmeyer, E. (2001). New textile applications of cyclodextrins. *Journal of Inclusion Phenomena and Macrocyclic Chemistry, 40*(3), 169-172.

Cavalli, R., Trotta, F., & Tumiatti, W. (2006). Cyclodextrin-based nanosponges for drug delivery. *Journal of Inclusion Phenomena and Macrocyclic Chemistry, 56*(1), 209-213.

Ceccato, M., Lo Nostro, P., & Baglioni, P. (1997). Alfa-Cyclodextrin/Polyethylene glycol polyrotaxane:A study of the threading process. *Langmuir, 13*(9), 2436-2439.

Challa, R., Ahuja, A., Ali, J., & Khar, R. (2005). Cyclodextrins in drug delivery: An updated review. *AAPS PharmSciTech, 6*(2), E329-E357.

Chen, C. Z., & Cooper, S. L. (2002). Interactions between dendrimer biocides and bacterial membranes. *Biomaterials, 23*(16), 3359-3368.

Chen, W., Tomalia, D. A., & Thomas, J. L. (2000). Unusual pH-dependent polarity changes in PAMAM dendrimers: Evidence for pH-responsive conformational changes. *Macromolecules, 33*(25), 9169-9172.

Chen, Y., & Liu, Y. (2010). ChemInform abstract: Cyclodextrin-based bioactive supramolecular assemblies. *ChemInform, 41*(22)

Cheng, Y., Li, M., & Xu, T. (2008). Potential of poly(amidoamine) dendrimers as drug carriers of camptothecin based on encapsulation studies. *European Journal of Medicinal Chemistry, 43*(8), 1791-1795.

Choi, H. S., Ooya, T., Lee, S. C., Sasaki, S., Kurisawa, M., Uyama, H., et al. (2004). pH dependence of polypseudorotaxane formation between cationic linear polyethylenimine and cyclodextrins. *Macromolecules, 37*(18), 6705-6710.

Choi, H. S., Ooya, T., Lee, S. C., Sasaki, S., Kurisawa, M., Uyama, H., et al. (2004). pH dependence of polypseudorotaxane formation between cationic linear polyethylenimine and cyclodextrins. *Macromolecules, 37*(18), 6705-6710.

Cooper, A. I., Londono, J. D., Wignall, G., McClain, J. B., Samulski, E. T., Lin, J. S., et al. (1997). Extraction of a hydrophilic compound from water into liquid CO2 using dendritic surfactants. *Nature, 389*(6649), 368-371.

Dai, S., & Tam, K. C. (2006). Isothermal titration calorimetric studies on the interaction between sodium dodecyl sulfate and polyethylene glycols of different molecular weights and chain architectures. *Colloids and Surfaces A: Physicochemical and Engineering Aspects, 289*(1-3), 200-206.

De, S. L., & Borsali, R. (2002). Static and dynamic light scattering from polyelectrolyte microcrystal cellulose. *Langmuir, 18*(4), 992-996.

De, S. L., Wong, J. T., Paillet, M., Borsali, R., & Pecora, R. (2003). Translational and rotational dynamics of rodlike cellulose whiskers. *Langmuir, 19*(1), 24-29.

Del Valle, E. M. M. (2004). Cyclodextrins and their uses: A review. *Process Biochemistry, 39*(9), 1033-1046.

Devarakonda, B., Hill, R. A., & de Villiers, M. M. (2004). The effect of PAMAM dendrimer generation size and surface functional group on the aqueous solubility of nifedipine. *International Journal of Pharmaceutics, 284*(1-2), 133-140.

Duchane, D., & Wouessidjewe, D. (1990). Pharmaceutical uses of cyclodextrins and derivatives. *Drug Development and Industrial Pharmacy, 16*(17), 2487-2499.

Duchêne, D., Bochot, A., Yu, S., Pépin, C., & Seiller, M. (2003). Cyclodextrins and emulsions. *International Journal of Pharmaceutics, 266*(1-2), 85-90.

Duchêne, D., Ponchel, G., & Wouessidjewe, D. (1999). Cyclodextrins in targeting: Application to nanoparticles. *Advanced Drug Delivery Reviews, 36*(1), 29-40.

Dufès, C., Uchegbu, I. F., & Schätzlein, A. G. (2005). Dendrimers in gene delivery. *Advanced Drug Delivery Reviews, 57*(15), 2177-2202.

Dufresne, A., Kellerhals, M. B., & Witholt, B. (1999). Transcrystallization in mcl-PHAs/Cellulose whiskers composites. *Macromolecules, 32*(22), 7396-7401.

Esfand, R., & Tomalia, D. A. (2001). Poly(amidoamine) (PAMAM) dendrimers: From biomimicry to drug delivery and biomedical applications. *Drug Discovery Today, 6*(8), 427-436.

Favier, V., Cavaille, J. Y., Canova, G. R., & Shrivastava, S. C. (1997). Mechanical percolation in cellulose whisker nanocomposites. *Polymer Engineering & Science, 37*(10), 1732-1739.

Favier, V., Chanzy, H., & Cavaille, J. Y. (1995). Polymer nanocomposites reinforced by cellulose whiskers. *Macromolecules, 28*(18), 6365-6367.

Fras Zemlji, L., Stenius, P., Laine, J., & Stana-Kleinschek, K. (2008). Topochemical modification of cotton fibres with carboxymethyl cellulose. *Cellulose, 15*(2), 315-321.

Fromming, K. H., & Szejtli, J.,. (1994). Cyclodextrins in pharmacy.

Furuta, T., Yoshii, H., Miyamoto, A., Yasunishi, A., & Hirano, H. (1993). Effects of water and alcohol on the formation of inclusion complexes of *d*-limonene and cyclodextrins. *Supramolecular Chemistry, 1*(3), 321.

Garcia de la Torre, J. & Bloomfield, V. A. (1981). Hydrodynamic properties of complex, rigid, biological macromolecules. theory and applications*14*, 81.

Garcia de, l. T., & Carrasco, B. (1998). Intrinsic viscosity and rotational diffusion of bead models for rigid macromolecules and bioparticles. *European Biophysics Journal, 27*(6), 549-557.

Górnas, P., Neunert, G., Baczynski, K., & Polewski, K. (2009). Beta-cyclodextrin complexes with chlorogenic and caffeic acids from coffee brew: Spectroscopic, thermodynamic and molecular modelling study. *Food Chemistry, 114*(1), 190-196.

Gupta, U., Agashe, H. B., Asthana, A., & Jain, N. K. (2006). A review of in vitro–in vivo investigations on dendrimers: The novel nanoscopic drug carriers. *Nanomedicine: Nanotechnology, Biology and Medicine, 2*(2), 66-73.

Habibi, Y., Lucia, L. A., & Rojas, O. J. (2010). Cellulose nanocrystals: Chemistry, self-assembly, and applications. *Chemical Reviews, 110*(6), 3479-3500.

Harada, A. (1996). Preparation and structures of supramolecules between cyclodextrins and polymers. *Coordination Chemistry Reviews, 148*, 115-133.

Harada, A. (1997). Construction of supramolecular structures from cyclodextrins, polymers. *Carbohydrate Polymers, 34*(3), 183-188.

Harada, A. (2001). Cyclodextrin-based molecular machines. *Accounts of Chemical Research, 34*(6), 456-464.

Harada, A., Li, J., & Kamachi, M. (1992). The molecular necklace: A rotaxane containing many threaded [alpha]-cyclodextrins. *Nature, 356*(6367), 325-327.

Harada, A., Nishiyama, T., Kawaguchi, Y., Okada, M., & Kamachi, M. (1997). Preparation and characterization of inclusion complexes of aliphatic polyesters with cyclodextrins. *Macromolecules, 30*(23), 7115-7118.

Harris, J. M., & Chess, R. B. (2003). Effect of PEGylation on pharmaceuticals. *Nat Rev Drug Discov, 2*(3), 214-221.

Hawker, C. J., & Frechet, J. M. J. (1990). Preparation of polymers with controlled molecular architecture. A new convergent approach to dendritic macromolecules. *Journal of the American Chemical Society, 112*(21), 7638-7647.

He, L., Huang, J., Chen, Y., & Liu, L. (2005). Inclusion complexation between comblike PEO grafted polymers and alfa-cyclodextrin. *Macromolecules, 38*(8), 3351-3355.

He, Y., Fu, P., Shen, X., & Gao, H. (2008). Cyclodextrin-based aggregates and characterization by microscopy. *Micron, 39*(5), 495-516.

Huh, K. M., Tomita, H., Ooya, T., Lee, W. K., Sasaki, S., & Yui, N. (2002). pH dependence of inclusion complexation between cationic poly(ε-lysine) and alfa-cyclodextrin. *Macromolecules, 35*(9), 3775-3777.

Ioelovich, M. &. F.,O. (2008). Nano-cellulose as promising biocarrier.*47-50*, 1286-1289.

Ishiwata, S., & Kamiya, M. (2000). Structural study on inclusion complexes of cyclodextrins with organophosphorus pesticides by use of rotational strength analysis method. *Chemosphere, 41*(5), 701-704.

Israelachvili, J. (1992). Intermolecular and surface forces. (2nd edition)

Jeffrey, C. L., James, A. R., Margareth H. W., & Paul E. W. (1998). Convergence properties of the Nedler-Mead Simplex Method in low dimensions. *SIAM Journal of Optimization, 9*, 112-147.

Kidowaki, M., Zhao, C., Kataoka, T., & Ito, K. (2006). Thermoreversible sol–gel transition of an aqueous solution of polyrotaxane composed of highly methylated α-cyclodextrin and polyethylene glycol. *Chemical Communications, 2006*(39), 4102-4103.

Kim, Y., Klutz, A. M., & Jacobson, K. A. (2008). Systematic investigation of polyamidoamine dendrimers surface-modified with poly(ethylene glycol) for drug delivery applications: Synthesis, characterization, and evaluation of cytotoxicity. *Bioconjugate Chemistry, 19*(8), 1660-1672.

Klajnert, B., & Bryszewska, M. (2001). Dendrimers: Properties and applications. *Acta Biochimica Polonica, 48*(1), 199-208.

Knapen, J. W. J., van, d. M., de Wilde, J. C., van Leeuwen, Piet W. N. M., Wijkens, P., Grove, D. M., et al. (1994). Homogeneous catalysts based on silane dendrimers functionalized with arylnickel(II) complexes. *Nature, 372*(6507), 659-663.

Kojima, C., Kono, K., Maruyama, K., & Takagishi, T. (2000). Synthesis of polyamidoamine dendrimers having poly(ethylene glycol) grafts and their ability to encapsulate anticancer drugs. *Bioconjugate Chemistry, 11*(6), 910-917.

Kolhe, P., Misra, E., Kannan, R. M., Kannan, S., & Lieh-Lai, M. (2003). Drug complexation, in vitro release and cellular entry of dendrimers and hyperbranched polymers. *International Journal of Pharmaceutics, 259*(1-2), 143-160.

Kvien I., Tanem B.S. and Oksman K. (2005). Investigation of the structure of cellulose whiskers and its nanocomposites by TEM,SEM,AFM, and X-ray diffraction.*8*

Kvien, I., Tanem, B. S., & Oksman, K. (2005). Characterization of cellulose whiskers and their nanocomposites by atomic force and electron microscopy. *Biomacromolecules, 6*(6), 3160-3165.

Lee, S. C., Choi, H. S., Ooya, T., & Yui, N. (2004). Block-selective polypseudorotaxane formation in PEI-b-PEG-b-PEI copolymers via pH variation. *Macromolecules, 37*(20), 7464-7468.

Li, J., Li, X., Ni, X., Wang, X., Li, H., & Leong, K. W. (2006). Self-assembled supramolecular hydrogels formed by biodegradable PEO-PHB-PEO triblock copolymers and α-cyclodextrin for controlled drug delivery. *Biomaterials, 27*(22), 4132-4140.

Li, J., & Loh, X. J. (2008). Cyclodextrin-based supramolecular architectures: Syntheses, structures, and applications for drug and gene delivery. *Advanced Drug Delivery Reviews, 60*(9), 1000-1017.

Li, J., Ni, X., & Leong, K. W. (2003). Injectable drug-delivery systems based on supramolecular hydrogels formed by poly(ethylene oxide)s and alpha-cyclodextrin. *Journal of Biomedical Materials Research Part A, 65A*(2), 196-202.

Liebert, T., and Heinze, T. (2008). Interactions of ionic liquids with polysaccharides. 5. solvents and reaction media for the modification of cellulose. *Macromolecular Rapid Communications, 3*(2), 576-601.

Lim A.H. (2008). Interactions of Amphiphilic Molecules with Dendrimers, Masters of Engineering Thesis, Nanyang Technological University.

Lima, M. M. d. S., & Borsali, R. (2004). Rodlike cellulose microcrystals: Structure, properties, and applications. *Macromolecular Rapid Communications, 25*(7), 771-787.

Liu, J., Sondjaja, H. R., & Tam, K. C. (2007). Alfa-cyclodextrin-induced self-assembly of a double-hydrophilic block copolymer in aqueous solution. *Langmuir, 23*(9), 5106-5109.

LLS Goniometer Instruction Manual. (2008). Brookhaven instruments limited: BI-200SM laser light scattering goniometer.

Loethen, S., Kim, J., & Thompson, D. H. (2007). Biomedical applications of cyclodextrin based polyrotaxanes. *Polymer Reviews, 47*(3), 383-418.

Loethen, S., Ooya, T., Choi, H. S., Yui, N., & Thompson, D. H. (2006). Synthesis, characterization, and pH-triggered dethreading of α-cyclodextrin-poly(ethylene glycol) polyrotaxanes bearing cleavable endcaps. *Biomacromolecules, 7*(9), 2501-2506.

Loftsson, T., & Duchêne, D. (2007). Cyclodextrins and their pharmaceutical applications. *International Journal of Pharmaceutics, 329*(1-2), 1-11.

Loftsson, T., Frikdriksdóttir, H., Sigurkdardóttir, A. M., & Ueda, H. (1994). The effect of water-soluble polymers on drug-cyclodextrin complexation. *International Journal of Pharmaceutics, 110*(2), 169-177.

Loftsson, T., Leeves, N., Bjornsdottir, B., Duffy, L., & Masson, M. (1999). Effect of cyclodextrins and polymers on triclosan availability and substantivity in toothpastes in vivo. *Journal of Pharmaceutical Sciences, 88*(12), 1254-1258.

Luo, D., Haverstick, K., Belcheva, N., Han, E., & Saltzman, W. M. (2002). Poly(ethylene glycol)-conjugated PAMAM dendrimer for biocompatible, high-efficiency DNA delivery. *Macromolecules, 35*(9), 3456-3462.

Malvern. (2008). Zeta potential tutorial.

Martin hubbe, Richarch A. Venditti,Orlando J. Rojas. (2007). "What happens to cellulosic fibers during papermaking and recycling? *Bioresources*, *2*(4), 739-788.

Matthews, J. F., Skopec, C. E., Mason, P. E., Zuccato, P., Torget, R. W., Sugiyama, J., et al. (2006). Computer simulation studies of microcrystalline cellulose I[beta]. *Carbohydrate Research, 341*(1), 138-152.

Memisoglu-Bilensoy, E., Åžen, M., & Hincal, A. A. (2006). Effect of drug physicochemical properties on in vitro characteristics of amphiphilic cyclodextrin nanospheres and nanocapsules. *Journal of Microencapsulation, 23*(1), 59-68.

Mias, S., Sudor, J., & Camon, H. (2008). PNIPAM: A thermo-activated nano-material for use in optical devices. *Microsystem Technologies, 14*(6), 747-751.

Michael Ioelovich. (2008). Cellulose as a nanostructured polymer: As short review. *Bioresources, 3*(4)

Mutalik, V., Manjeshwar, L. S., Wali, A., Sairam, M., Raju, K. V. S. N., & Aminabhavi, T. M. (2006). Thermodynamics/hydrodynamics of aqueous polymer solutions and dynamic mechanical characterization of solid films of chitosan, sodium alginate, guar gum, hydroxy ethyl cellulose and hydroxypropyl methylcellulose at different temperatures. *Carbohydrate Polymers, 65*(1), 9-21.

Nagahori, N., Lee, R. T., Nishimura, S., Pagé, D., Roy, R., & Lee, Y. C. (2002). Inhibition of adhesion of type 1 fimbriated *escherichia coli* to highly mannosylated ligands. *ChemBioChem, 3*(9), 836-844.

Ni, X., Cheng, A., & Li, J. (2009). Supramolecular hydrogels based on self-assembly between PEO-PPO-PEO triblock copolymers and alpha-cyclodextrin. *Journal of Biomedical Materials Research Part A, 88A*(4), 1031-1036.

NumanoÄŸlu, U., Åžen, T., Tarimci, N., Kartal, M., Koo, O., & Ã–nyÃ¼ksel, H. (2007). Use of cyclodextrins as a cosmetic delivery system for fragrance materials: Linalool and benzyl acetate. *AAPS PharmSciTech, 8*(4), 34-42.

Okada, M., Kawaguchi, Y., Okumura, H., Kamachi, M., & Harada, A. (2000). Complex formation of cyclodextrins with poly(propylene glycol) derivatives. *Journal of Polymer Science Part A: Polymer Chemistry, 38*(S1), 4839-4849.

Oksman, K., Mathew, A. P., Bondeson, D., & Kvien, I. (2006). Manufacturing process of cellulose whiskers/polylactic acid nanocomposites. *Composites Science and Technology, 66*(15), 2776-2784.

Okumura, H., Okada, M., Kawaguchi, Y., & Harada, A. (2000). Complex formation between poly(dimethylsiloxane) and cyclodextrins: New pseudo-polyrotaxanes containing inorganic polymers. *Macromolecules, 33*(12), 4297-4298.

Ooya, T., Choi, H. S., Yamashita, A., Yui, N., Sugaya, Y., Kano, A., et al. (2006). Biocleavable polyrotaxane plasmid DNA polyplex for enhanced gene delivery. *Journal of the American Chemical Society, 128*(12), 3852-3853.

Ooya, T., Ito, A., & Yui, N. (2005). Preparation of α-Cyclodextrin-Terminated polyrotaxane consisting of β-Cyclodextrins and pluronic as a building block of a biodegradable network. *Macromolecular Bioscience, 5*(5), 379-383.

Ooya, T., Lee, J., & Park, K. (2003). Effects of ethylene glycol-based graft, star-shaped, and dendritic polymers on solubilization and controlled release of paclitaxel. *Journal of Controlled Release, 93*(2), 121-127.

O'Suillivan, A. (1997). *Cellulose: The structure slowly unravels* Springer Netherlands.

Philp, D., & Stoddart, J. F. (1996). Self-assembly in natural and unnatural systems. *Angewandte Chemie International Edition in English, 35*(11), 1154-1196.

Piel, G., Evrard, B., Fillet, M., Llabres, G., & Delattre, L. (1998). Development of a non-surfactant parenteral formulation of miconazole by the use of cyclodextrins. *International Journal of Pharmaceutics, 169*(1), 15-22.

Prasad, N., Strauss, D., & Reichart, G. (1999). Cyclodextrins inclusion for food,cosmetics and pharmaceuticals.*1,084,625*

Pun, S. H., & Davis, M. E. (2002). Development of a nonviral gene delivery vehicle for systemic application. *Bioconjugate Chemistry, 13*(3), 630-639.

Rekharsky, M. V., & Inoue, Y. (1998). Complexation thermodynamics of cyclodextrins. *Chemical Reviews, 98*(5), 1875-1918.

Rodriguez-Fernandez, J., Perez-Juste, J., Luis M. Liz-Marzan, & Lang, P. R. (2007). Dynamic light scattering of short au rods with low aspect ratios. *The Journal of Physical Chemistry C, 111*(13), 5020-5025.

Sabadini, E., Cosgrove, T., & Taweepreda, W. (2003). Complexation between alfa-cyclodextrin and poly(ethylene oxide) physically adsorbed on the surface of colloidal silica. *Langmuir, 19*(11), 4812-4816.

Saenger, W., Jacob, J., Gessler, K., Steiner, T., Hoffmann, D., Sanbe, H., et al. (1998). Structures of the common cyclodextrins and their larger AnaloguesBeyond the doughnut. *Chemical Reviews, 98*(5), 1787-1802.

Saint Aman, E., & Serve, D. (1990). A conductimetric study of the association between cyclodextrins and surfactants--application to the electrochemical study of a mixed aqueous system: Substrate, cyclodextrin, surfactant. *Journal of Colloid and Interface Science, 138*(2), 365-375.

Sanchez-Garcia, M., & Lagaron, J. (2010). *On the use of plant cellulose nanowhiskers to enhance the barrier properties of polylactic acid* Springer Netherlands.

Scott Loethen. (May 2008). Cyclodextrin Based pseudopolyrotoxanes and polyrotoxanes for Biological Application. *Doctor of Philosophy presented to Purdue University*

Seo, T., Kajihara, T., & Iijima, T. (1987). The synthesis of poly(allylamine) containing covalently bound cyclodextrin and its catalytic effect in the hydrolysis of phenyl esters. *Die Makromolekulare Chemie, 188*(9), 2071-2082.

Shechter, I., Ramon, O., Portnaya, I., Paz, Y., & Livney, Y. D. (2010). Microcalorimetric study of the effects of a chaotropic salt, KSCN, on the lower critical solution temperature (LCST) of aqueous poly(N-isopropylacrylamide) (PNIPA) solutions. *Macromolecules, 43*(1), 480-487.

Sidhu, J., Bloor, D. M., Couderc Azouani, S., Penfold, J., Holzwarth, J. F., & Wyn-Jones, E. (2004). Interactions of poly(amidoamine) dendrimers with the surfactants SDS, DTAB, and C12EO6:An equilibrium and structural study using a SDS selective electrode, isothermal titration calorimetry, and small angle neutron scattering. *Langmuir, 20*(21), 9320-9328.

Siqueira, G., Bras, J., & Dufresne, A. (2009). Cellulose whiskers versus microfibrils: Influence of the nature of the nanoparticle and its surface functionalization on the thermal and mechanical properties of nanocomposites. *Biomacromolecules, 10*(2), 425-432.

Sojo, M. M., Nunez-Delicado, E., Garcia-Carmona, F., & Sanchez-Ferrer, A. (1999). Cyclodextrins as activator and inhibitor of latent banana pulp polyphenol oxidase. *Journal of Agricultural and Food Chemistry, 47*(2), 518-523.

Sriupayo, J., Supaphol, P., Blackwell, J., & Rujiravanit, R. (2005). Preparation and characterization of [alpha]-chitin whisker-reinforced chitosan nanocomposite films with or without heat treatment. *Carbohydrate Polymers, 62*(2), 130-136.

Stella, V. J., & Rajewski, R. A. (1997). Cyclodextrins: Their future in drug formulation and delivery. *Pharmaceutical Research, 14*(5), 556-567.

Szejtli J. 1998. Introduction and General Overview of Cyclodextrin Chemistry. Chem Rev 98:1743-1754.

Szejtli J. 1984. Inclusion Compounds. 3: Academic Press, London, Vol. 3. p. 331

Szejtli J. 1982. Cyclodextrin and their Inclusion Complexes. Akademiai Kiado, Cambridge, MA

Szente, L., & Szejtli, J. (1986). Molecular encapsulation of natural and synthetic coffee flavor with β-cyclodextrin. *Journal of Food Science, 51*(4), 1024-1027.

Szente, L., & Szejtli, J. (2004). Cyclodextrins as food ingredients. *Trends in Food Science & Technology, 15*(3-4), 137-142.

Takata, T. (2006). Polyrotaxane and polyrotaxane network: Supramolecular architectures based on the concept of dynamic covalent bond chemistry. *Polymer Journal, 38*(1), 1-20.

Tamura, M., Gao, D., & Ueno, A. (2001). A polyrotaxane series containing *alpha*-cyclodextrin and naphthalene-modified *alpha*-cyclodextrin as a light-harvesting antenna system. *Chemistry, 7*(7), 1390-1397.

Terech, P., Chazeau, L., & Cavaille, J. Y. (1999). A small-angle scattering study of cellulose whiskers in aqueous suspensions. *Macromolecules, 32*(6), 1872-1875.

Tomalia, D. A. and Durst, H.D. Topics in current chemistry: Directed synthesis and molecular recognition.*165,* 93-313.

Tomalia, D. A., & Dvornic, P. R. (1994). What promise for dendrimers? *Nature, 372*(6507), 617-618.

Tomalia, D. A. (1994). Starburst/Cascade dendrimers: Fundamental building blocks for a new nanoscopic chemistry set. *Advanced Materials, 6*(7-8), 529-539.

Tomasik, P., & Schilling, C. H. (1998). Complexes of starch with inorganic guests. In Derek Horton (Ed.), *Advances in carbohydrate chemistry and biochemistry* (pp. 263-343) Academic Press.

Topchieva, I. N., Tonelli, A. E., Panova, I. G., Matuchina, E. V., Kalashnikov, F. A., Gerasimov, V. I., et al. (2004). Two-phase channel structures based on alfa-cyclodextrin polyethylene glycol inclusion complexes. *Langmuir, 20*(21), 9036-9043.

Tu, C., Kuo, S., & Chang, F. (2009). Supramolecular self-assembly through inclusion complex formation between poly(ethylene oxide-b-N-isopropylacrylamide) block copolymer and α-cyclodextrin. *Polymer, 50*(13), 2958-2966.

Ulya, N., Tangül, S., Nilüfer, T., Murat, K., Otilia, M. Y. K., & & Hayat, Ö. (2007). Use of cyclodextrins as a cosmetic delivery system for fragrance materials:Linalool and benzyl acetate.*8*(4)

University Tutorial. (2003). NMR theory tutorial.

Van Zanten, J. H., & Monbouquette, H. G. (1991). Characterization of vesicles by classical light scattering. *Journal of Colloid and Interface Science, 146*(2), 330-336.

Van, d. M., Vermonden, T., van Nostrum, C. F., & Hennink, W. E. (2009). Cyclodextrin-based polymeric materials: Synthesis, properties, and Pharmaceutical/Biomedical applications. *Biomacromolecules, 10*(12), 3157-3175.

Van, d. Z., Dhont, J. K. G., Bahmer, M. R., & Philipse, A. P. (2000). Colloidal dispersions of gold rods characterized by dynamic light scattering and electrophoresis. *Langmuir, 16*(2), 459-464.

Vancha, A., Govindaraju, S., Parsa, K., Jasti, M., Gonzalez-Garcia, M., & Ballestero, R. (2004). Use of polyethyleneimine polymer in cell culture as attachment factor and lipofection enhancer. *BMC Biotechnology, 4*(1), 23.

VP-ITC Instruction Manual. (2001).

Wang, C., & Tam, K. C. (2002). New insights on the interaction mechanism within oppositely charged Polymer/Surfactant systems. *Langmuir, 18*(17), 6484-6490.

Wang, C., Wyn-Jones, E., Sidhu, J., & Tam, K. C. (2007). Supramolecular complex induced by the binding of sodium dodecyl sulfate to PAMAM dendrimers. *Langmuir, 23*(4), 1635-1639.

Wang, J., Marlowe, E. M., Miller-Maier, R., & Brusseau, M. L. (1998). Cyclodextrin-enhanced biodegradation of phenanthrene. *Environmental Science & Technology*, *32*(13), 1907-1912.

Wenz, G. (1994). Cyclodextrins as building blocks for supramolecular structures and functional units. *Angewandte Chemie International Edition in English, 33*(8), 803-822.

Wenz, G., Han, B., & Miller, A. (2006). Cyclodextrin rotaxanes and polyrotaxanes. *Chemical Reviews, 106*(3), 782-817.

Wiener, E. C., Auteri, F. P., Chen, J. W., Brechbiel, M. W., Gansow, O. A., Schneider, D. S., et al. (1996). Molecular dynamics of ion chelate complexes attached to dendrimers. *Journal of the American Chemical Society, 118*(33), 7774-7782.

Wiseman, T., Williston, S., Brandts, J. F., & Lin, L. (1989). Rapid measurement of binding constants and heats of binding using a new titration calorimeter. *Analytical Biochemistry, 179*(1), 131-137.

Yamakawa, T., & Nishimura, S. (2003). Liquid formulation of a novel non-fluorinated topical quinolone, T-3912, utilizing the synergic solubilizing effect of the combined use of magnesium ions and hydroxypropyl-[beta]-cyclodextrin. *Journal of Controlled Release, 86*(1), 101-113.

Yang, C., Wang, X., Li, H., Goh, S. H., & Li, J. (2007). Synthesis and characterization of polyrotaxanes consisting of cationic alfa-cyclodextrins threaded on poly[(ethylene oxide)-ran-(propylene oxide)] as gene carriers. *Biomacromolecules, 8*(11), 3365-3374.

Yang, H., & Lopina, S. T. (2006). *In vitro* enzymatic stability of dendritic peptides. *Journal of Biomedical Materials Research Part A, 76A*(2), 398-407.

Yang, H., Morris, J. J., & Lopina, S. T. (2004). Polyethylene glycol-polyamidoamine dendritic micelle as solubility enhancer and the effect of the length of polyethylene glycol arms on the solubility of pyrene in water. *Journal of Colloid and Interface Science, 273*(1), 148-154.

Zhao, H., Kwak, J. H., Conrad Zhang, Z., Brown, H. M., Arey, B. W., & Holladay, J. E. (2007). Studying cellulose fiber structure by SEM, XRD, NMR and acid hydrolysis. *Carbohydrate Polymers, 68*(2), 235-241.

Zheng, P. J., Wang, C., Hu, X., Tam, K. C., & Li, L. (2005). Supramolecular complexes of azocellulose and α-cyclodextrin: Isothermal titration calorimetric and spectroscopic studies. *Macromolecules, 38*(7), 2859-2864.

Zhu, S., Hong, M., Zhang, L., Tang, G., Jiang, Y., & Pei, Y. (2010). PEGylated PAMAM dendrimer-doxorubicin conjugates: In vitro evaluation and in vivo tumor accumulation. *Pharmaceutical Research, 27*(1), 161-174.

Zhuo, R. X., Du, B., & Lu, Z. R. (1999). In vitro release of 5-fluorouracil with cyclic core dendritic polymer. *Journal of Controlled Release, 57*(3), 249-257.